Department of Energy
Washington, DC 20585

QA: N/A
DOCKET NUMBER 63-001

April 13, 2009

ATTN: Document Control Desk
John H. (Jack) Sulima, Project Manager
Project Management Branch Section B
Division of High-Level Waste Repository Safety
Office of Nuclear Material Safety and Safeguards
U.S. Nuclear Regulatory Commission
EBB-2B2
11545 Rockville Pike
Rockville, MD 20852-2738

YUCCA MOUNTAIN – REQUEST FOR ADDITIONAL INFORMATION – SAFETY EVALUATION REPORT, VOLUME 3 – POSTCLOSURE CHAPTER 2.2.1.3.1 – DEGRADATION OF ENGINEERED BARRIERS 2ND SET – (U.S. DEPARTMENT OF ENERGY'S SAFETY ANALYSIS REPORT SECTION 2.3.6.8)

Reference: Ltr, Sulima to Williams, dtd 03/16/09, "Yucca Mountain – Request for Additional Information – Safety Evaluation Report, Volume 3 – Postclosure Chapter 2.2.1.3.1 – Degradation of Engineered Barriers 2nd Set – (U.S. Department of Energy's Safety Analysis Report Section 2.3.6.8)"

The purpose of this letter is to transmit the U.S. Department of Energy's (DOE) responses to ten (10) of the eleven (11) Requests for Additional Information (RAI) identified in the above-referenced letter regarding DOE's License Application Section 2.3.6.8. Each RAI response (for RAIs Numbers 1 through 10) is provided as a separate enclosure. Due to the subject matter, the response to the RAI Number 11 of this set was transmitted to NRC separately on April 8, 2009.

Most of the DOE references cited in the RAI responses have previously been provided with the License Application (LA) or the LA update. Any DOE references cited in the RAI responses, which have not been previously provided to the NRC, are included with this submittal.

There is a commitment in the enclosed response to RAI Number 3. If you have any questions regarding this letter, please contact me at (202) 586-9620, or by email to jeff.williams@rw.doe.gov.

Jeffrey R. Williams, Supervisor
Licensing Interactions Branch
Regulatory Affairs Division
Office of Technical Management

OTM: CJM-0629

Printed with soy ink on recycled paper

NMSS05

Enclosures (11):
Responses to 10 Requests for Additional Information
SER Volume 3, Chapter 2.2.1.3.1, Set 2, Numbers 1 through 10
Enclosure 11
Horn, J.; Martin, S.; Carrillo, C.; and Lian, T. 2005. *Microbial Effects on Nuclear Waste Packaging Materials*. UCRL-TR-213915 Rev. 1. Livermore, California: Lawrence Livermore National Laboratory. ACC: MOL.20050728.0312.

cc w/encl:
B. J. Benney, NRC, Rockville, MD
J. C. Chen, NRC, Rockville, MD
J. R. Davis, NRC, Rockville, MD
A. S. Mohseni, NRC, Rockville, MD
N. K. Stablein, NRC, Rockville, MD
D. B. Spitzberg, NRC, Arlington, TX
J. D. Parrott, NRC, Las Vegas, NV
L. M. Willoughby, NRC, Las Vegas, NV
Jack Sulima, NRC, Rockville, MD
Christian Jacobs, NRC, Rockville, MD
Lola Gomez, NRC, Rockville, MD
W. C. Patrick, CNWRA, San Antonio, TX
Budhi Sagar, CNWRA, San Antonio, TX
Bob Brient, CNWRA, San Antonio, TX
Rod McCullum, NEI, Washington, DC
B. J. Garrick, NWTRB, Arlington, VA
Bruce Breslow, State of Nevada, Carson City, NV
Alan Kalt, Churchill County, Fallon, NV
Irene Navis, Clark County, Las Vegas, NV
Ed Mueller, Esmeralda County, Goldfield, NV
Ron Damele, Eureka County, Eureka, NV
Richard Cervantes, Inyo County, Independence, CA
Chuck Chapin, Lander County, Battle Mountain, NV
Connie Simkins, Lincoln County, Pioche, NV
Linda Mathias, Mineral County, Hawthorne, NV
Darrell Lacy, Nye County, Pahrump, NV
Jeff VanNeil, Nye County, Pahrump, NV
Joe Kennedy, Timbisha Shoshone Tribe, Death Valley, CA
Mike Simon, White Pine County, Ely, NV
K. W. Bell, California Energy Commission, Sacramento, CA
Barbara Byron, California Energy Commission, Sacramento, CA
Susan Durbin, California Attorney General's Office, Sacramento, CA
Charles Fitzpatrick, Egan, Fitzpatrick, Malsch, PLLC

EIE Document Components:

001_NRC_Trans_Letter_3.2.2.1.3.1_Set_2_No_2.pdf	
002_Enclosures_1_thru_10_3.2.2.1.3.1_Set_2.pdf	3,890 KB
003_MOL.20060911.0067_UCRL_TR_213915_R01.pdf	2,334 KB

RAI: Volume 3, Chapter 2.2.1.3.1, Second Set, Number 1:

Provide additional technical bases to support: (1) the range of activation energy values used in TSPA, (2) the selection of the mean activation energy as 40.78 kJ/mol, and (3) an evaluation of whether the range or the estimate of the central tendency in the activation energy controls consequence estimates. These should all include a discussion of the extrapolation of activation energy for Alloy 22 passive dissolution to the range of temperatures and water chemistries expected for repository conditions during the performance period.

Basis: The model for passive dissolution of Alloy 22 uses a mean activation energy of 40.78 kJ/mol to represent all temperatures and water conditions analyzed in the general corrosion model (SAR Section 2.3.6.3; SNL, 2007, Section 6.4.3.4). Available information in the literature shows that mean activation energies can be roughly 50 percent lower for solution chemistries and temperatures that may occur during repository closure (e.g., Gordon, 2002; Hua and Gordon, 2004; BSC, 2004). Hua and Gordon (2004) also indicate that activation energy for Alloy 22 varied with time. DOE has not provided a technical basis to address why these apparent solution chemistry, temperature, or time-dependent effects are not considered in the selection of the mean activation energy used in the Alloy 22 corrosion model. This information suggests that the mean activation energy, which has a potentially significant effect on expected annual dose (SNL, 2008a), may be lower than used in the current model. This requested information is needed to assess the use of these activation energy data in the performance assessment used to demonstrate compliance with 10 CFR 63.21(c)(15) and 63.114(b).

1. RESPONSE

The technical basis for the use of a range of activation energies for Alloy 22 over a range of temperatures and water chemistries as presented in *General Corrosion and Localized Corrosion of Waste Package Outer Barrier* (SNL 2007a). The Alloy 22 general corrosion model used in the total system performance assessment (TSPA) is corroborated by newly-derived data (discussed in the response to RAI: 3.2.2.1.3.1-2-003) and is summarized here. Although the newly-derived data indicates that the apparent activation energy for Alloy 22 general corrosion is lower than that used in TSPA, it also indicates that the Alloy 22 general corrosion rate is lower than that used in TSPA. Overall, it is concluded that despite the reduction in the mean apparent activation energy, the preliminary results presented in the response to RAI: 3.2.2.1.3.1-2-003, when propagated through the TSPA, is not expected to result in an increase in expected annual dose.

1.1 AN ASSESSMENT OF THE TEMPERATURE-DEPENDENT GENERAL CORROSION MODEL

As discussed in Section 6.4.3.4 of *General Corrosion and Localized Corrosion of Waste Package Outer Barrier* (SNL 2007a), the general corrosion rate of Alloy 22 depends on temperature. A temperature dependent model was developed based upon data from short-term

polarization resistance (PR) measurements. These data were then corroborated with longer-term weight-loss test results.

The PR tests were conducted at three temperatures (60°C, 80°C, and 100°C) in nine solutions with a range of chloride to nitrate ratios from 2 to 20 (SNL 2007a, Table 6-8) which covers the anticipated chloride to nitrate ratio range reported in *Engineered Barrier System: Physical and Chemical Environment* (SNL 2007b, Figures 6.13-9 to 6.13-12). These environments correspond to moderate relative humidity (RH) conditions under which seepage is expected to occur. Based on analysis of the PR data, the apparent activation energy of Alloy 22 general corrosion is represented by a normal distribution with a mean of 40.78 kJ/mol and a standard deviation of 11.75 kJ/mol. Because short-term tests are unlikely to achieve steady state, these results were compared to a calculated apparent activation energy based on analysis of the measured weight-loss of Alloy 22 specimens immersed for five years in simulated concentrated water (SCW) at 60°C and 90°C (SNL 2007a, p. 6-52). However, that activation energy analysis was based on weight-loss specimens left in an indeterminate final state that necessitated re-cleaning and reevaluation (RAI response 3.2.2.1.3.1-2-003). The newly-derived Alloy 22 general corrosion rates (based on the re-cleaned specimens) were used to recalculate the apparent activation energy as summarized in the response to RAI: 3.2.2.1.3.1-2-003, Section 1.4. The apparent activation energy distribution obtained for the re-cleaned weight-loss specimens immersed in SCW solution for five years is shown in Figure 9 of that response. The Bootstrap distribution has a mean of about 32.26 kJ/mol and minimum and maximum values of 3.37 and 60.05 kJ/mol, respectively.

Figure 9 of response to RAI: 3.2.2.1.3.1-2-003 also shows the apparent activation energy distribution used in the total system performance assessment (TSPA) (SAR Section 2.3.6.3.3.1), which is based on a normal distribution with a mean of 40.78 kJ/mol and a standard deviation of 11.75 kJ/mol truncated between −3 standard deviations (5.54 kJ/mol) and +2 standard deviations (64.28 kJ/mol). This range of activation energies was based upon Bootstrap evaluation of the SCW 60°C and 90°C weight-loss specimens prior to re-cleaning. The use of the non-uniform truncation ensures that sufficiently low activation energies are captured. The apparent activation energy distribution determined from the Bootstrap evaluation of the re-cleaned weight-loss specimens has a lower mean and slightly lower minimum and maximum values than the apparent activation energy distribution used in TSPA. The range of apparent activation energies determined from the Bootstrap evaluation of the re-cleaned five-year weight-loss specimens is adequately represented by the apparent activation energy distribution used in the TSPA. The only potentially substantive difference is the reduction in the mean apparent activation energy from approximately 41 kJ/mol to approximately 32 kJ/mol. The potential impact on the predicted Alloy 22 general corrosion rate and the expected annual dose of a decrease in the mean activation energy and the use of the general corrosion rates of the re-cleaned specimens are evaluated in the response to RAI: 3.2.2.1.3.1-2-003 and Section 1.2 of this RAI response, respectively.

As described in SAR Section 2.3.6.3, the Alloy 22 general corrosion rate distribution used at 60°C is conservatively based upon corrosion data obtained for 60°C and 90°C. The SCW-immersed specimens exhibited the highest corrosion rates of 8.08 nm/yr and 13.98 nm/yr at 60°C and 90°C, respectively. Using the mean activation energy of approximately 32 kJ/mol, at 25°C these rates equate to 2.06 and 3.56 nm/yr, respectively. If only the 60°C data were used with an

activation energy of 20 kJ/mol, the extrapolated maximum corrosion rate at 25°C would be 3.46 nm/yr. This calculation demonstrates that even if the actual mean activation energy were 20 kJ/mol the TSPA model overestimates maximum corrosion rates at 25°C.

In summary, the mean value of 40.78 kJ/mol and the range of 5.5 kJ/mol to 64.3 kJ/mol for the apparent activation energy used in the Alloy 22 waste package outer corrosion barrier general corrosion model were developed using data collected over a wide range of water chemistries at three temperatures (60°C, 80°C, and 100°C). The model is corroborated by an analysis of the re-cleaned weight-loss specimen data as reported in the response to RAI: 3.2.2.1.3.1-2-003 that calculated an activation energy distribution based on general corrosion rates from specimens immersed in SCW at two temperatures, 60°C and 90°C, for approximately 5 years. In addition, as reported in *General Corrosion and Localized Corrosion of Waste Package Outer Barrier* (SNL 2007a, Table 6-9), the apparent activation energy range adequately represents the Alloy 22 general corrosion response to a wide range of solution chemistries and temperatures.

1.2 COMPARISON OF MODEL DATA TO LITERATURE VALUES

Several literature studies were evaluated in *General Corrosion and Localized Corrosion of Waste Package Outer Barrier* (SNL 2007a, Sections 6.4.3.4 and 7.2.1) (EPRI 2002; Smailos et al. 1987; Dunn et al. 1999; Dunn et al. 2004 ; Dunn et al. 2005 ; Hua and Gordon 2004 ; Pensado et al. 2002). In general, it was shown that for short-term tests (from a few hours to a few weeks) apparent activation energy values for the general corrosion of Alloy 22 are higher than for long-term (greater than a few weeks) tests. For example, Smailos et al. (1987) conducted a series of tests using a C-4 alloy (similar to Alloy 22) and it was found that the apparent activation energy which was in the short-term (100 days) approximately 40 kJ/mol was reduced by half after approximately 1,000 days. In contrast, Hua and Gordon (2004) observed a modest increase in apparent activation energy from approximately 19 kJ/mol (after four weeks of exposure) to approximately 25 kJ/mol (after eight weeks of exposure). Some tests reported activation energies of approximately 46 kJ/mol (slightly higher than the DOE value of approximately 41 kJ/mol) (Lloyd 2003; Dunn et al. 2004; Pensado et al. 2002).

1.3 AN EVALUATION OF THE IMPACT OF MEAN ACTIVATION ENERGY FOR THE GENERAL CORROSION OF ALLOY 22 ON TOTAL MEAN DOSE

The model for the general corrosion of Alloy 22 is described in SAR Section 2.3.6.3.3.1, and includes two uncertain quantities:

C_1 = a constant equaling the apparent activation energy divided by the universal gas constant. The value of C_1 is fixed for all waste packages in a given realization.

C_0 = a constant defined by $C_0 = \ln(R_0) + \frac{C_1}{333.15}$, where R_0 is the general corrosion rate of Alloy 22 at 60°C. The value for R_0 is sampled independently for each patch on each waste package from a scaled Weibull distribution that, for a given realization, is selected from three possible distributions.

The apparent activation energy and the distribution for the general corrosion rate of Alloy 22 at 60°C are classified as epistemic uncertainties in the TSPA.

The model for general corrosion is applied to each of a large number of patches on each waste package (SAR Section 2.3.6.3.3.1). For a given realization, the patches with the fastest general corrosion rates are those for which the value for R_0 is sampled from the upper tail of the scaled Weibull distribution because the value for C_1 is fixed. Across all realizations, the most rapid general corrosion rates result from the combination of low sampled values for C_1 and high sampled values for R_0; high values for R_0 are more likely to occur in realizations in which the scaled Weibull distribution representing the highest 5% uncertainty partition is selected.

Consequences from radionuclide releases from the repository are quantified (SAR Figure 2.4-154) as estimates of the expected annual dose (where the expectation is over aleatory uncertainty in events that may affect the repository) to the reasonably maximally exposed individual (RMEI). Sensitivity analyses are performed to determine the influence of uncertain parameters on the estimates of expected annual dose. Sensitivity analyses results are summarized in SAR Section 2.4.2.3.3.7 and presented in SAR Figures 2.4-154 and 2.4-155. These results show that uncertainty in apparent activation energy (denoted by *WDGCA22* and also termed temperature dependence coefficient) is among the most influential variables contributing to the uncertainty in estimates of expected annual dose. The scatterplot presented at SAR Figure 2.4-155c indicates that low values of apparent activation energy (denoted by *WDGCA22*) preclude low values of expected annual dose at 500,000 years postclosure; the partial-rank correlation coefficients presented in SAR Figures 2.4-154c indicate that this effect persists between roughly 300,000 and 1,000,000 years postclosure. Thus, the mean and the range of the apparent activation energy are both influential to estimates of consequence.

The base model in the TSPA for the general corrosion of Alloy 22 used a set of general corrosion rates based upon mass loss studies of crevice geometry specimens that had not been properly cleaned (see response to RAI: 3.2.2.1.3.1-2-003). Re-cleaning of the weight-loss geometry specimens that were exposed for 5 years indicates that the general corrosion rates at 60°C (i.e., R_0) are significantly lower than the general corrosion rates used in the base model. Also, from this new data, a new distribution for apparent activation energy was calculated (see response to RAI: 3.2.2.1.3.1-2-003, Section 1.4), which indicated a lower mean apparent activation energy. However, combining the newly derived general corrosion rates with the newly calculated distribution for apparent activation energy, the resulting Alloy 22 general corrosion rates are generally lower across a wide range of temperatures than those predicted by the base model (see response to RAI: 3.2.2.1.3.1-2-003, Figures 10, 11, and 12). Thus, despite the reduction in the mean apparent activation energy, the preliminary results presented in the response to RAI: 3.2.2.1.3.1-2-003, when propagated through the performance assessment, are not expected to result in an increase in expected annual dose.

In summary, this response justifies the DOE selection of the range and mean value of activation energies used within TSPA, and documents that both the mean and the low values of activation energy are important to consequence estimates. Finally the response describes that changes in the mean activation energy as a result of analyses of the re-cleaned 5-year specimens are not expected to result in an increase in expected annual dose.

2. COMMITMENTS TO NRC

None.

3. DESCRIPTION OF PROPOSED LA CHANGE

None.

4. REFERENCES

Dunn, D.S.; Cragnolino, G.A.; Pan, Y.M.; and Tang, L.T. 2004. "Effect of Fabrication Processes on Alloy 22 Corrosion Resistance." *Corrosion/2004, 59th Annual Conference & Exposition, March 28-April 1, 2004, New Orleans*. Paper No. 04698. Houston, Texas: NACE International.

Dunn, D.S.; Pan, Y-M.; and Cragnolino, G.A. 1999. *Effects of Environmental Factors on the Aqueous Corrosion of High-Level Radioactive Waste Containers—Experimental Results and Models*. CNWRA 99-004. San Antonio, Texas: Center for Nuclear Waste Regulatory Analyses.

Dunn, D.S.; Pensado, O.; and Cragnolino, G.A. 2005. "Performance Assessment of Alloy 22 as a Waste Package Outer Barrier." *Corrosion/2005, 60th Annual Conference & Exposition, 1945-2005, April 3-7, 2005, George R. Brown Convention Center, Houston, Texas*. Paper No. 05588. Houston, Texas: NACE International.

Hua, F. and Gordon, G. 2004. "Corrosion Behavior of Alloy 22 and Ti Grade 7 in a Nuclear Waste Repository Environment." *Corrosion, 60,* (8), 764-777. Houston, Texas: NACE International.

Lloyd, A.C.; Shoesmith, D.W.; McIntyre, N.S.; and Noël, J.J. 2003. "Effects of Temperature and Potential on the Passive Corrosion Properties of Alloys C22 and C276." *Journal of the Electrochemical Society, 150,* (4), B120-B130. New York, New York: Electrochemical Society.

Pensado, O.; Dunn, D.S.; Cragnolino, G.A.; and Jain, V. 2002. *Passive Dissolution of Container Materials—Modeling and Experiments*. CNWRA 2003-01. San Antonio, Texas: Center for Nuclear Waste Regulatory Analyses.

Smailos, E. and Köster, R. 1987. "Corrosion Studies on Selected Packaging Materials for Disposal of High Level Wastes." *Materials Reliability in the Back End of the Nuclear Fuel Cycle, Proceedings of a Technical Committee Meeting, Vienna, 2-5 September 1986*. IAEA TECHDOC-421, 7-24. Vienna, Austria: International Atomic Energy Agency.

SNL (Sandia National Laboratories) 2007a. *General Corrosion and Localized Corrosion of Waste Package Outer Barrier*. ANL-EBS-MD-000003 REV 03. Las Vegas, Nevada: Sandia National Laboratories. ACC: DOC.20070730.0003.

SNL 2007b. *Engineered Barrier System: Physical and Chemical Environment*. ANL-EBS-MD-000033 REV 06. Las Vegas, Nevada: Sandia National Laboratories.
ACC: DOC.20070907.0003.

RAI Volume 3, Chapter 2.2.1.3.1, Second Set 2, Number 2:

Provide additional technical basis to show that the range of general corrosion rates extrapolated to low temperatures (e.g., 25 °C) in the current DOE model accounts for published experimental data at this temperature.

Basis: In SAR Section 2.3.6.3.4.2, the Alloy 22 general corrosion rates at 25 °C are extrapolated to be 1.13, 3.04, and 6.50 nm/yr at the 50th, 95th, and 99.99th percentiles, respectively; however, no experimental data are given to support these rates at this temperature. Literature information shows that some measured corrosion rates at ~25 °C are relatively high, ranging from 7 to 137 nm/yr (Dunn, et al., 2005; McMillion, et al., 2005). DOE has not provided a technical basis to assess the significance of these data or explained how the current range of uncertainty in extrapolated general corrosion rates accounts for these data. This requested information is needed to assess the use of these corrosion rates in the performance assessment used to demonstrate compliance with 10 CFR 63.21(c)(15) and 63.114(b).

1. RESPONSE

The extrapolation of the Alloy 22 general corrosion rates to low temperatures, as presented in the response to RAI: 3.2.2.1.3.1-2-003 and supporting analyses, is summarized herein. As demonstrated below, the short-term corrosion studies cited in the basis statement (Dunn et al., 2005; McMillion et al., 2005) are consistent with the DOE-projected Alloy 22 general corrosion rates at 25°C.

1.1 SUMMARY OF GENERAL CORROSION RATES EXTRAPOLATED TO LOW TEMPERATURES

Owing to the extreme corrosion resistance of Alloy 22, low-temperature studies have been generally limited to electrochemical methods such as electrochemical impedance spectroscopy (EIS) or passive current density measurements in relatively aggressive solutions (e.g., ≥ 4 M NaCl) (McMillion et al. 2005; Dunn et al. 2005). Under these environmental conditions, the results of very short-term experiments have reported values up to 137 nm/yr for the general corrosion rate of Alloy 22 at 30°C (McMillion et al. 2005, p. 1,140). Although McMillion et al. (2005) conducted EIS experiments at about 30°C and 60°C, careful review of the report indicates that the general corrosion rate of 137 nm/yr was measured at 60°C, not 30°C (McMillion et al. 2005, Figures 8 to 11). McMillion et al. (2005, Figures 8 to 11 and surrounding text) indicate that the measured current densities at 60°C were 14 and 62 nA/cm^2, which correspond to general corrosion rates of 137 and 608 nm/yr, respectively (McMillion et al. 2005, Table I). McMillion et al. (2005) conducted their EIS measurements in a carefully deaerated 4 M sodium chloride solution buffered to a pH of 6 using a sodium acetate/acetic acid buffer. The EIS measurements were obtained under polarized conditions (−200 mV vs. Ag/AgCl at 30°C and −250 mV vs. Ag/AgCl at 60°C). These exposure conditions are not relevant to the repository since repository exposure conditions will be oxic as compared to the anoxic test conditions, and the waste packages will not be externally polarized.

The McMillion et al. (2005) experiments were run for up to a maximum of 352 hours, which is approximately 15 days or 0.04 years. Short-term Alloy 22 general corrosion rates at 90°C are reported in *General Corrosion and Localized Corrosion of Waste Package Outer Barrier* (SNL 2007, Table 7-1). After an exposure time of one day, Alloy 22 general corrosion rates of 460 nm/yr and 1,250 nm/yr are reported for simulated acidified water (SAW) and simulated concentrated water (SCW) aqueous environments respectively. Alloy 22 general corrosion rates of 100 and 182 nm/yr are reported after seven and 56 days of exposure, respectively. As shown in the response to RAI: 3.2.2.1.3.1-2-003 (Figure 3), the measured Alloy 22 general corrosion rate after five years of exposure at 90°C can be as high as 14 nm/yr. Overall, these results show that the Alloy 22 general corrosion rate decreases markedly with time (e.g., by about 100× from one day to five years). If the 137 nm/yr Alloy 22 general corrosion rate reported by McMillion et al. (2005) was to decrease by one order of magnitude, at an exposure time of five years it would be within the variation of the Alloy 22 general corrosion model at 60°C and even at 25°C (response to RAI: 3.2.2.1.3.1-2-003, Figures 8 and 10). Therefore, the Alloy 22 general corrosion rates reported by McMillion et al. (2005) are consistent with the DOE-projected Alloy 22 general corrosion rates at 60°C and 25°C.

The foregoing discussion is also applicable to the lower Alloy 22 general corrosion rates reported by Dunn et al. (2005) at 25°C. Thus, the DOE-projected Alloy 22 general corrosion rates are consistent with the very short-term values referred to in the RAI Basis.

1.2 SUMMARY OF IMPLEMENTATION OF THE ALLOY 22 GENERAL CORROSION MODEL

Waste package general corrosion is modeled by sampling Alloy 22 general corrosion rates for about 1,400 patches (sub areas) per modeled waste package (SAR Section 2.4.2.3.2.1.5). Although the general corrosion rate for Alloy 22 is expected to decrease with exposure time (SNL 2007, Section 7.2.1), the Alloy 22 general corrosion rate model used by the total system performance assessment (TSPA) conservatively assumes that the Alloy 22 general corrosion rate remains constant with time for a given temperature (SNL 2007, Assumption 5.2). This assumption is conservative because the general corrosion rate of metals and alloys tends to decrease with time (SNL 2007, Section 7.2.1).

Although the Alloy 22 general corrosion rate for the 60°C experimental results reported by McMillion et al. (2005) extrapolated to longer times is within the variation of the Alloy 22 general corrosion model at 60°C and even 25°C (response to RAI: 3.2.2.1.3.1-2-003 Figure 10), it corresponds to a general corrosion rate which would be around the 95th percentile of the cumulative probability distribution at 25°C. However, as discussed in response to RAI: 3.2.2.1.1-004, a relatively small fraction of the waste package surface needs to be breached by general corrosion to allow all of the drift seepage to enter the waste package; for example, when 4% of the waste package surface (about 56 patches) is penetrated by general corrosion, the fraction of seepage that flows through a commercial spent nuclear fuel waste package ranges from 0 to 1.0, with a median fraction of seepage of 0.92 flowing through the waste package. Similar results are obtained for codisposal waste packages. These results indicate that the upper 4% of the measured general corrosion rates will determine the fraction of seepage that can enter the waste packages. For diffusive releases, as indicated by the analysis of the effect of seismic

damaged area fraction on the annual dose at 10,000 years presented in *Total System Performance Assessment Model/Analysis for the License Application* (SNL 2008, Figure 7.3.2-12), beyond a waste package damage fraction of about 10^{-5}, annual dose does not increase significantly with increasing waste package damage fraction. Given that the consequences of seismic ground motion events are approximated by examining only damaged waste packages under intact drip shields (SAR Section 7.3.2.6.1.3), where only diffusive releases can occur, the effect of seismic damaged area fraction on annual dose at 10,000 years indicates that diffusive releases are insensitive to increases in failed patch area fractions above 10^{-5} (much less than one failed patch). Therefore, although the Alloy 22 general corrosion model predicts a range of general corrosion rates, some of which are low, the general corrosion rates at the high end of the distribution are most relevant to assessment of performance.

As demonstrated above, the short-term corrosion studies reported by Dunn et al. (2005) and McMillion et al. (2005) are consistent with the DOE-projected range of Alloy 22 general corrosion rates at low temperatures.

2. COMMITMENTS TO NRC

None.

3. DESCRIPTION OF PROPOSED LA CHANGE

None.

4. REFERENCES

Dunn, D.S.; Pensado, O.; Pan, Y.-M.; Pabalan, R.T.; Yang, L.; He, X.; and Chiang, K.T. 2005. *Passive and Localized Corrosion of Alloy 22 - Modeling and Experiments.* CNWRA 2005-02. REV 01. San Antonio, Texas: Center for Nuclear Waste Regulatory Analyses.

McMillion, L.G., Sun, A.; Macdonald, D.D. and Jones, D.A. 2005. "General Corrosion of Alloy 22: Experimental Determination of Model Parameters from Electrochemical Impedance Spectroscopy Data." *Metallurgical and Materials Transactions A. 36A*, 1129–1141.

SNL (Sandia National Laboratories) 2007. *General Corrosion and Localized Corrosion of Waste Package Outer Barrier.* ANL-EBS-MS-000003 REV 03. Sandia National Laboratories. ACC: DOC.20070730.0003.

SNL 2008. *Total System Performance Assessment Model /Analysis for the License Application.* MDL-WIS-PA-000005 REV 00 AD 01. Las Vegas, Nevada: Sandia National Laboratories. ACC: DOC.20080312.0001.

RAI: Volume 3, Chapter 2.2.1.3.1, Second Set, Number 3:

1. Assess the effects of apparent experimental errors for the 5-year weight loss data for Alloy 22 (SNL, 2008b, 2008c) on the uncertainties in associated corrosion rates used to develop the general corrosion model.

2. Assess how the post-test specimen cleaning operations used for the 5-year weight loss Alloy 22 experiments are equivalent to the cleaning procedures given in ASTM G1-90, specifically with regard to the use of uncorroded control specimens and the uncertainty in the weight-loss data resulting from repetitive cleaning cycles.

Basis: DOE uses data from 5-year experiments to develop the general corrosion model (SAR Section 2.3.6.3.4.2). Information from SNL (2008b, Section 3.4; 2008c) indicates there may be unquantified experimental uncertainties on the corrosion rates derived from the 5-year Alloy 22 weight loss experiments due to incomplete cleaning and sample preparation errors. Proper sample preparations and complete cleaning of the 5-year coupons could result in larger weight loss, generating higher general corrosion rates than are currently used for the general corrosion model. DOE has not quantified explicitly the effects of these experimental uncertainties nor assessed how these uncertainties could affect Alloy 22 general corrosion rates. This requested information is needed to assess the use of the Alloy 22 general corrosion rates in the performance assessment used to demonstrate compliance with 10 CFR 63.21(c)(15) and 63.114(b).

1. RESPONSE

Alloy 22 crevice and weight-loss specimens were immersed for five years in the DOE Long-Term Corrosion Test Facility (LTCTF). After immersion, the specimens were removed, cleaned, and analyzed. The measured weight-loss of the crevice specimens was used to determine a distribution of general corrosion rates, which, in turn, was used to represent the general corrosion rate of the Alloy 22 waste package outer corrosion barrier at 60°C. It was subsequently determined that the initial specimen cleaning was unsatisfactory because unexposed specimens cleaned according to the same procedures experienced weight loss of the same order of magnitude as specimens exposed for five years. The LTCTF specimens are in the process of being re-cleaned and reanalyzed. The results presented within this RAI response are based on preliminary re-analyses that are not expected to change upon finalization.

Experimental artifacts on the crevice specimens (e.g., mill-annealed oxides and surface contamination, which were not present on the weight-loss specimens) led to the calculation of an artificially high Alloy 22 general corrosion rate. The initial evaluation of the weight-loss specimens indicates that the general corrosion rate of Alloy 22 at 60°C and 90°C is much lower than the general corrosion rates used in the license application, which were based on the initial cleaning of the crevice specimens. In addition, an evaluation of the temperature dependence of the re-cleaned weight-loss specimens is presented herein. Although the newly-derived apparent activation energy for Alloy 22 general corrosion is lower than that used in the license

application, combining the newly-derived general corrosion rates and apparent activation energy, results in predicted Alloy 22 general corrosion rates that are generally lower across a wide range of temperatures than those used in the license application.

1.1 CREVICE SPECIMENS

The surface roughness of the weight-loss specimens was specified to be RMS32 (approximately 150 grit). Inspection of the weight-loss specimens upon removal from the LTCTF revealed that they have a unidirectional surface finish approximately equal to a 600-grit wet finish. The surface roughness of the back side of the crevice specimens was specified to be RMS32, but the front side roughness was specified to be RMS16 (approximately 240 grit). The back side of the crevice specimens had a surface finish that is not characteristic of paper grinding. Inspection of the front surfaces of the crevice specimens upon removal from the LTCTF revealed that they have a unidirectional surface finish approximately equal to a 600-grit wet finish. However, the crevice specimens were tested without removing the mill-annealed oxide coating from the unpolished back sides of the specimens at the time of their immersion into the test electrolytes.

An analysis of the effect of the re-cleaning process on weight-loss and crevice control specimens (specimens that were never exposed to the test solutions) indicates that the mill-annealed oxide coating on the back side of the crevice specimens is at least partially removed by the cleaning process. Additionally, there is evidence of surface contamination (a matrix of Fe and O with particles rich in Si and O distributed throughout them) on some of the as-received crevice specimens, which could also be totally or partially removed during cleaning. This surface contamination was not present on the as-received weight-loss specimens. Unlike the mill-annealed oxide, which was present only on the back side of the crevice specimens, the surface contamination was found on both the front and back sides of the crevice specimens including under the crevice formers. Thus, the initial weight of the crevice specimens was artificially high (due to the presence of mill-annealed oxide and surface contamination). Because there was at least partial removal of the mill-annealed oxide and surface contamination during specimen cleaning, this led to artificially high measured weight loss and calculated corrosion rates for the crevice specimens. Therefore, the weight-loss data from the crevice specimens provide a conservative estimate for the general corrosion rate of the Alloy 22 waste package outer corrosion barrier in the repository. Because there is no evidence of contamination or the presence of a mill-annealed oxide film on the as-received weight-loss specimens, the most accurate estimate available for the extent of corrosion of specimens exposed in the LTCTF is derived from the data for the re-cleaned five-year weight-loss specimens.

1.2 SPECIMEN RE-CLEANING

The initial cleaning of the five-year exposed Alloy 22 specimens used solutions recommended in ASTM G 1-90, *Standard Practice for Preparing, Cleaning, and Evaluating Corrosion Test Specimens*. However, the cleaning procedure did not include the recommendation in ASTM G 1-90 (1999, Figure 1) to graph mass loss as a function of cleaning cycle. Such a graph can assist in determining when the specimens are sufficiently cleaned such that additional cleaning cycles would result in loss of the base metal. The initial cleaning discussed above was determined to be unsatisfactory after a series of scoping tests, in which unexposed Alloy 22

control samples were cleaned, resulting in higher than anticipated weight losses. The weight loss experienced by the control samples was of the same magnitude or greater than many of the weight loss values reported for specimens exposed for five years. For this reason, the exposed specimens are presently being re-cleaned and analyzed again. Re-cleaning is being accomplished in a manner consistent with ASTM G 1-03, *Standard Practice for Preparing, Cleaning, and Evaluating Corrosion Test Specimens*. In particular, the specimens were:

(1) Immersed in an acetone solution under the swirling action of a magnetic stirrer for two minutes. Each specimen was canted to maximize the area being cleaned. The specimens were rinsed in flowing deionized water for at least 30 seconds followed by blow drying with filtered dry nitrogen.

(2) Then immersed in a cleaning solution (prepared by diluting 150 mL of HCl [12.1 N, 1.19 g/cm^3] with deionized water to make 1,000 mL of solution) for three minutes at ambient temperature (between 20°C and 25°C) under the swirling action of a magnetic stirrer. Each specimen was canted to maximize the area being cleaned. The specimens were then rinsed in flowing deionized water for two minutes, blow dried with filtered dry nitrogen, and dried for 15 minutes in a recirculating hot air dryer (between 90°C and 105°C). Specimens were then cooled in an inert nitrogen cabinet at ambient temperature for at least one hour.

During re-cleaning, all specimens were subjected to the process steps outlined in (1) only once, followed by several cycles (typically three or more) of the process steps outlined in (2), until the cycle-to-cycle weight loss of the test specimens was less than the uncertainty in the mass measurements or indistinguishable from the weight loss of unexposed control specimens. After re-cleaning, selected specimens were subjected to ultrasonication in deionized water to evaluate whether further cleaning was accomplished by this method. A typical cleaning curve (weight change per cleaning cycle versus cleaning cycle) obtained during the re-cleaning process is shown in Figure 1. In Figure 1, "Initial Clean" refers to the total weight change of the specimens after the initial cleaning discussed in the first paragraph of this section and the process steps outlined in (1) above. The cleaning curve is equivalent to that shown in Figure 1 of ASTM G 1-03, which is in terms of cumulative mass loss (weight change) versus cleaning cycle.

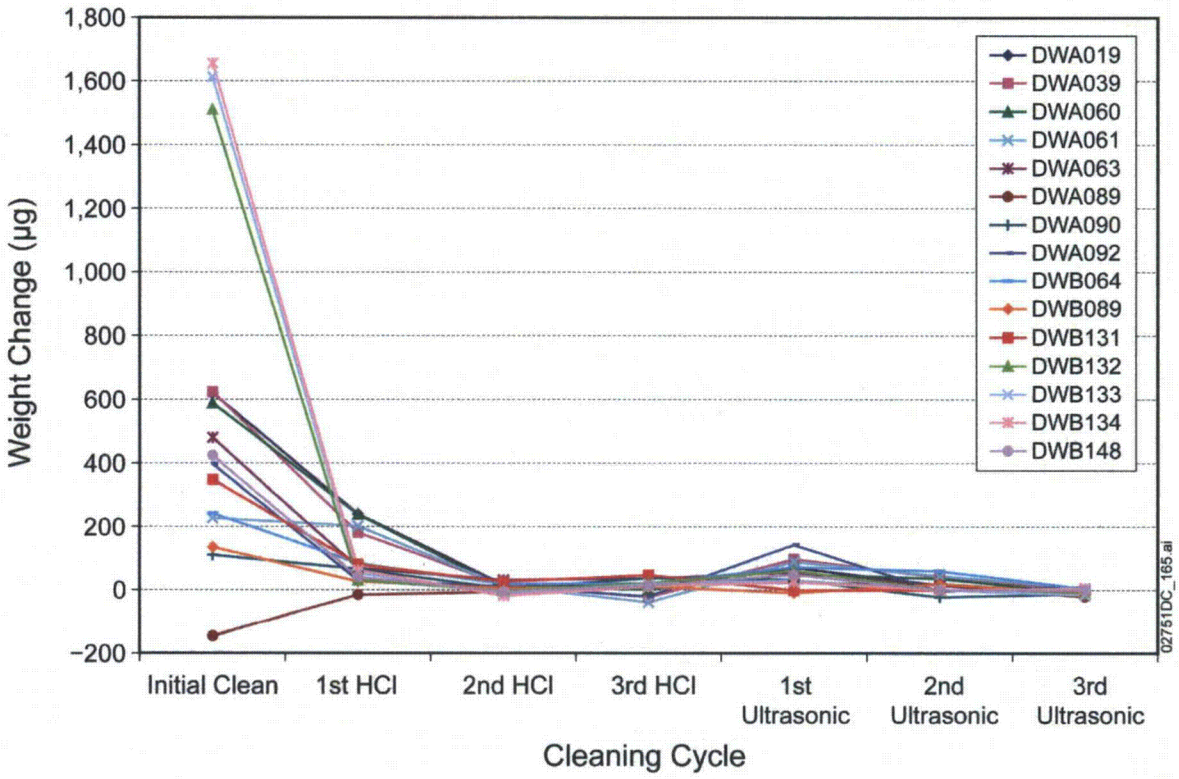

Figure 1. Typical Cleaning Curve Showing Weight Loss Resulting from Repeated Cleaning Cycles

Figure 1 indicates that the majority of the weight loss due to re-cleaning occurred during the "Initial Clean." Subsequent HCl cleaning cycles resulted in very little weight loss and the deionized water ultrasonic cleaning cycles had a minimal effect on the total weight loss. Therefore, deionized water ultrasonic cleaning cycles were not applied to all specimens. In addition to ultrasonic cleaning in deionized water, the effects of ultrasonic cleaning in a 10% by volume Brulin 815 GD solution (an alkaline industrial cleaning solution) in a water solvent were investigated for selected specimens. As shown in Figure 2, Brulin cleaning cycles did not result in significant weight loss as compared to the "Initial Clean." Therefore, Brulin cleaning cycles were not applied to all specimens.

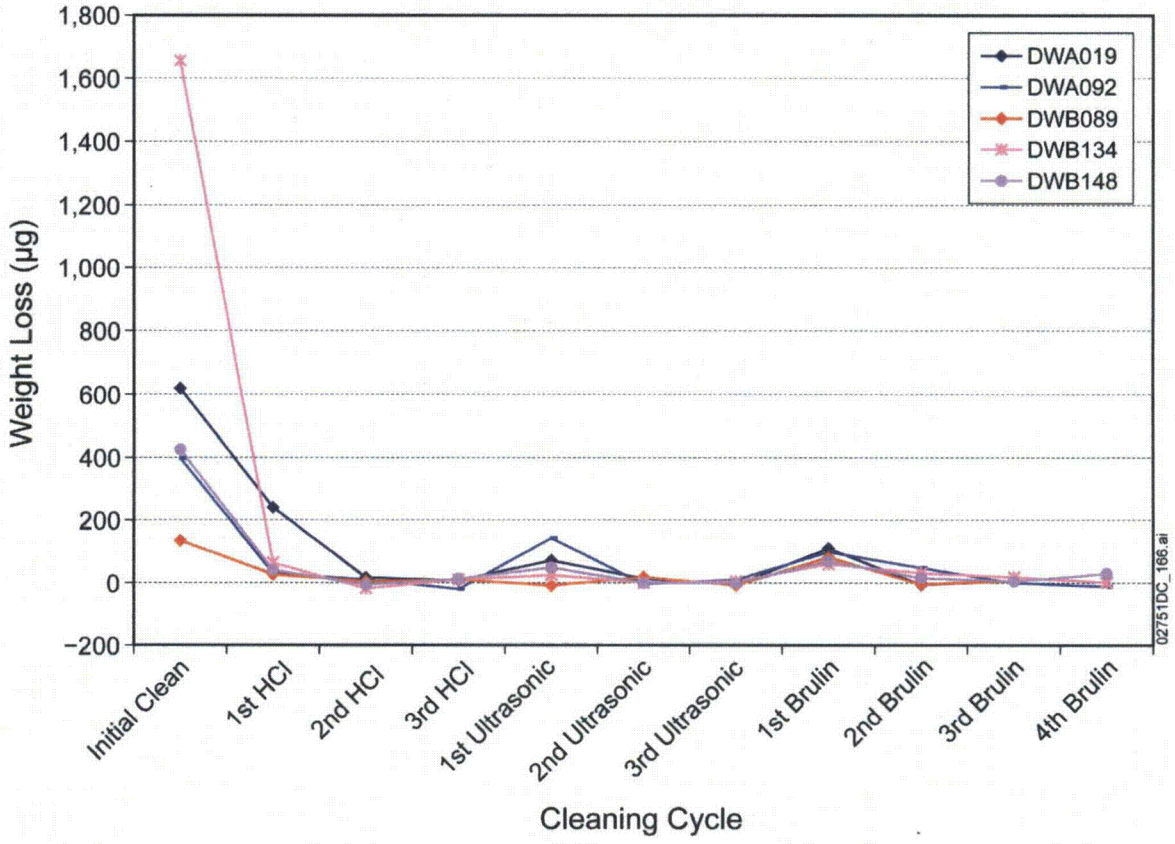

Figure 2. Typical Cleaning Curve Showing Weight Loss Resulting from Repeated Cleaning Cycles

1.3 WEIGHT-LOSS SPECIMEN DATA ANALYSIS

The formula used to calculate the general corrosion rate from weight-loss specimens is shown in Equation 1 (ASTM G 1-03, Section 8):

$$Corrosion\ Rate = \frac{8.76 \times 10^{10} \cdot \Delta w}{\rho \cdot A \cdot t} \qquad \text{(Eq. 1)}$$

where 8.76×10^{10} is a proportionality constant (nm × cm^{-1} × hr × yr^{-1}), Δw is the weight loss in grams after more than five years, ρ is the density of Alloy 22 (8.69 g/cm^3), A is the exposed surface area of each specimen (cm^2), and t is the exposure time (hours).

Figure 3 summarizes the calculated corrosion rates for the Alloy 22 weight-loss specimens exposed to the simulated acidified water (SAW), simulated concentrated water (SCW), and simulated dilute water (SDW) solutions at 60°C and 90°C for over five years. Specimens were either immersed in solution, exposed in the vapor above the test solution, or located at the waterline. As can be seen in Figure 3, the highest corrosion rates were observed in SCW liquid at 90°C. The remainder of the calculated corrosion rates are not significantly different from each

other. Figure 4 shows the average corrosion rates (plotted as filled squares) and 1.96 standard deviation (5 to 95 percentile ranges) (calculated based on the use of a normal distribution) for each exposure condition. Also plotted (as open squares) are the corrosion rates of the specimens exposed at the waterline. The waterline specimens (with the exception of those in SCW solution at 90°C) appear to behave similarly to specimens exposed in the liquid phase. Because there were no significant differences between mill-annealed and as-welded general corrosion rates (Figure 5), the calculated general corrosion rates of these specimens were combined in Figures 3 and 4.

The non-negative corrosion rates for the weight-loss specimens ranged from about 1.0 to 14 nm/yr (Figure 3), with the lowest mean rates generally observed for the specimens in the SDW solution (Figure 4). For the weight-loss specimens, the corrosion rates were generally lower for specimens exposed to vapor than for those immersed in liquid, regardless of the test temperature or electrolyte solution. Overall, the specimens immersed in the SCW solution at 90°C exhibited higher corrosion rates.

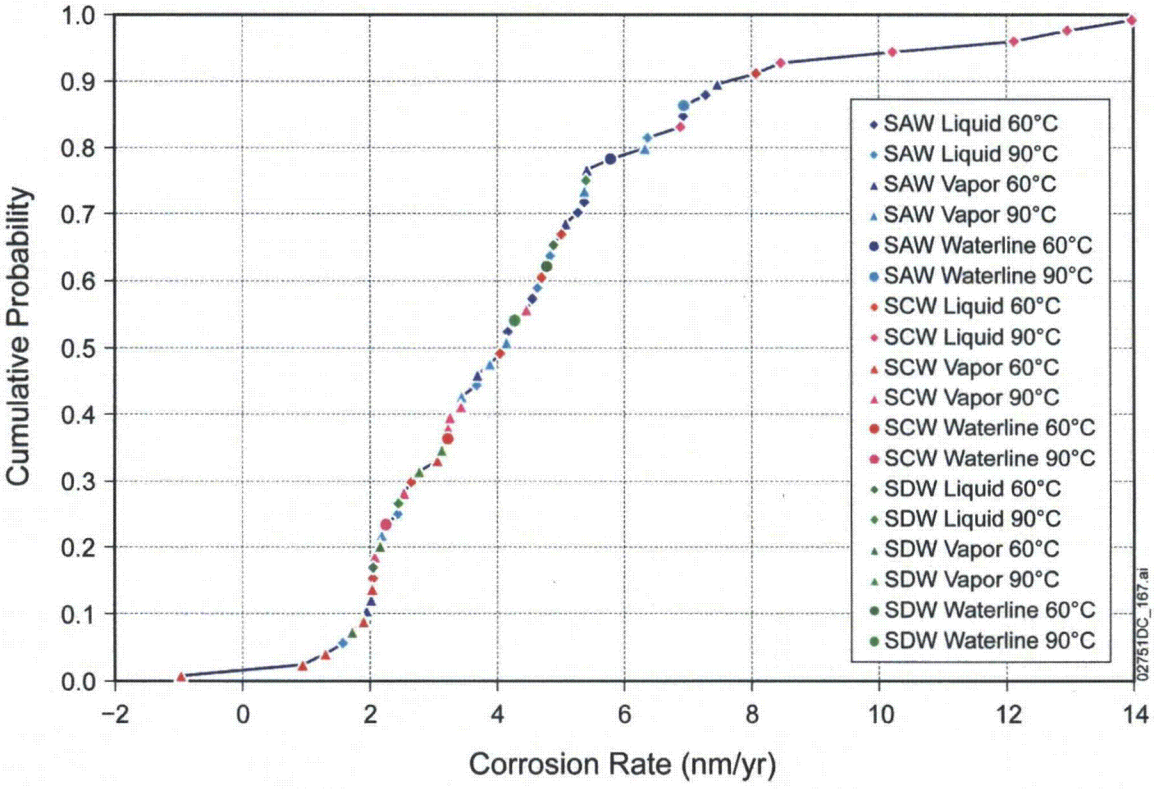

Figure 3. Corrosion Rates for Alloy 22 Weight-Loss Specimens in SAW, SCW, and SDW

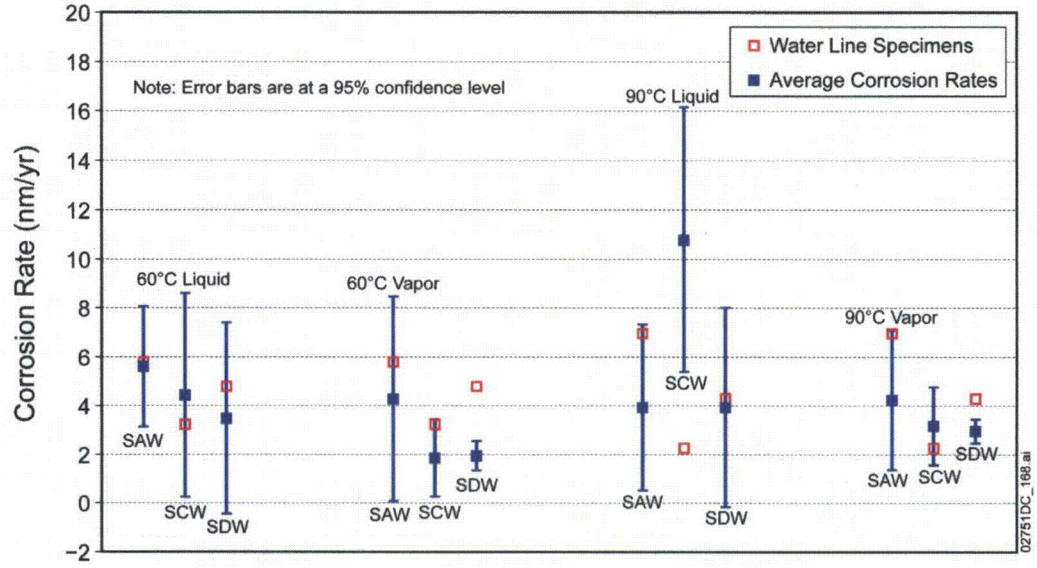

Figure 4. Corrosion Rates for Alloy 22 Weight-Loss Specimens in SAW, SCW, and SDW

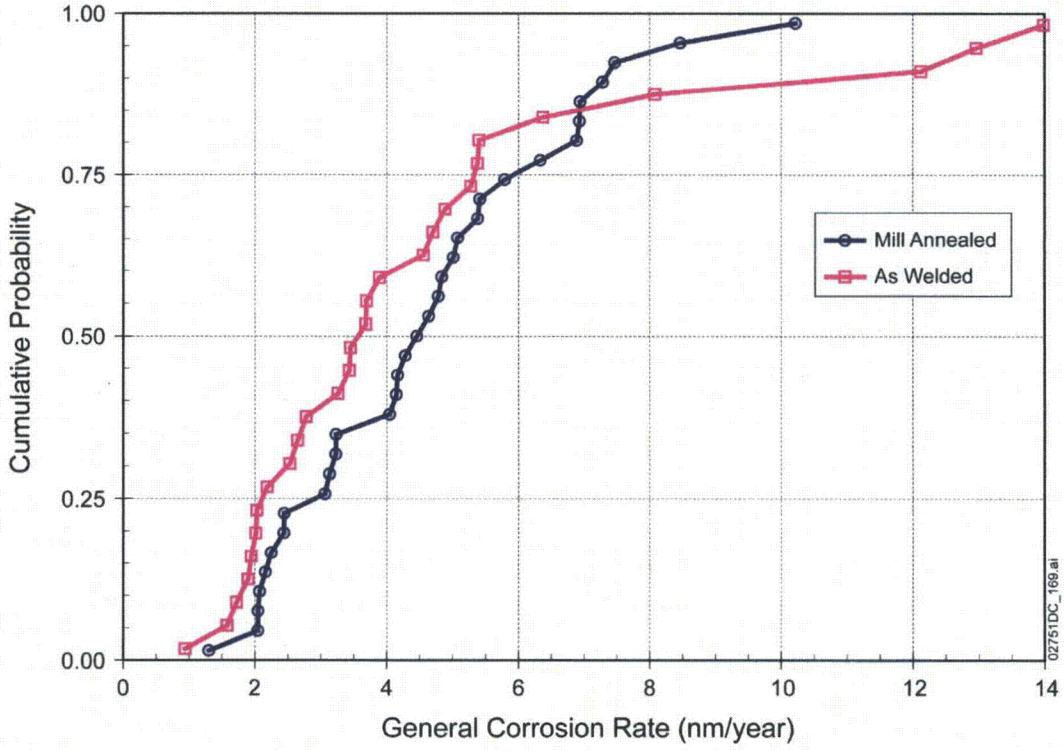

Figure 5. Empirical Cumulative Distribution Functions for General Corrosion Rate of Mill-Annealed and As-Welded Alloy 22 Weight-Loss Samples after Five-Year Exposure in the Aqueous and Vapor Phases of SAW, SCW, and SDW in the LTCTF

In general, for corrosion processes, the corrosion rate increases with increases in temperature. However, because the determined general corrosion rates were very low and within the uncertainty range of the measurement technique, a clear dependence on the temperature could not be established for these data (Figure 6), with the exception of the results from weight-loss specimens immersed in the SCW solution. As shown in Figure 3, the upper tail of the 90°C cumulative distribution function is determined by specimens exposed to SCW liquid phase. The temperature dependence of Alloy 22 general corrosion rates of weight-loss specimens immersed in the SCW solution is evaluated in Section 1.4.

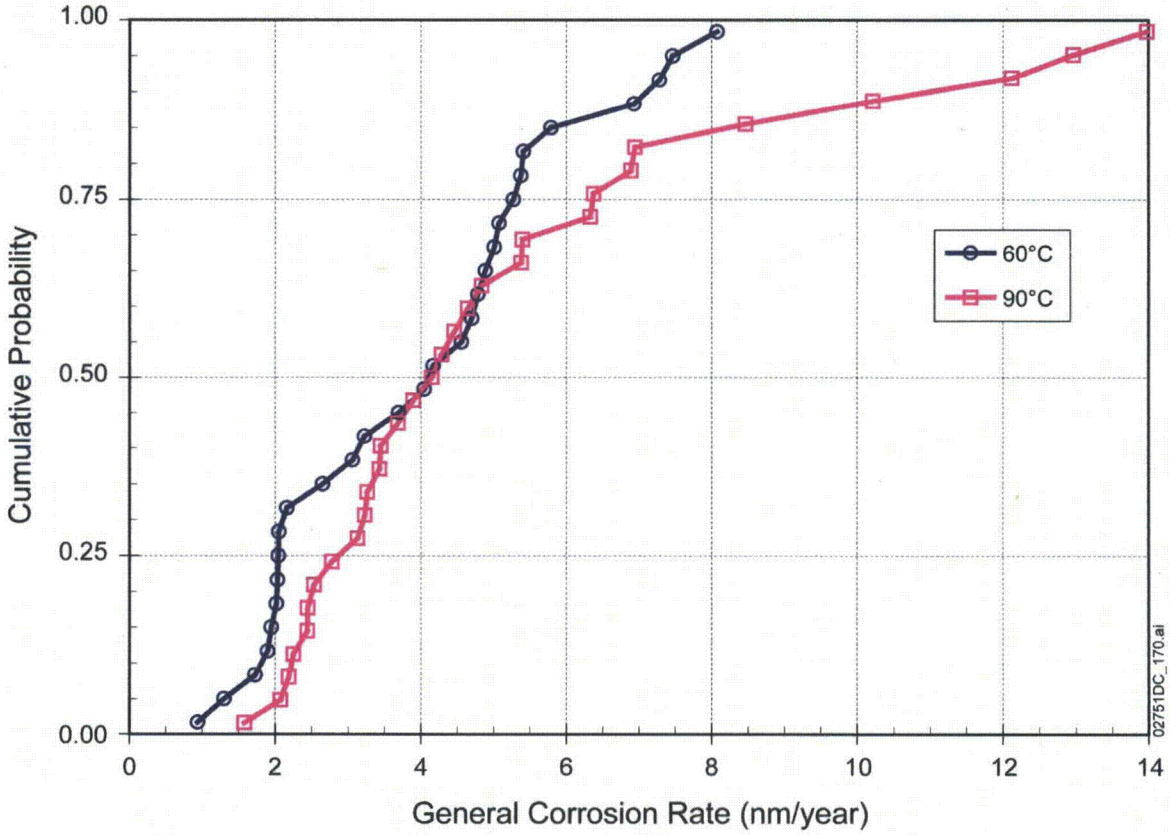

Figure 6. Empirical Cumulative Distribution Functions for General Corrosion Rate of Alloy 22 Weight-Loss Specimens at 60°C and 90°C after Five-Year Exposure in the Aqueous and Vapor Phases of SAW, SCW, and SDW in the LTCTF

Figure 7 illustrates that exposure conditions (i.e., solution composition and temperature) had little effect on the calculated corrosion rates, with the exception of those for SCW liquid phase at 90°C.

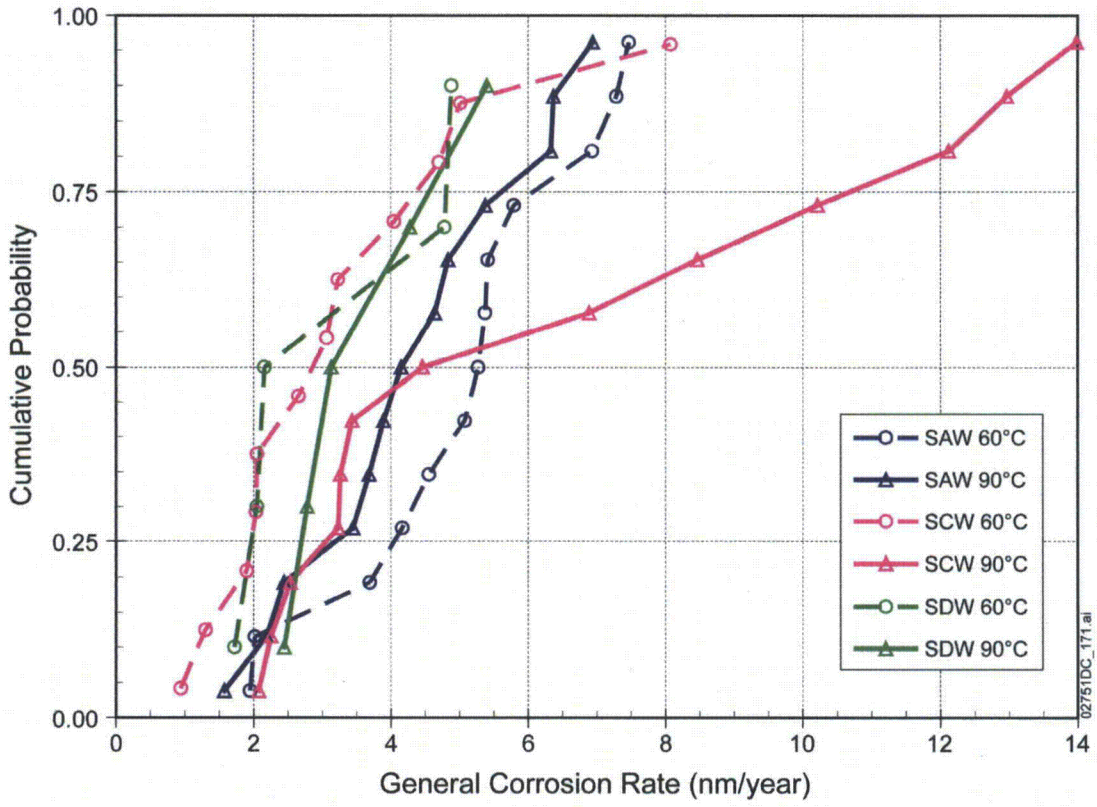

Figure 7. Empirical Cumulative Distribution Functions for General Corrosion Rate of Alloy 22 Weight-Loss Samples Tested in Three Different Solution Types at 60°C and 90°C after Five-Year Exposure in the LTCTF

1.3.1 Weight-Loss Specimen Data Uncertainty Analysis

The dominant source of uncertainty in the calculated general corrosion rates is due to uncertainty in the measurement of weight loss. In what follows, this uncertainty is evaluated in this section, and the general corrosion rates of Alloy 22 calculated from the re-cleaned five-year weight-loss specimen measurements are compared to the Alloy 22 general corrosion model developed in *General Corrosion and Localized Corrosion of Waste Package Outer Barrier* (SNL 2007, Section 6.4.3).

1.3.1.1 Uncertainty in General Corrosion Rates Calculated from the Re-cleaned Five-Year Weight Loss Specimens

Following the approach in *General Corrosion and Localized Corrosion of Waste Package Outer Barrier* (SNL 2007, Section 6.4.3.3.1), the combined uncertainty of a measurement result y, designated by Δy, is given by Equation 2:

$$\Delta y = \sqrt{\sum_{i=1}^{N}\left(\frac{\partial f}{\partial x_i}\right)^2 \Delta x_i^2 + 2\sum_{i=1}^{N-1}\sum_{j=i+1}^{N}\frac{\partial f}{\partial x_i}\frac{\partial f}{\partial x_j}\Delta x_i x_j} \qquad \text{(Eq. 2)}$$

In Equation 2, the partial derivatives $\frac{\partial f}{\partial x_i}$ are the sensitivity coefficients, Δx_i is the standard uncertainty associated with the input estimate x_i, and $\Delta x_i x_j$ is the estimated covariance associated with x_i and x_j. Referring to Equation 1, and letting y be the five-year general corrosion rate, the combined uncertainty of y is estimated by Equation 3:

$$\Delta y = \sqrt{\left(\frac{\partial y}{\partial w}\right)^2 \Delta w^2 + \left(\frac{\partial y}{\partial \rho}\right)^2 \Delta \rho^2 + \left(\frac{\partial y}{\partial t}\right)^2 \Delta t^2 + \left(\frac{\partial y}{\partial a}\right)^2 \Delta a^2 + \left(\frac{\partial y}{\partial b}\right)^2 \Delta b^2 + \left(\frac{\partial y}{\partial c}\right)^2 \Delta c^2 + \left(\frac{\partial y}{\partial d}\right)^2 \Delta d^2} \qquad \text{(Eq. 3)}$$

where t is the time of exposure in hours; w is the total weight loss, in grams, during the time, t; ρ is the density in grams per cubic centimeter; a, b, and c are specimen external dimensions; and d is the diameter of the hole in the specimen (used for mounting). w, ρ, t, a, b, c, and d are considered independent; hence, the covariance terms in Equation 2 disappear. Values used for the parameters of interest are listed in Table 1.

Table 1. Values Used for Measurement Uncertainty Analysis of General Corrosion Rates Based upon Weight-Loss Specimen Measurements after Five-Year Exposure

Parameter	Units	Weight-Loss Specimens
w	g	6.21×10^{-4}
ρ	g/cm^3	8.69
t	hour	43,800
a	cm	5.08
b	cm	2.54
c	cm	0.3175
d	cm	0.7925
Δw	g	3.29×10^{-4}
$\Delta \rho$	g/cm^3	0.1
Δt	hour	24
Δa	cm	0.00254
Δb	cm	0.00254
Δc	cm	0.00254
Δd	cm	0.00254

Weight measurement is expected to be the main source of uncertainty due to the extremely low corrosion rates of the alloy in the test media. The uncertainty in the initial weight was evaluated by obtaining balance accuracy information typical of the balance used and estimating the accuracy of the balance readings. The accuracy for the balance was estimated to be 0.001% of the balance reading plus 0.2 mg. The upper and lower bounds of this uniform distribution are about 0.5 mg and −0.5 mg, respectively. Several measurements of final weight were made for each specimen and the uncertainty in the final weight was represented by a normal distribution with a different standard deviation for each specimen. The standard deviation for each specimen varies between about 9 μg and 20 μg. To evaluate the total uncertainty, 50,000 realizations of the initial and final weight measurement uncertainties were generated, from which the standard uncertainty of the uncertainty in the weight-loss measurement (Δw) can be estimated to be about 0.329 mg (Table 1).

The combined standard uncertainty in the corrosion rate was estimated with Equation 3 using the expected values of the input variables and their estimated standard uncertainties in Table 1. The combined standard uncertainty is estimated to be approximately 2.49 nm/yr (Table 2) for the weight-loss specimens. This estimate corresponds to one standard deviation. Therefore, using one standard deviation, about 54% (2.49/4.58) of the variation in the measured general corrosion rate is due to measurement uncertainty and about 46% of the variation is from the variations of the general corrosion rate among the specimens. Using two standard deviations, all of the variation in the calculated general corrosion rate is due to measurement uncertainty. However, it is reasonable to suppose that any measurement over three standard deviations (i.e., about 7.5 nm/yr), such as those in SCW liquid at 90°C, is significant. Thus, the data supports the modeling assumption that there is some chemical dependence (variability) in the obtained general corrosion rates. In addition, although the primary contributor to uncertainty in the general corrosion rates is due to the weight-loss uncertainty, which is dominated by the uniformly distributed initial weight uncertainty, the distribution of general corrosion rates based on the re-cleaned weight-loss data is not uniformly distributed (Figure 3) even if the data from specimens immersed in SCW at 90°C were not considered. This indicates that there is variability within the re-cleaned weight-loss specimen data set.

Table 2. Summary of Measurement Uncertainty Analysis for Corrosion Rates Based on Weight-Loss Measurements after Five-Year Exposure in the LTCTF

Specimen Configuration	Combined Standard Uncertainty in General Corrosion Rate (nm/yr)	Mean General Corrosion Rate (nm/yr)	Standard Deviation of General Corrosion Rate (nm/yr)
Weight-Loss	2.49	4.58	2.76

It is also reasonable to expect that there will be variability in the general corrosion rates of the waste packages in the repository at the waste package-surface level. Sources of variability would include variations in material properties (e.g., composition and metallurgical condition of the base material and the passive film formed) and in chemical exposure conditions (e.g., dripping water contact versus non-dripping water contact and the chemistry of the dripping

water and/or variations in dust compositions on the waste package surface), as well as local temperature variations across the waste package surface.

Furthermore, the use of variability is expected to be conservative with respect to assessment of waste package outer barrier performance. This can be seen by considering the barrier capability of a waste package breached by general corrosion to divert seepage water. As discussed in the response to RAI: 3.2.2.1.1-004, a relatively small fraction of the waste package surface needs to be breached by general corrosion to allow, when modeled, all of the drift seepage to enter the waste package; for example, if the drip shield is no longer functioning, when 4% of the waste package surface is penetrated by general corrosion, the fraction of seepage that flows through a commercial spent nuclear fuel waste package is modeled to range from 0 to 1.0, with a median fraction of seepage of 0.92 flowing through the waste package. Similar results are obtained for codisposal waste packages. These results indicate that the upper range of the measured general corrosion rates will determine the fraction of seepage that can enter the waste packages. As can be seen in Figure 3, the upper range of the measured general corrosion rates is defined by the measurements obtained for specimens immersed in the SCW solution at 90°C. The assignment of the variation in general corrosion rate to variability is conservative in that waste package general corrosion is modeled by independently and randomly sampling the general corrosion rate distribution for about 1,400 patches (sub areas) per modeled waste package, resulting in the expected assignment of a very high general corrosion rate (equivalent to the 99.9th percentile value) to at least one patch on each waste package (SAR Section 2.4.2.3.2.1.5).

1.3.2 Comparison of Re-cleaned Weight-Loss Data to Alloy 22 General Corrosion Model

The Alloy 22 general corrosion model (i.e., the base model) makes use of three distributions corresponding to low, medium, and high levels of uncertainty (SAR Section 2.3.6.3.3.1). The scale and shape parameters for these three distributions at 60°C are shown in Table 3.

Table 3. Scale and Shape Parameters Used for the Weibull Distributions That Represent the Alloy 22 General Corrosion Rate at 60°C

Uncertainty Level	Scale Parameter, *b* (nm/yr)	Shape Parameter, *c* (no units)
Low	6.628	1.380
Medium	8.134	1.476
High	9.774	1.578

Source: SAR Section 2.3.6.3.3.1.

Figure 8 shows a comparison between the base model Alloy 22 general corrosion rate distributions at 60°C (Table 3) and the Alloy 22 general corrosion rates obtained from the re-cleaned weight-loss data (i.e., the updated model). Horizontal error bars corresponding to ±2.5 nm/yr (i.e., the measurement uncertainty in the updated model from Table 2) are also plotted along with the general corrosion rates obtained from the weight-loss specimens. In considering the horizontal error bars, it should be realized that the measurement uncertainty is unbiased (i.e., the measured weight loss is equally likely to be higher or lower than the "true" weight loss). Therefore, it is not reasonable to postulate that every general corrosion rate would be higher than that calculated from the measured value based on measurement uncertainty. For

example, if the true weight loss of the specimen at the 75th percentile were lower than the measured value and the true weight loss of the specimen at the 25th percentile were higher than the measured value, these specimens might simply change places in the cumulative distribution function, leaving its general shape unchanged. As can be seen in Figure 8, the general corrosion rates of the updated model can be higher than the base model at low cumulative probabilities. However, as discussed in Section 1.3.1.1, only the general corrosion rates at the upper end of the Alloy 22 general corrosion rate cumulative distribution (e.g., the general corrosion rates with cumulative probabilities above 0.96) are important in determining waste package performance. At these higher cumulative probabilities, the general corrosion rates predicted by the base model are significantly higher than those predicted using the re-cleaned weight-loss data. Therefore, use of the Alloy 22 general corrosion base model is not expected to underestimate repository performance (see response to RAI: 3.2.2.1.3.1-2-001).

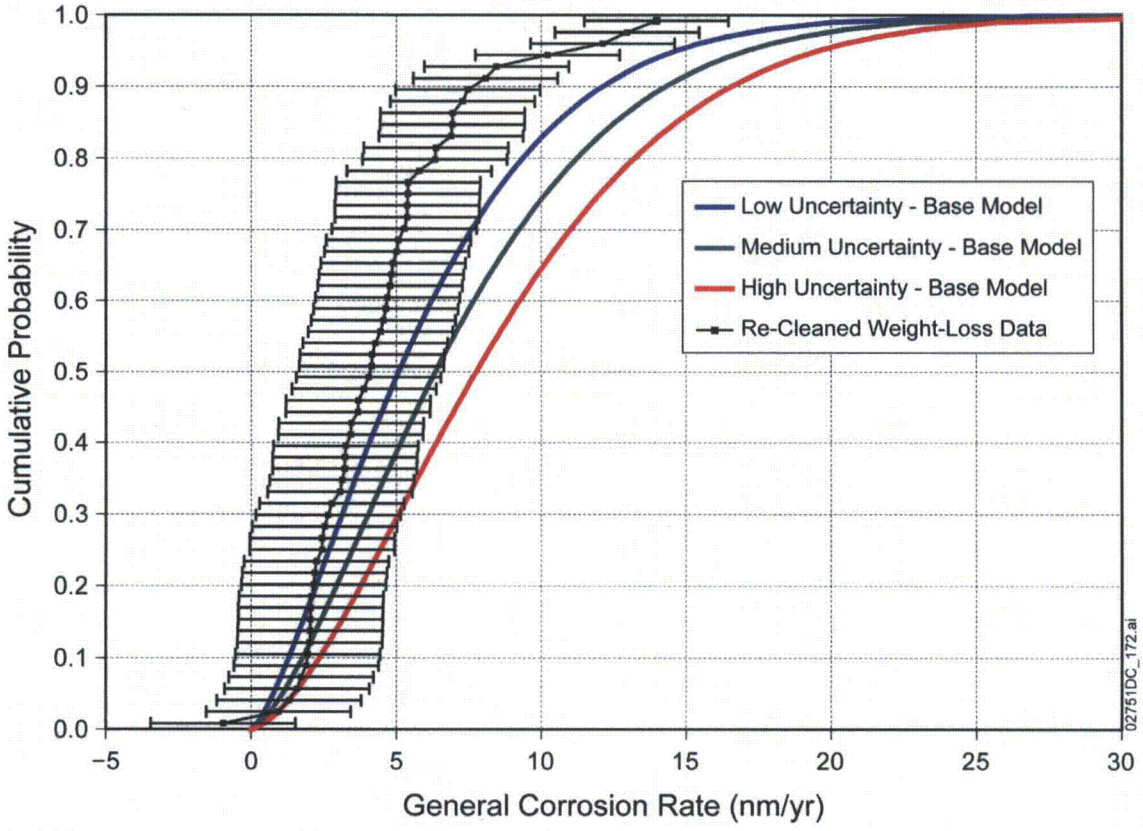

Figure 8. Empirical Cumulative Distribution for General Corrosion Rate of Alloy 22 Weight-Loss Specimens Tested in Three Different Solutions at 60°C and 90°C after Five-Year Exposure (re-cleaned weight-loss data) with Error Bars Corresponding to ±2.5 nm/yr and Weibull Distributions Used to Represent the General Corrosion Rate of Alloy 22 at 60°C (base model)

1.4 TEMPERATURE DEPENDENCE OF ALLOY 22 GENERAL CORROSION BASED ON SCW WEIGHT-LOSS SPECIMENS EXPOSED AT 60°C AND 90°C

As discussed in Section 1.3, no temperature dependence was observed in the Alloy 22 general corrosion rates, with the exception of the results from weight-loss specimens immersed in the SCW solution. In *General Corrosion and Localized Corrosion of Waste Package Outer Barrier* (SNL 2007, Section 6.4.3.4), these data (before re-cleaning) were used to evaluate the temperature dependence of Alloy 22 general corrosion for comparison to the temperature dependence of the Alloy 22 general corrosion model used in the Total System Performance Assessment (TSPA). Given that these specimens have been re-cleaned, it is appropriate to re-evaluate the temperature dependence of the re-cleaned data. For this analysis, only specimens immersed in solution, excluding those specimens exposed at the waterline, were used. Using the same Bootstrap analysis technique (Efron and Gong 1983) discussed in *General Corrosion and Localized Corrosion of Waste Package Outer Barrier* (SNL 2007, Section 6.4.3.4), the apparent activation energy distribution obtained for the re-cleaned weight-loss specimens immersed in SCW solution is shown in Figure 9. The Bootstrap distribution has a mean of about 32.26 kJ/mol and minimum and maximum values of 3.37 and 60.05 kJ/mol, respectively.

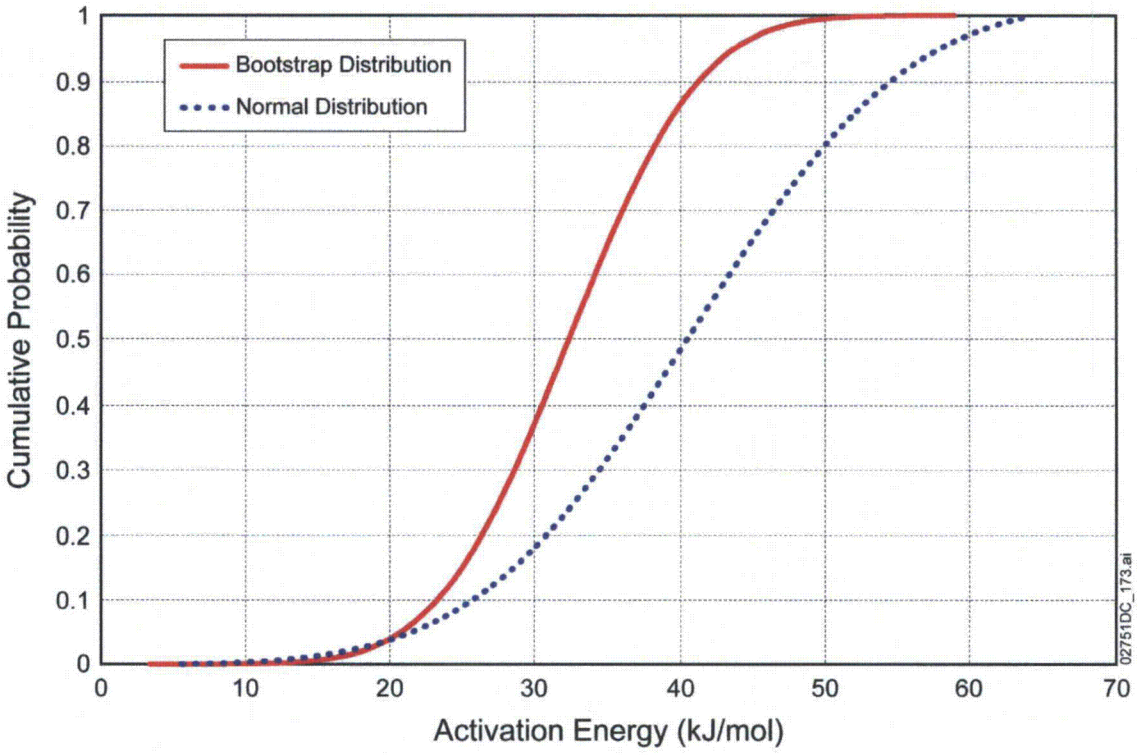

Figure 9. Apparent Activation Energy Cumulative Distribution Function Used in the TSPA (normal distribution) versus Apparent Activation Energy Cumulative Distribution Function Generated by Bootstrap Analysis of Alloy 22 Weight-Loss Specimens Immersed in SCW for Five Years at 60°C and 90°C

Also shown in Figure 9 is the apparent activation energy distribution used in the TSPA (SAR Section 2.3.6.3.3.1), which is based on a normal distribution with a mean of 40.78 kJ/mol and a standard deviation of 11.75 kJ/mol truncated between −3 standard deviations (5.54 kJ/mol) and +2 standard deviations (64.28 kJ/mol). The apparent activation energy distribution determined from the Bootstrap evaluation of the re-cleaned weight-loss specimens has a lower mean and slightly lower minimum and maximum values than the apparent activation energy distribution used in the TSPA.

Figure 10 shows the Alloy 22 general corrosion rate distributions obtained from both models at an exposure temperature of 25°C. The solid lines correspond to the use of the medium uncertainty level and lowest (5.54 kJ/mol; in red), mean (40.78 kJ/mol; in blue), and highest (64.28 kJ/mol; in green) apparent activation energies for the base Alloy 22 general corrosion model (SAR Section 2.3.6.3.3.1). The points (updated model) correspond to applying the lowest (3.37 kJ/mol; in red), mean (32.26 kJ/mol; in blue), and highest (60.05 kJ/mol; in green) apparent activation energies (obtained for the re-cleaned weight-loss specimens immersed in SCW solution) to the empirical cumulative distribution function of re-cleaned weight-loss specimen corrosion rates (i.e., the distribution shown in Figure 3 without the negative general corrosion rate). Similar comparisons at 100°C and 200°C are shown in Figures 11 and 12, respectively. As can be seen in Figure 10 through Figure 12, at all temperatures considered, the updated model results in lower predicted Alloy 22 general corrosion rates than the base model, except at very low cumulative probabilities. As discussed in Section 1.3.1.1, only the general corrosion rates at the upper end of the Alloy 22 general corrosion rate cumulative distribution (e.g., the general corrosion rates with cumulative probabilities above 0.96) are important in determining waste package performance. Therefore, use of the Alloy 22 general corrosion base model is not expected to underestimate repository performance.

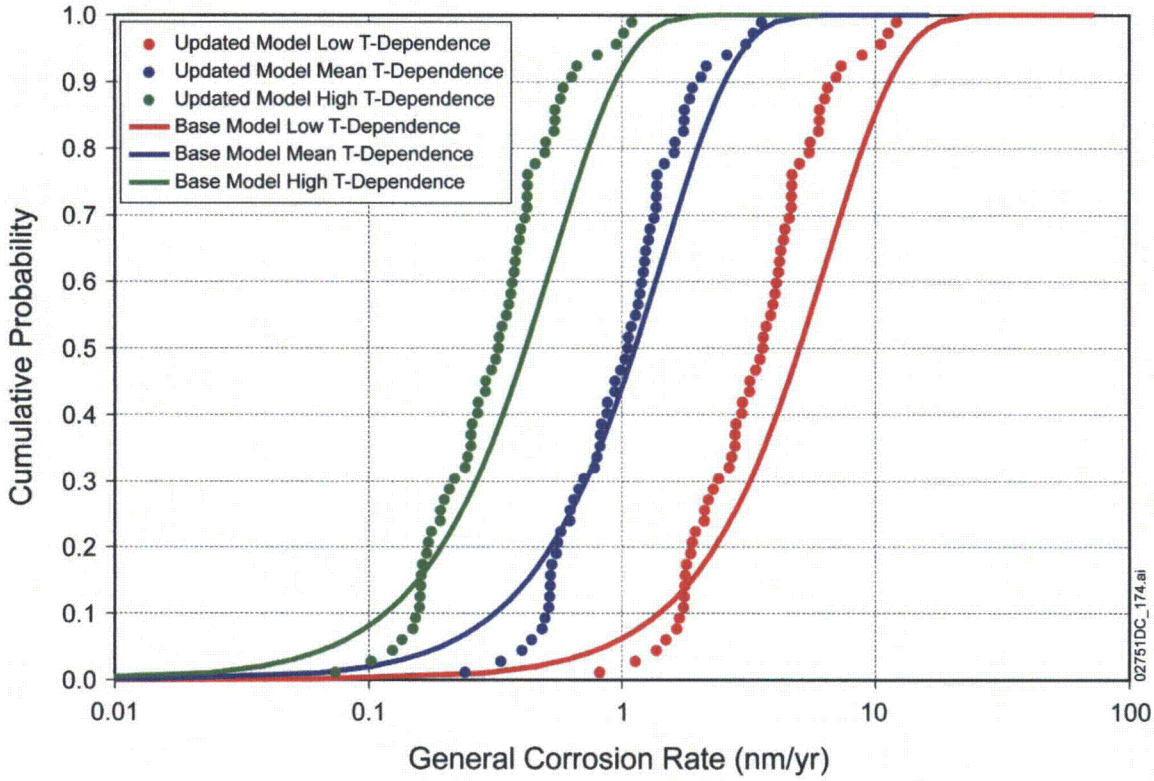

Figure 10. Comparison (at 25°C) of Base-Case Alloy 22 General Corrosion Model to General Corrosion Rates Predicted Using the Re-Cleaned Weight-Loss Specimens and the Apparent Activation Energy Generated by Bootstrap Analysis of Re-Cleaned Alloy 22 Weight-Loss Specimens Immersed in SCW for Five Years at 60°C and 90°C (updated model)

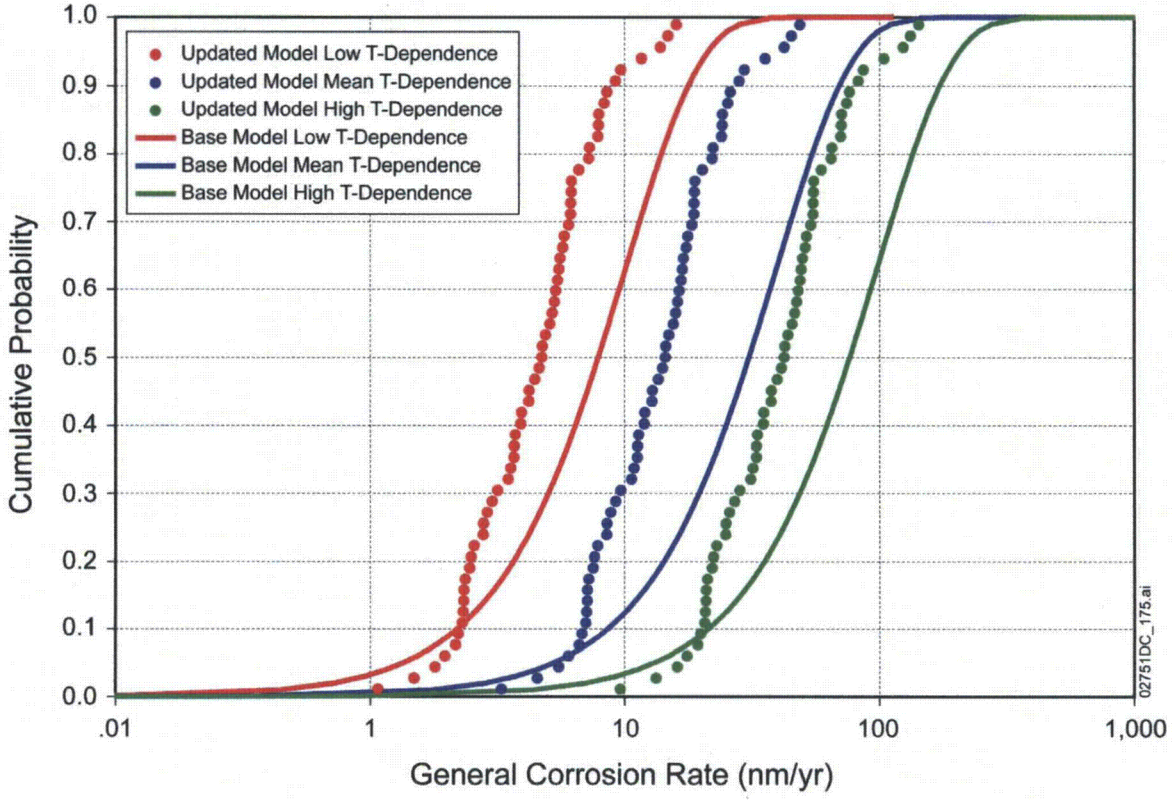

Figure 11. Comparison (at 100°C) of Base-Case Alloy 22 General Corrosion Model to General Corrosion Rates Predicted Using the Re-Cleaned Weight-Loss Specimens and the Apparent Activation Energy Generated by Bootstrap Analysis of Re-Cleaned Alloy 22 Weight-Loss Specimens Immersed in SCW for Five Years at 60°C and 90°C (updated model)

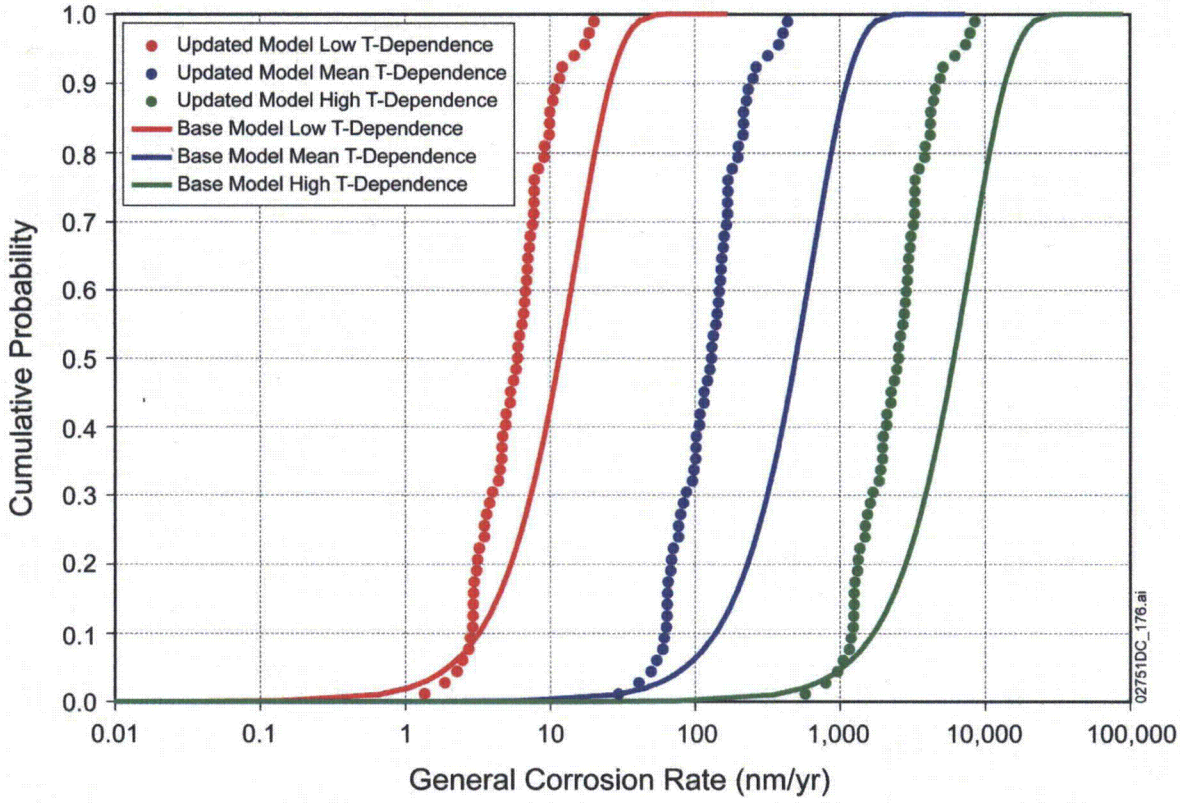

Figure 12. Comparison (at 200°C) of Base-Case Alloy 22 General Corrosion Model to General Corrosion Rates Predicted Using the Re-Cleaned Weight-Loss Specimens and the Apparent Activation Energy Generated by Bootstrap Analysis of Re-Cleaned Alloy 22 Weight-Loss Specimens Immersed in SCW for Five Years at 60°C and 90°C (updated model)

1.5 SUMMARY

As discussed above, experimental artifacts on the crevice specimens (e.g., mill-annealed oxides and surface contamination, which were not present on the weight-loss specimens) led to the calculation of an artificially high Alloy 22 general corrosion rate. A preliminary evaluation of the weight-loss specimens indicates that the general corrosion rate of Alloy 22 at 60°C and 90°C is much lower than is predicted based on the initial cleaning of the crevice specimens. In addition, the temperature dependence of the re-cleaned weight-loss specimens was evaluated. The Alloy 22 general corrosion model based on the re-cleaned weight-loss data (updated model) predicts lower Alloy 22 general corrosion rates than the Alloy 22 general corrosion rate model developed in *General Corrosion and Localized Corrosion of Waste Package Outer Barrier* (SNL 2007, Section 6.4.3) (base model), except at very low cumulative probabilities, which are less important to predictions of repository performance. Therefore, use of the Alloy 22 general corrosion base model is not expected to underestimate repository performance.

2. COMMITMENTS TO NRC

The final results of the re-cleaning and re-analysis of the weight-loss specimens will be documented in an addendum to *General Corrosion and Localized Corrosion of Waste Package Outer Barrier* (SNL 2007) and a revision of SAR Section 2.3.6. The change to the SAR will be included in a future license application update.

3. DESCRIPTION OF PROPOSED LA CHANGE

SAR Section 2.3.6.3 text will be revised to reflect changes due to re-cleaning of the weight-loss specimens. The change will be included in a future license application update.

4. REFERENCES

ASTM G 1-03 2003. *Standard Practice for Preparing, Cleaning, and Evaluating Corrosion Test Specimens.* West Conshohocken, Pennsylvania: American Society for Testing and Materials.

ASTM G 1-90 (Reapproved 1999) 1999. *Standard Practice for Preparing, Cleaning, and Evaluating Corrosion Test Specimens.* West Conshohocken, Pennsylvania: American Society for Testing and Materials.

Efron, B. and Gong, G. 1983. "A Leisurely Look at the Bootstrap, the Jackknife, and Cross-Validation." *The American Statistician, 37*, (1), 36-48. Washington, D.C.: American Statistical Association.

SNL (Sandia National Laboratories) 2007. *General Corrosion and Localized Corrosion of Waste Package Outer Barrier.* ANL-EBS-MD-000003 REV 03. Las Vegas, Nevada: Sandia National Laboratories. ACC: DOC.20070730.0003.

RAI: Volume 3, Chapter 2.2.1.3.1, Second Set, Number 4:

Provide additional technical basis to assess uncertainties in Alloy 22 corrosion rates associated with the long-term persistence of the passive film on Alloy 22 with regard to the structure, composition, and thickness of the passive film. Assess the potential effects of foreign deposits (e.g., silicon oxide) during the repository performance period.

Basis: DOE assumed a constant general corrosion rate of Alloy 22 at a given temperature (i.e., time independent) (SAR, Section 6.3.2.3). This assumption relies on the long-term stability of the thin and adherent passive oxide film formed on the alloy surface, which is mainly composed of chromium and nickel oxides. Lloyd, et al. (2003, 2004) indicated that the structure and composition of the oxide film was a function of temperature and redox condition. However, DOE has provided limited information on oxide film characterization of Alloy 22 under simulated repository conditions (SNL 2007, Orme 2005). The data in SNL (2007, Figure 6-7) showed a decrease of chromium and nickel concentrations in the film as the immersion time in a test solution increases while silicon concentration increases. The 5 years' long-term data (Orme, 2005) did not clearly support the assumption of the long-term stability of the passive film. The data that characterizes the evolution of the thickness, composition, and structure of the passive film for a range of potential repository environmental conditions is not available, as commented in the pre-licensing evaluation of Container Life and Source Term (CLST) Key Technical Issue (KTI) Agreement CLST 1.08 and 1.09 (NRC, 2004). DOE has not assessed the potential effects changes of the oxide structure, composition, and thickness of the oxide on the long-term stability of the oxide film, nor has DOE provided a technical basis to demonstrate that these effects would not significantly affect general corrosion rates of Alloy 22 during the performance assessment period. This requested information is needed to assess the use of a constant general corrosion rate at a given temperature in the general corrosion model for Alloy 22 in the performance assessment used to demonstrate compliance with 10 CFR 63.114(f).

1. RESPONSE

This response describes the new and previously available studies and analyses used to determine the uncertainties associated with the long-term persistence of the passive film on Alloy 22 with regard to the structure, composition, and thickness of the passive film. These studies conclusively demonstrate the long-term stability of the passive oxide film on Alloy 22 under a wide range of repository relevant conditions. Though the structure and composition of the film does vary with the conditions under which it was formed, the protective nature is preserved.

Additional potential effects of foreign deposits during the repository performance period are discussed in Response Section 1.2 and include experimentation performed in an effort to determine the impact that silica scale, or other foreign matter, might have on the oxide stability, and therefore general corrosion rate, of Alloy 22. Silica deposited on the surface of the Alloy 22

coupons during exposure to silicate-bearing solutions does not have a discernable impact on the stability of the passive oxide, and hence the general corrosion rate, of Alloy 22.

1.1 PROPERTIES OF THE PASSIVE OXIDE ON ALLOY 22 AS A FUNCTION OF EXPOSURE CONDITIONS AND TIME

The model for general corrosion in the total system performance assessment (TSPA) conservatively use a constant rate of general corrosion based on the weight loss observed over the first 5 years of exposure, rather than a time-varying corrosion. Effectively, the model assumes that the passive film breaks down or spalls off completely and a new material surface is introduced every 5 years. Thus, the model does not take credit for the fact that the general corrosion rate will decrease with time over the entire repository performance period, but rather, offers a highly conservative constant value for the corrosion rate based on short-term, 5-year test duration data.

To assess the long-term stability of the passive oxide layer on Alloy 22, a series of experiments were performed to observe its properties as a function of the conditions through which it was produced, as well as its behavior under repository relevant conditions.

To establish the nature of the oxide responsible for the passivation of Alloy 22, oxide films were grown electrochemically at different applied potentials in solutions of varying pH and composition. In all cases, passivity was found to be the result of a thin, conformal oxide layer rich in chromium oxide. Consistent with the observations of Lloyd et al. (2003; 2004), the thickness and composition of this layer varied with the aggressiveness of the exposure condition, but was generally 5 nm or less. In addition, under some conditions a porous oxide layer was formed on the top of the compact protective layer, though this did not have a detrimental effect on the properties of the protective layer. In alkaline solutions, a thin silica-rich layer was deposited on the surface of the oxide layer, with the origin of the silica speculated as being from the dissolution of the glass vessel in which the experiment was performed. Again, in all cases passivity appeared to be the result of a thin chromium oxide layer at the metal surface.

Oxide-growth process kinetics were evaluated electrochemically at various applied potentials, temperatures, and solution chemistries. Oxide growth was observed to exhibit an initial logarithmic stage, followed in time by a dramatic reduction and stabilization of the current. This behavior has been attributed to the initial formation of the oxide layer, followed by the gradual reduction in defects/consolidation of the oxide. This process results in the oxide becoming increasingly protective, leading to the observed reduction in current. The implication of this, relative to the long-term stability of the oxide layer, is that the protective chromium-rich layer will tend to become "stronger" over time in terms of its ability to protect the underlying metal substrate and that, therefore, passivity will be maintained.

To further evaluate the long-term stability of the oxide, potentiostatic experiments were performed in solutions of varying pH at a temperature of 90°C, and the impact which that polarization had on the stability of the oxide layer was evaluated. Chromium oxides are the primary species in the barrier layer for the range of pH and potential values tested. The equilibrium speciation modeling suggests that the Cr_2O_3 that forms at pH = 2.8 and the $NiCr_2O_4$

that forms at pH = 7.5 are thermodynamically stable in concentrated solutions (e.g., 1 g of metal was dissolved into 1 kg of NaCl solution, or approximately 0.01 M dissolved Alloy 22). In potentiostatic experiments, the measured currents provide an estimate of the metal transferred to solution. With the assumption that the entire current is due to metal dissolution, the resulting metal concentrations are approximately 10^{-5} to 10^{-6} M. At these concentrations, it is very unlikely that chromium oxides are the thermodynamically stable oxide phase (i.e., based upon a Pourbaix type diagram, chromium oxide is not the most stable form of chromium under the conditions in question). Thus, the obtained results (indicating that the corrosion rate remained low) suggest that a kinetically stable oxide layer forms on the metal surface, hindering further dissolution, and hence limiting the buildup of metal ions in solution.

1.2 IMPACT OF SILICA OR OTHER THIN SURFACE DEPOSITS ON THE PROPERTIES OF THE PASSIVE OXIDE FORMED ON ALLOY 22

If seepage of silicate containing groundwater comes into contact with the waste package, there is the potential for a silica-rich layer to be deposited on the surface. The impact of such solutions was explored via an experimental program in which Alloy 22 was exposed to a series of solutions containing varying concentrations of silicate as well as varying pH, chloride concentration, and temperature. The presence of silicate had no significant impact on the observed open circuit potentials, or on the corrosion rate under any of the conditions evaluated. Furthermore, results from long-term exposure tests performed in silicate-bearing solutions in the Long-Term Corrosion Test Facility (LTCTF) also indicated that neither the silicate in solution, nor the silica-rich deposits on the specimen, enhanced dissolution. As such, it may be concluded that silicate did not alter the electrochemistry occurring on the metal surface sufficiently to either destabilize the oxide or increase the general corrosion rate.

In addition to not accelerating general corrosion, deposits which might form on the waste package surface due to evaporation of seepage water will not enhance localized corrosion. In order to induce localized corrosion experimentally, a sufficiently tight crevice on the surface of an Alloy 22 coupon under relevant environmental conditions is necessary. To create a sufficiently tight crevice, the DOE utilized a polytetrafluoroethylene- (PTFE-) coated ceramic crevice former pressed firmly onto the sample surface. Research has demonstrated that this approach is effectively a "worst case" scenario. Other designs, such as a bare ceramic crevice former combined with anodic polarization, were insufficient to initiate crevice corrosion, demonstrating the necessity of a very tight crevice geometry for localized corrosion initiation in Alloy 22. The geometry utilized by the DOE is more severe, and therefore, is more effective at enabling the initiation and propagation of localized corrosion than any anticipated crevices that could potentially be formed by materials within a drift contacting a waste package surface.

In a study performed by Badwe et al. (2006), the effect of the salt layer on the corrosion behavior of Alloy 22 was evaluated by exposing the material to a series of multi-ionic solutions that were evaporated to dryness on the metal surface. In no case was localized corrosion observed beneath the salt deposits, including within aqueous solutions with an initial pH as low as 3. These observations reinforce the conclusion that deposits of foreign material on the surface of the waste package will not result in locally enhanced dissolution.

2. COMMITMENTS TO NRC

None.

3. DESCRIPTION OF PROPOSED LA CHANGE

None.

4. REFERENCES

Badwe, S., Raja, K.S., Misra, M. 2006 "A Study of Corrosion Behavior of Ni-22Cr-13Mo-3W Alloy Under Hydroscopic Salt Deposits on Hot Surface," *Electrochimica Acta, Vol. 51*, No. 26, pp. 5836-5844.

Lloyd, A.C., Shoesmith, D.W., McIntyre, N.S., and Noël, J.J. 2003. "Effects of Temperature and Potential on the Passive Corrosion Properties of Alloys C22 and C276." *Journal of the Electrochemical Society. Vol. 150.* pp. B120–130.

Lloyd, A.C., Noël, J.J., McIntyre, N.S., Shoesmith, D.W. 2004. "Cr, Mo and W alloying additions in Ni and their effect on passivity." *Electrochimica Acta. Vol. 49.* pp.3015–3027.

Orme, C.A. 2005. "The Passive Film on Alloy 22." UCRL–TR–215277. Livermore, California: Lawrence Livermore National Laboratory.

SNL (Sandia National Laboratories) 2007. *General Corrosion and Localized Corrosion of Waste Package Outer Barrier.* ANL-EBS-MD-000003 REV 03. Las Vegas, Nevada: Sandia National Laboratories. ACC: DOC.20070730.0003; DOC.20070807.0007; LLR.20080414.0018; DOC.20090126.0002.

RAI: Volume 3, Chapter 2.2.1.3.1, Second Set, Number 5:

Provide a technical basis to show that the assumed role of molybdenum in Alloy 22 in eliminating the deleterious effect of sulfur on passivity is supported by available information.

Basis: In SNL (2007, Section 6.4.1.1.4), DOE notes that the dissolution of molybdenum sulfides is expected in the anticipated oxic repository environment. Therefore, potentially deleterious effects of anodic sulfur segregation on Alloy 22 passivity will be avoided. However, this effect has not been demonstrated experimentally and may not be consistent with available information. Some published information shows sulfur enrichment on Alloy 22 can occur even in the presence of molybdenum in an oxidizing environment (Windisch, et al., 2007; Wong, et al., 2004, Figures 2 and 3). This information apparently was not considered by DOE, and DOE did not provide a technical basis to support the assumed role of molybdenum in mitigating the potential effects of sulfur segregation on passive film stability for Alloy 22. This requested information is needed to assess the use of Alloy 22 general corrosion rates in the performance assessment used to demonstrate compliance with 10 CFR 63.114(f).

1. RESPONSE

This response provides additional technical basis regarding the role of molybdenum and chromium in mitigating the deleterious effect of sulfur on Alloy 22 passivity. The response also summarizes the relevant details of the publications cited in the basis statement (Windisch et al. 2007; Wong et al. 2004) and explains how those publications are consistent with the corrosion studies presented in the SAR. Finally, the response discusses the time to reach one monolayer of sulfur at the outer surface of Alloy 22, based on both calculation results and experimental observations.

Unlike Alloy 22, some nickel and nickel-iron alloys (without molybdenum and chromium additions) can undergo sulfur enrichment at the metal/passive film interface under long-term exposure potentially leading to deleterious enhanced general corrosion rates and localized corrosion. Because of the relatively high molybdenum (and chromium) content in Alloy 22, it is not expected, based on the information presented below, that sulfur-enhanced corrosion degradation of the waste package outer corrosion barrier will occur in the repository environment. Molybdenum exhibits an affinity for sulfur under aqueous conditions and the resulting molybdenum sulfide tends to dissolve under repository relevant oxic conditions. This sulfide dissolution, along with the formation of a very stable chromium oxide-rich passive film, is expected to mitigate any deleterious effect resulting from long-term sulfur enrichment at the metal/oxide interface of a corroding Alloy 22 waste package outer barrier. Also, because of drip shields, contact between potentially corrosive seepage waters and the waste packages is not expected until well after 10,000 years (RAI 3.2.2.1.2.1-4-005).

1.1 ROLE OF MOLYBDENUM AND CHROMIUM IN MITIGATING DELETERIOUS SULFUR EFFECTS ON PASSIVITY IN NICKEL ALLOYS

1.1.1 Beneficial Role of Molybdenum

Under normal waste package exposure conditions, sulfur can potentially enrich at a metal surface through thermal segregation, deposition from the environment and/or anodic (corrosion-induced) dissolution (Marcus and Maurice 2000, pp. 160 to 162; Jones et al. 2006). Although thermal segregation in nickel base alloys has been observed at higher temperatures (e.g., 800°C to 1,100°C), these thermal conditions are not relevant to repository conditions. Thermal segregation is considerably more sluggish and complex at lower temperatures and may not occur in Alloy 22 below 200°C (Jones et al. 2006, p.5). The waste packages will be cooler than 200°C for the entire repository period following the initial about 100 years of the thermal pulse as indicated in SAR Figure 2.3.5-33. Deposition of sulfur from the environment will not occur under repository relevant oxic conditions (Jones 2006, p. 4).

In passive alloys such as Alloy 22, anodic sulfur segregation can potentially occur as selective cations (e.g., nickel) diffuse through the passive film through a defect mechanism and react at or near the outermost surface/solution interface, resulting in enrichment of species present at the metal/film interface. However, to be detrimental to corrosion resistance, the interfacial sulfur must approach one monolayer in thickness and must remain in a reduced form (Jones et al. 2006, p.6). If the sulfur reaches this critical concentration of about one monolayer, it can potentially lead to enhanced corrosion rates or local breakdown of the passive film of nickel and nickel iron alloys (Marcus and Maurice 2000, p. 161; Jung et al. 2007, Section 4.1.1.2.2).

The presence of molybdenum counteracts this deleterious effect of sulfur present at about the monolayer level by forming bonds with sulfur (either adsorbed sulfur or sulfur exposed at sites of passive film breakdown) and the resulting molybdenum sulfide then dissolves, thus mitigating the detrimental effects of sulfur (Marcus and Maurice 2000, p. 158; Jung et al. 2007, Section 4.1.1). Alloy 22 contains a significant amount of molybdenum (12.5 wt % to 14.5 wt %) (ASTM B 575-94 1994). Jung et al. (2007, Section 4.1.3.1) present Mo-S-H_2O potential-pH (Poubaix) thermodynamic stability diagrams for aqueous systems at 25°C and 90°C indicating that MoS_2 and MoS_3 are stable phases over a range of pH values under reducing conditions. Marcus and Moscatelli (1989) indicate that the adsorbed sulfur can be dissolved via other soluble molybdenum sulfides (e.g., Mo_2S or MoS for nickel-molybdenum or stainless steel, respectively), or molybdenum-sulfur clusters with water. Evidence of MoS_2 dissolution in aqueous media is presented in *Corrosion* (ASM International 1987, p. 962), which indicates that MoS_2 is not stable at pH values greater than 4.5. As pointed out by Jung et al. (2007, Section 4.1.3.3), the dissolved sulfur species could be either in the form of reduced sulfur or, under more oxidizing conditions, oxidized sulfur (e.g., SO_4^{2-}) depending on the solution chemistry and temperature. The removal of segregated sulfur in this manner permits the regeneration of the chromium oxide passive film on Alloy 22.

1.1.2 Beneficial Role of Chromium

In addition to its high molybdenum content, Alloy 22 also contains a significant amount of chromium (20.0 wt % to 22.5 wt %) (ASTM B-575-94 1994). Corrosion test results (Jung et al. 2007, Section 4.1.1.2.1) show that the chromium in Ni-xCr-10Fe alloys (x = 8, 19, and 34 atomic percent (at %)) counteracts the detrimental effects of sulfur by promoting the passivation of the alloys, whereas the passivation is precluded by sulfur in nickel or nickel-iron alloys (no chromium) under similar conditions. The thermodynamic stability diagrams for the Cr–S–H_2O system and the Ni–S–H_2O system (Jung et al. 2007, Section 4.1.3.1) confirm that the formation of chromium oxide (Cr_2O_3) is strongly favored in a wide range of potential and pH regions over sulfide formation. This superior stability of chromium oxide over any forms of sulfide explains why chromium is beneficial to the corrosion resistance of chromium containing nickel-based alloys with adsorbed or alloyed sulfur. The effect of sulfur enrichment on passivation in chromium containing nickel alloys is expected to be different than that in nickel-chromium-molybdenum alloys. Whereas molybdenum combines with the sulfur as soluble sulfides, chromium does not cause a reduction in adsorbed sulfur concentration, but instead promotes passivation in spite of the presence of adsorbed sulfur (Marcus 2002, pp. 300 to 301).

For sulfur-enriched nickel-chromium alloys, surface analysis confirmed the coexistence of nickel sulfide and chromium oxide (Jung et al. 2007, p. 4-5). In the presence of sulfur, chromium forms a continuous layer of Cr_2O_3 at the metal/film interface essentially covering the nickel sulfide (Ni_3S_2) islands.

1.2 EFFECT OF SULFUR ENRICHMENT ON ALLOY 22 GENERAL CORROSION

Sulfur enrichment approaching one monolayer at the surface of passive metals and alloys is an extremely slow kinetic process; therefore, to study the enrichment effect on subsequent corrosion behavior, it is necessary to use accelerated approaches to produce sulfur enrichment in test specimens (Jung et al. 2007, Section 4.1.1). Such experimental approaches include ion-implantation, sulfur doping by exposure to high temperature gaseous environments, exposure to dissolved sulfur in aqueous solutions, and alloying to produce a range of sulfur contents.

1.2.1 Summary of Experimental Study by Windisch et al.

To assess the potential for sulfur enrichment to degrade the corrosion performance of Alloy 22, Windisch et al. (2007) used a sulfur ion-implantation technique to produce specimens containing a sulfur-enriched surface layer with a maximum sulfur concentration of about 2 at % at a depth of 20 to 25 nm. After implantation, they sputtered most of the sulfur-enriched specimens to achieve the maximum concentration of sulfur at the sample outermost surface. Argon ion implanted specimens were also prepared to use as controls. The sulfur-enriched specimens were then evaluated along with the control specimens in room temperature, deaerated (nitrogen sparged) 1 M NaCl solutions (a reducing environment) at pH values of 8.15 and 3.67, using short-term electrochemical corrosion tests (corrosion potential and potentiodynamic polarization behavior).

In addition, one sulfur-implanted specimen was subjected to a 29-day exposure to the deaerated, pH = 3.67, 1 M NaCl solution to obtain evidence of any sulfur accumulation at the surface over longer times. Following testing, the specimen surfaces were analyzed using x-ray photoelectron spectroscopy (XPS) to determine film thicknesses and compositional gradients, with particular emphasis on the amount and chemical state of any sulfur present. Based on this limited corrosion study, Windisch et al. (2007, p. 2,504) found that the measured passive currents for the tested conditions (i.e., sulfur-implanted and argon ion-implanted) are generally very small, indicating no obvious enhancement of general corrosion due to sulfur. The sulfur concentration profiles left after the sputtering step remained the same in the alloy after polarization.

XPS data (e.g., Windisch et al. 2007, Figure 8 and p. 2,509) indicate that for the 29-day exposed specimen examined after testing, there is an enhancement of molybdenum and sulfur at the surface, consistent with an inhibitory role for molybdenum. An increase in the outermost (about 1 nanometer) surface sulfur content from about 2 at % to between 3.5 at % and 5 at % was observed during the 29-day exposure test. The authors concluded:

- There was very little, if any, reproducible influence from the sulfur on the passive corrosion current in the short term when initially present in the surface layers of the alloy at concentrations up to 2 at %.

- The presence of sulfur caused a significant and reproducible negative corrosion potential offset (about 100 mV) to the alloy (separate from the effects of ion implantation) and the effect appears to be related to the amount of sulfur present.

- There is strong evidence that sulfur can enrich on the surface of Alloy 22 during corrosion under normally passive conditions in deaerated solutions. Studies on the impact of this buildup would require samples with even higher levels of surface-sulfur than were tested in this work.

- In aerated environments, for example, it is possible that the sulfur may be significantly oxidized and removed (by dissolution) from the surface, thus ameliorating the long-term effects of the sulfur on corrosion.

The conclusion in the fourth bullet, along with the observation of aqueous dissolution of molybdenum sulfides discussed and the molybdenum enrichment observed at the outer surface following these corrosion tests, is expected in the oxic repository environment.

1.2.2 Summary of Surface Analysis Study by Wong et al. 2004

The study by Wong et al. (2004) summarized results on the characterization of the surface deposits as well as the corrosion rates for over 100 Alloy 22 corrosion specimens after more than five years exposure at 60°C or 90°C in the Long-Term Corrosion Test Facility (LTCTF). Each tank contained 1,000 liters of repository relevant aerated seepage water solutions designated as either simulated dilute water (SDW, pH ~10), simulated concentrated water (SCW, pH ~ 10) or simulated acidified water (SAW, pH ~3) (SAR Table 2.3.6-1). Of the 134 Alloy 22 specimens

evaluated, 122 were chemically descaled and weighed to obtain corrosion rates and 12 specimens representing each of the different test conditions were set aside for surface analysis.

To characterize the composition of the surface deposits present on specimens exposed to various LTCTF environments, surface analysis of the deposits (Wong et al. 2004, Figures 2 and 3) was performed by energy dispersive spectroscopy (EDS). In addition to the alloying constituents of Alloy 22, the elemental analyses also indicated the presence of the elements carbon, oxygen, silicon, aluminum, chlorine, sulfur, and phosphorus. This is not unexpected since the individual LTCTF tanks had a range of relatively concentrated ionic constituents, including Na^+, K^+, Mg^{2+}, Ca^{2+}, Cl^-, NO_3^-, SO_4^{2-}, HCO_3^-, and SiO_2 (aq), as well as specimens fabricated from several less corrosion resistant alloys. Some of these ionic constituents plated out on specimens shown in Figure 3 (Wong et al. 2004), which were immersed in the liquid phase or carried over in various chemical forms into the vapor phase and deposited onto the surfaces of the specimen shown in Figure 2 (Wong et al. 2004), which was located just above the test solution. The scanning electron microscope images and the EDS-determined elemental compositions at several locations are shown for the specimen exposed to 90°C SAW vapor in Figure 2, and for the two specimens in Figure 3 (Wong et al. 2004), one exposed to 90°C SAW liquid (pH ~3) and the other exposed to 90°C SCW liquid (pH ~10). Analyses are reported for locations containing deposits or surface particles as well as regions between the thicker deposits. Although the elemental compositions of the EDS-measured surface deposits vary somewhat from specimen to specimen, there is a similarity in the type and quantity of the analyzed constituents not associated with the major Alloy 22 alloying additions. Although sulfur is among the elements measured in the deposits and adjacent surfaces (reported values varying from about 0.16 wt % to between 2 wt % and 3 wt %), the EDS signal is likely to have come from the SO_4^{2-} ions present at high levels in both SAW (~40,000 ppm SO_4^{2-}) and SCW (~20,000 ppm SO_4^{2-}). This is fully consistent with the analysis described in Section 1.3 of this RAI response for the estimated time required to reach a monolayer of sulfur on the surface of Ni-Fe alloys. After 5 years at 90°C, the analysis predicts formation of a single monolayer of sulfur for a Ni-Fe alloy with 100 ppm initial sulfur content at a corrosion rate of 100 nm/yr and even less than a single monolayer at the lower measured 5-year corrosion rates (~2 to 15 nm/yr) for Alloy 22 exposed in 90°C SAW and SCW (Wong et al. 2004, Table 3). The EDS technique used to obtain the surface elemental analyses shown in Figures 2 and 3 of the Wong et al. (2004) report is not capable of resolving elements at the monolayer level as it has a depth resolution of about 1 μm (~1,000 nm). Consequently, the sulfur detected was likely present in thicker surface deposits formed from ionic species present in the test solutions. Thus, these surface analysis results do not support the RAI basis statement that Wong et al. (2004, Figures 2 and 3) show the occurrence of sulfur enrichment on Alloy 22.

1.3 ESTIMATE OF THE TIME TO REACH ONE MONOLAYER OF SULFUR AT THE OUTER SURFACE OF ALLOY 22

1.3.1 Summary of Calculation to Assess Time for Sulfur Monolayer Formation

Jung et al. (2007, Section 4.1.3.2) estimated the induction time for potential Alloy 22 passive film degradation (i.e., enhanced general corrosion rate and/or initiation of localized corrosion) due to surface sulfur enrichment. The authors used an equation developed for Ni-Fe alloys (no chromium or molybdenum additions) and assumed it was valid for Alloy 22. The equation

describes the time needed to form one monolayer of sulfur equivalent to about 40 nanograms/cm^2 at the metal surface. Based on their calculations, they developed a table, listing the estimated time to passive film breakdown at 25°C and 90°C for various initial bulk sulfur concentrations. For a 90°C exposure, it was concluded:

> Considering a maximum sulfur concentration (e.g., maximum 0.02 wt % = 200 ppm by weight) and a generally low passive current density (e.g., < 10^{-8} A/cm^2 [6.5 × 10^{-8} A/ft^2]) in Alloy 22, the calculation indicates that the film breakdown on Alloy 22 could occur after 2.5 years or longer under deaerated conditions, assuming sulfur in the alloy segregates at the metal–film interface without dissolving into the solution. Based on the currently available long-term corrosion test data for Alloy 22, such as obtained at the DOE LTCTF, there is no evidence or any indication of sulfur-induced film breakdown for Alloy 22, suggesting that the beneficial role of alloying elements (e.g., molybdenum and chromium) overcome any potential anodic sulfur segregation.

It was also concluded:

> As the beneficial effects of chromium and molybdenum have been previously demonstrated in nickel-molybdenum and nickel-chromium-iron alloys as discussed, it can be also expected that the beneficial role of alloying elements (molybdenum and chromium) in Alloy 22 counteract the detrimental sulfur effects. Long-term studies using higher sulfur concentrations in the alloy may be useful to examine the potentially beneficial and/or aggravating effects of these elements on corrosion induced by anodic sulfur segregation in Alloy 22.

The cited current density of < 10^{-8} A/cm^2 corresponds to a corrosion rate of > 100 nm/yr.

1.3.2 Comparison of Calculation Results with Experimental Observations for Alloy 22

As indicated in SAR Section 2.3.6.4.4.2.1 and Table 2.3.6-12, there have been no observations of accelerated general corrosion and/or localized corrosion on any of the Alloy 22 corrosion specimens examined after up to 5 years exposure at 60°C and 90°C in the LTCTF. It is important to consider the actual sulfur content of the material tested when comparing these LTCTF observations to the predictions made by Jung et al. (2007, Table 4-2) of the time to reach a critical surface sulfur concentration for accelerated general corrosion and/or localized corrosion (one monolayer) described in Section 1.3.1. Examination of the material certifications for Alloy 22 sheet material used to prepare these corrosion specimens indicates a range of bulk sulfur contents from about 20 to 80 wt ppm. These values are lower than the Alloy 22 specification limit of 200 wt ppm sulfur discussed in the previous section, but are typical of values to be expected from modern melting practices. Based on the Jung et al. (2007, Table 4-2) calculation results, for 80 wt ppm sulfur, the time at 90°C to form a monolayer of sulfur at the alloy surface (potentially leading to accelerated corrosion) should be about 6 years. There have been no observations of accelerated corrosion on any of the approximately one hundred Alloy 22 specimens with up to 80 wt ppm sulfur that were examined after 5 years exposure as well as on a few U-bend and crevice specimens examined visually after 9.5 years exposure. The lack of an

observed sulfur-enhanced general corrosion rate or localized corrosion after 5 years exposure in the LTCTF indicates that, if sufficient sulfur-enrichment were to ultimately occur at the oxide metal interface, and if it unexpectedly resulted in oxide breakdown and/or spalling, subsequent sulfur dissolution and reformation of the highly stable chromium oxide passive film would result in another cycle of passive corrosion (of at least 5 years) with the rate equal to the currently measured rates after 5 years exposure. This is consistent with the conclusion of Pensado et al. (2002, p. 5-24) that, "it is not anticipated that the sulfur-enhanced dissolution process, if it occurs, can be sustained for extended periods."

In addition to the DOE long-term exposure results described above, highly successful field experience and specimen test results following exposure in a number of power plant flue gas desulfurization systems are summarized for Alloy 22 (Haynes International 1992). Many of the reported results are for exposures at or over 10 years in several very aggressive environments at temperatures up to at least 177°C.

1.4 SUMMARY AND CONCLUSIONS

Experimental results (Sections 1.2) and theoretical results (Sections 1.1 and 1.3) reviewed in this response indicate that the potential for the occurrence of deleterious sulfur enrichment in Alloy 22 is highly unlikely considering the relatively high molybdenum (and chromium) levels in this alloy. Therefore, the relevance of this potential corrosion degradation mechanism is unexpected for the waste package outer corrosion barrier. Molybdenum exhibits an affinity for sulfur under aqueous conditions. The resulting molybdenum sulfide tends to dissolve under repository relevant oxic conditions. This expected sulfide dissolution, along with the formation of a very stable chromium oxide rich passive film, will mitigate any deleterious effect resulting from long-term sulfur enrichment at the metal/oxide interface of a corroding Alloy 22 waste package outer barrier. Due to the drip shields, contact of potentially corrosive seepage waters with the waste packages is not expected until well after 10,000 years. Thus, the literature, including the references cited by this RAI, support the beneficial role of molybdenum in mitigating potential deleterious sulfur effects as described in *General Corrosion and Localized Corrosion of Waste Package Outer Barrier* (SNL 2007, Section 6.4.1.1.4).

2. COMMITMENTS TO NRC

None.

3. DESCRIPTION OF PROPOSED LA CHANGE

None.

4. REFERENCES

ASM International 1987. *Corrosion.* Volume 13 of *Metals Handbook.* 9th Edition. Metals Park, Ohio: ASM International.

Haynes International 1992. *Field Experience with Nickel-Base Alloys and Future Trends in Flue Gas Desulfurization Systems.* H-2059B. Kokomo, Indiana: Haynes International.

Jones, R.H., Baer, D.R., Windisch, Jr., C.F., and Rebak, R.B. 2006. "Corrosion Enhanced Enrichment of Sulfur and Implications for Alloy 22." *Corrosion/2006, Paper 06621, San Diego, 12-16 March 2006.*

Jung, H.; Mintz, T.; Dunn, D.S.; Pensado, O. and Ahn, T. 2007. *A Review of the Long-Term Persistence of the Passive Film on Alloy 22 in Potential Yucca Mountain Repository Environments.* San Antonio, Texas: Center for Nuclear Waste Regulatory Analyses.

Marcus, P. and Moscatelli, M. 1989. "The Role of Alloyed Molybdenum in the Dissolution and the Passivation of Nickel-Molybdenum Alloys in the Presence of Adsorbed Sulfur." *Journal of the Electrochemical Society, 135* (6), 1634-1637. Pennington, New Jersey: The Electrochemical Society, Inc.

Marcus, P. and Maurice, V. 2000. "Passivity of Metals and Alloys." Chapter 3 of *Corrosion and Environmental Degradation.* Schütze, M., ed. Volume I. Materials Science and Technology Volume 19. New York, New York: Wiley-VCH.

Marcus, P., ed. 2002. *Corrosion Mechanisms in Theory and Practice.* Second Edition, Revised and Expanded. Corrosion Technology 17. New York, New York: Marcel Dekker.

Martin, S.; Horn, J.; and Carillo, C. 2004. "Micron-Scale MIC of Alloy 22 After Long Term Incubation in Saturated Nuclear Waste Repository Microcosms." *Corrosion/2004, 59th Annual Conference & Exposition, March 28–April 1, 2004, New Orleans.* Paper No. 04596. Houston, Texas: NACE International.

Pensado, O.; Dunn, D.S.; Cragnolino, G.A.; and Jain, V. 2002. *Passive Dissolution of Container Materials—Modeling and Experiments.* CNWRA 2003-01. San Antonio, Texas: Center for Nuclear Waste Regulatory Analyses.

SNL (Sandia National Laboratories) 2007. *General Corrosion and Localized Corrosion of Waste Package Outer Barrier.* ANL-EBS-MD-000003 REV 03. Las Vegas, Nevada: Sandia National Laboratories. ACC: DOC.20070730.0003; DOC.20070807.0007; LLR.20080414.0018.

Windisch, C.F., Baer, D.R., Jones, R.H., and Engelhard, M.H. 2007. "Electrochemical Effects of Sulfur Accumulation on Ion-Implanted Alloy 22 in 1 M NaCl Solutions," *Corrosion Science, 49,* 2497-2511.

Wong, L.L.; Lian, T.; Fix, D.V.; Sutton, M.; and Rebak, R.B. 2004. "Surface Analysis of Alloy 22 Coupons Exposed for Five Years to Concentrated Ground Waters." *Corrosion/2004, 59th Annual Conference & Exposition, March 28 - April 1, 2004, New Orleans.* Paper No. 04701. Houston, Texas: NACE International.

RAI: Volume 3, Chapter 2.2.1.3.1, Second Set, Number 6:

Provide a technical basis to assess the potential effects of dripping and evaporation of seepage water on the long-term persistence of passive film, and subsequent effects on the general corrosion rates of Alloy 22.

Basis: DOE used data from immersion experiments to derive general corrosion rates for Alloy 22. Corrosion conditions in the potential repository, however, may include the dripping of seepage water in contacting the waste package surface (SAR Section 2.1.2.24, page 2.1-66). Literature information (Lee and Solomon, 2006) showed localized corrosion (i.e., pitting) of Alloy 22 occurred under dripping and evaporation conditions, which is not observed in DOE immersion tests. This information indicates that the stability of passive film and general corrosion rates may be altered under dripping water conditions, relative to immersion conditions. DOE did not provide a technical basis to assess the potential effects of dripping water conditions on the passivity and general corrosion rates of Alloy 22. This requested information is needed to assess the use of Alloy 22 general corrosion rates in the performance assessment used to demonstrate compliance with 10 CFR 63.114(f).

1. RESPONSE

This response provides a technical basis to assess the potential effects of a scenario involving seepage water dripping and evaporation. As demonstrated in the following sections, such a scenario would not result in an increase in the observed general or localized corrosion rates under repository-relevant conditions.

1.1 IMPLICATIONS OF DRIPPING CONDITIONS VERSUS IMMERSION CONDITIONS ON THE SOLUTION CHEMISTRIES EVALUATED IN THE SAR

As presented in SAR Section 2.3.6.4.4.1, seepage will not occur until the drift wall temperature is below 100°C, at which point the waste package surface temperature will be below 120°C. In the study by Lee and Solomon (2006), an experiment was run where the metal surface was held at a temperature of 200°C, and a liquid phase was formed on the surface (which was unstable, and rapidly dried out) while continuously dripping water onto the surface. The metastable solution, or "salt puddle," formed in the Lee and Solomon (2006) drip test experiment is not well characterized. Lee and Solomon (2006, p. 122) concluded, "with well controlled situation the solution was stable at about 140°C for a few hours at the most." Moreover, the brine formed in the Lee and Solomon (2006) experiment requires temperatures greater than 120°C, yet seepage will not occur with the drift walls above 100°C, which is the condition that would result in waste package temperatures above 120°C (SAR Section 2.3.6.4.4.1). Therefore, seepage conditions are not conducive to the formation of this brine on the waste package.

Waste package surfaces will not undergo corrosion similar to that described by Lee and Solomon (2006). While localized corrosion was observed by Lee and Solomon (2006), a potential contribution to this behavior is the condition of the material which was used in that study. The

Alloy 22 test samples used by Lee and Solomon (2006, Figure 1) were not solutionized, and significant tetrahedrally close-packed (TCP) phase precipitation is visible. Material in this condition is expected to have inherently inferior performance under aggressive environmental conditions. TCP-phase and carbide precipitates that form in Alloy 22 are generally rich in chromium and/or molybdenum (Raghavan et al. 1984). Because these elements are responsible for the high corrosion resistance of Alloy 22, precipitation of TCP phases and carbides, especially at grain boundaries, can lead to an increased susceptibility to localized corrosion in the alloy. The high-temperature solutionizing treatment described in SAR Section 1.5.2.7.1 is necessary to either remove altogether, or limit the potentially detrimental impact of these phases on the corrosion resistance of the waste package outer barrier. The solutionizing treatment consists of exposing the waste package outer barrier to a temperature of 2,050°F (1,121°C) +50°F (+28°C) / −0°F (−0°C) for a period of at least 20 minutes followed by rapid quenching at a rate greater than 275°F/min (153°C/min) to below 700°F (371°C) (SAR Section 1.9, Table 1.9-9, Parameter 03-16). This heat treatment will dissolve the majority of second phase particles within the microstructure (e.g., TCP phases and long-range ordering [LRO] phases), and compositionally homogenize the material, eliminating the deleterious chromium or molybdenum composition gradients which may exist due to the formation of these phases (see response to RAI: 3.2.2.1.2.1-2-017 for detailed discussion). Since the material evaluated by Lee and Solomon (2006) did not receive such a treatment, solute-depleted regions are expected in the material around the TCP phases, and these regions could be susceptible to localized corrosion under the experimental conditions used by Lee and Solomon (2006) while the surrounding matrix would not be expected to be susceptible under these conditions.

The solution chemistries that are expected to form due to evaporative concentration of seepage water have been accounted for in the experiments performed to date (SNL 2007a, Sections 6.2 and 6.5.1; SNL 2007b, Section 6.4.3.1.3). As such, the solution which might form on the waste package surface due to dripping of seepage water has been accounted for. Furthermore, since the current implementation of both the general and localized corrosion models applies to the entire surface area of the waste package, rather than just local regions where seepage water may have dripped, it is a far more conservative representation of the impact which general and localized corrosion will have on the waste package surface (i.e., the fact that seepage is anticipated to contact only a small portion of the surface area of a waste package is, conservatively, not considered).

1.2 IMPLICATIONS OF DRIPPING CONDITIONS VS. IMMERSION CONDITIONS ON THE SOLUTION VOLUME AND OXYGEN CONCENTRATION

A limited volume of solution, such as would be present under the dripping scenario, could have an impact on the corrosion behavior of the waste package outer barrier by providing an increased availability of oxygen (and hence a potentially larger cathodic current density) as well as by dictating the available surface area available for anodic and/or cathodic sites. In the bulk electrolyte experiments performed within the Long-Term Corrosion Test Facility (LTCTF) tanks, the solution volume was large relative to the surface area of coupons inside the tank, and the tank was continuously stirred such that the solution remained in equilibrium with the oxygen concentration in the air blanket over the top of the tank (which occupied a similar volume to the solution, and was continuously replenished). This was verified experimentally, as presented by

Farmer et al. (2000, Figure 4) where the oxygen concentrations in the simulated acidified water (SAW), simulated concentrated water (SCW), and simulated diluted water (SDW) tanks were verified as being in equilibrium with the oxygen partial pressure of air. The low corrosion rate (and thus, the low rate of oxygen reduction) of Alloy 22 is insufficient to result in significant depletion of the oxygen within a bulk electrolyte, and thus a thinner electrolyte layer would not result in an increased availability of oxygen over the bulk case. This result is further confirmed by the observation of samples placed at the waterline of the test solution, where the overall corrosion rates observed were comparable to those observed for completely submerged samples. Also, no increased corrosion was observed at any position of the waterline coupons, including regions close to the waterline itself.

Another result of reduced solution volume (such as would occur under the dripping scenario) is that the available anodic and cathodic surface areas are reduced, along with the spatial separation of anodic and cathodic sites. Further, in a bulk solution, the anode and cathode may be separated spatially, such that reactions occurring at the cathode do not act to alter the chemistry of the bulk electrolyte. As the volume of solution becomes small, so does the potential distance between the anodic and cathodic regions of the surface. Cathodic reactions will act to increase the pH value of the limited volume of solution, further reducing the current-delivering capacity of the cathode and significantly reducing the corrosiveness of any solution which is in contact with the waste package outer barrier.

To summarize, the experiments performed to date under bulk/immersion conditions adequately address the corrosion behavior under thin film conditions because neither the oxygen availability nor the differing wetted surface area effects would result in the total immersion condition underestimating the corrosion rate.

1.3 PHYSICAL EFFECTS OF A DRIPPING ELECTROLYTE ON THE WASTE PACKAGE OUTER BARRIER

The dripping of seepage water onto the waste package will not have a detrimental physical effect on the metal surface by disrupting the passive oxide layer on the surface via either mechanical or thermal shock. Both effects require conditions which are not representative of repository conditions. In the case of the repository, the following two considerations are relevant:

- Dripping seepage water will be close in temperature to the waste package outer barrier (e.g., temperatures are approximately 20°C apart when the peak waste package temperature is 120°C). The temperature difference between the drift wall and the waste package surface will continue to decrease with time. Under conditions when the drip shield is present, the temperature difference between the underside of the drip shield and the waste package surface will be even less than that between the drift wall and the waste package surface. As such, the thermal shock associated with seepage from the drift wall or condensation formed on the underside of the drip shield contacting the waste package will be minimal.

- The distance between the drift wall and the waste package outer barrier will be approximately 6 to 10 feet (depending on the type of waste package and the radial position where the drop lands), and the distance from the underside of the drip shield to

the waste package will be 1 to 2 feet—as such, sporadic drips (or even a steady stream of solution) will not have sufficient kinetic energy to result in physical damage of the oxide on the surface of the waste package outer barrier. Erosion corrosion due to water drop impingement is typically associated with very high-impact velocities, such as seen for a helicopter rotor striking rain drops. (ASM International 2003, p. 328)

1.4 SUMMARY

Although the dripping scenario differs from the total immersion conditions in tests used as a basis for the models presented in the SAR, such dripping conditions would not result in an increase in the observed general or localized corrosion rates. As such, the approach currently utilized in the TSPA accounts for the corrosion behavior that would be expected under dripping conditions.

2. COMMITMENTS TO NRC

None.

3. DESCRIPTION OF PROPOSED LA CHANGE

None.

4. REFERENCES

ASM International 2003, ASM Handbook Vol. 13A – Corrosion: Fundamentals, Testing, and Protection, Materials Park, OH: ASM International.

Lee, S.G. and Solomon, A.A. 2006. "Localized Corrosion of Alloy C22 Nuclear Waste Canister Material under Limiting Conditions." Materials Science and Engineering. Vol. A 434. pp. 114–123.

Farmer, J., McCright, D.; Gdowski, G.; Wang, F.; Summers, T.; Bedrossian, P.; Horn, J.; Lian, T.; Estill, J.; Lingenfelter, A.;Halsey, W. 2000. "General and Localized Corrosion of Outer Barrier of High-Level Waste Container in Yucca Mountain" Report UCRL-JC-138890, Livermore, CA: Lawrence Livermore National Laboratory.

Raghavan, M.; Mueller, R.R.; Vaughn, G.A.; and Floreen, S. 1984. "Determination of Isothermal Sections of Nickel Rich Portion of Ni-Cr-Mo System by Analytical Electron Microscopy." *Metallurgical Transactions A, 15A, (5)*, pp. 783-792. New York, New York: Metallurgical Society of American Institute of Mining, Metallurgical, and Petroleum Engineers.

SNL (Sandia National Laboratories) 2007a. *General Corrosion and Localized Corrosion of the Drip Shield.* ANL-EBS-MD-000004 REV 02 AD 01. Las Vegas, Nevada: Sandia National Laboratories. ACC: DOC.20060427.0002; DOC.20070807.0004; DOC.20071003.0019; LLR.20080423.0006.

SNL 2007b. *General Corrosion and Localized Corrosion of Waste Package Outer Barrier.* ANL-EBS-MD-000003 REV 03. Las Vegas, Nevada: Sandia National Laboratories. ACC: DOC.20070730.0003; DOC.20070807.0007; LLR.20080414.0018.

RAI: Volume 3, Chapter 2.2.1.3.1, Second Set, Number 7:

Provide additional support to show that DOE's localized corrosion initiation model appropriately accounts for the effects of planned fabrication processes on the repassivation potential of Alloy 22, including welding, solution annealing, and surface mitigation at high temperature and high chloride concentrations.

Basis: In SAR Section 2.3.6.4.4.2.1, DOE indicates that it does not adjust the localized corrosion initiation model for fabrication effects. SNL (2007, Section 6.4.6.2) indicates that in high chloride conditions, the repassivation potential for as-welded material decreases with increasing temperature more rapidly than observed for mill-annealed material. At high temperatures and high chloride concentrations representative of some early in-drift conditions, this effect may lead to lower repassivation potentials for as-welded samples than calculated by the DOE repassivation potential model. SNL (2007) states that low plasticity burnishing and/or laser shock peening would mitigate the effect of welding by increasing the repassivation potential. However, this conclusion is inconsistent with the information in SAR Section 2.3.6.4.4.2.1, which states that the repassivation potential for both welded and surface stress-mitigated samples was very similar. This requested information is needed to assess the Alloy 22 localized corrosion model in the performance assessment used to demonstrate compliance with 10CFR 63.21(c)(15) and 10CFR 63.114(f).

1. RESPONSE

The technical basis for the localized corrosion initiation model, as presented in *General Corrosion and Localized Corrosion of Waste Package Outer Barrier* (SNL 2007, Section 6.4.4), and supporting analyses are clarified and discussed herein. The model was developed using repassivation and long-term open-circuit potentials measured for Alloy 22 samples that included differing sample configurations and metallurgical conditions in a wide range of exposure environments. The effect of surface mitigation techniques is also small and well within the range of model uncertainty; therefore, no credit is taken for such techniques in the model.

1.1 A SUMMARY OF LOCALIZED CORROSION INITIATION MODEL DATA DEVELOPMENT

A series of electrochemical corrosion tests was conducted to generate the data for the localized corrosion initiation model (SNL 2007, Section 6.4.4). As illustrated in the aforementioned document, two key potentials are utilized to determine whether localized corrosion will occur. These two potentials are the open circuit potential (E_{corr}) and the repassivation potential (E_{rcrev}). The model provides that localized corrosion occurs when $E_{corr} - E_{rcrev} \geq 0$.

The repassivation potential is obtained through cyclic potentiodynamic polarization (CPP) experiments. A series of CPP tests was performed for Alloy 22 samples over a wide range of exposure conditions. Included in the tests were a variety of solution chemistries, exposure temperatures, sample geometries, and metallurgical conditions (i.e., mill-annealed and

as-welded) (SNL 2007, Section 6.4.4.2). Solution chemistries included a series of chloride and chloride + nitrate salt solutions at concentrations up to near saturation. Only data obtained at test temperatures of 120°C or below were used, as seepage cannot occur until the drift wall temperature is below 100°C, corresponding to a waste package surface temperature of 120°C (SAR Section 2.3.6.4.4.1). Furthermore, as a conservative measure, only experiments where the onset of localized corrosion was verified with either optical or scanning electron microscopy were used to develop the model. In other words, if a sample did not undergo localized corrosion, the potential corresponding to the onset of transpassive dissolution was not used in place of the repassivation potential, as this would render the mean critical potential more positive under such situations. The details of the effects of high temperatures and solution compositions are displayed in *General Corrosion and Localized Corrosion of Waste Package Outer Barrier* (SNL 2007, Figures 6-31 and 6-32).

Section 6.4.6.2 of *General Corrosion and Localized Corrosion of Waste Package Outer Barrier* (SNL 2007) notes that as the temperature increases for high-chloride solutions, the E_{rcrev} becomes more negative, and that this effect is more pronounced for as-welded material than for mill-annealed material. The data summarized by Evans et al. (2005, Table 1) shows that for a high-chloride solution (5 M $CaCl_2$), as the temperature is increased from 45°C to 120°C, the repassivation potential for as-welded and mill-annealed both become more negative, and more importantly, that they are virtually indistinguishable from one another. In addition, careful inspection of repassivation data as a function of chloride concentration (see SNL 2007, Appendix IX) reveals that the majority of the E_{rcrev} data, and particularly the lower bound for both metallurgical conditions, are nominally identical. Thus, the welding process does not result in a more pronounced reduction in E_{rcrev} with increasing temperature, and the E_{rcrev} for the two metallurgical conditions are nominally identical.

The second critical potential utilized by the localized corrosion model, the open-circuit potential (E_{corr}), was obtained through a series of long-term exposure tests. These experiments were performed under conditions similar to those utilized in establishing the repassivation potential. Open-circuit potentials were measured for both as-welded and mill-annealed samples, the results of which are presented in *General Corrosion and Localized Corrosion of Waste Package Outer Barrier* (SNL 2007, Figures 6-38 to 6-40). As illustrated by those figures, there is no significant difference in open-circuit potential between the as-welded and mill-annealed samples as a function of chloride concentration (0 to 12 molal), nitrate concentration (from 0.001 to 10 molal), or solution pH (2 to 10).

In summary, it has been experimentally verified that as-welded and mill-annealed Alloy 22 exhibit nominally identical behaviors to one another in terms of parameters relevant to the localized corrosion model (i.e., E_{corr} and E_{rcrev}). In constructing the localized corrosion model, data from both metallurgical conditions were utilized interchangeably. As such, the localized corrosion model captures the behavior of Alloy 22 in all relevant metallurgical conditions under repository-relevant environmental conditions.

1.2 AN ASSESSMENT OF THE EFFECT OF SURFACE MITIGATION ON THE REPASSIVATION POTENTIAL OF ALLOY 22

The welding process may introduce surface stresses upon the closure weld, which could be potentially detrimental with regard to stress corrosion cracking. In order to mitigate the impact of these stresses, low-plasticity burnishing (LPB) of the closure weld will be performed (laser shock peening will not be used). The LPB process will introduce compressive stresses near the surface, which mitigates the potentially detrimental stresses relative to stress corrosion crack initiation. Examination of Figures 6-58 and 6-59 of *General Corrosion and Localized Corrosion of Waste Package Outer Barrier* (SNL 2007) indicates that LPB only increases the repassivation potential by 10 to 25 mV in a 6-molal chloride solution at 100°C (a more aggressive environment than the waste packages will experience especially considering drip shields), which is well within two standard deviations of the measurement uncertainty. In other words, the impact of LPB surface mitigation on E_{rcrev} is negligible compared to measurement uncertainty, and thus credit is not taken in the model for this effect.

2. COMMITMENTS TO NRC

None.

3. DESCRIPTION OF PROPOSED LA CHANGE

None.

4. REFERENCES

Evans, K.J., A. Yilmaz, S.D. Day, L.L. Wong, J.C. Estill, and R. Rebak. 2005. "Using Electrochemical Methods to Determine Alloy 22's Crevice Corrosion Repassivation Potential." *Journal of Metals*. Jan. pp. 56-61.

SNL (Sandia National Laboratories) 2007. *General Corrosion and Localized Corrosion of Waste Package Outer Barrier*. ANL-EBS-MD-000003 REV 03. Las Vegas, Nevada: Sandia National Laboratories. ACC: DOC.20070730.0003.

RAI: Volume 3, Chapter 2.2.1.3.1, Second Set, Number 8:

Provide additional technical basis to show that the effects of chloride or nitrate on crevice corrosion (SAR Figures 2.3.6-24 and 2.3.6-26) are supported by available experimental evidence in the literature.

Basis: The results of the localized corrosion repassivation potential model described in SAR Section 2.3.6.4.3.1.2 indicate that at pH 7, as chloride concentration is increased or the nitrate concentration is decreased, the localized corrosion susceptibility decreases. However, some published experimental investigations show opposite trends (Dunn, et al., 2005; King, et al., 2005). In these experiments, higher chloride concentrations increase crevice corrosion susceptibility, whereas higher concentrations of nitrate decrease crevice corrosion susceptibility of Alloy 22. This published information was not considered by DOE in developing the technical basis to support the evaluation of crevice corrosion. The requested information is needed to assess the potential effects of crevice corrosion in the performance assessment used to demonstrate compliance with 10 CFR 63.21(c)(15) and 63.114 (f).

1. RESPONSE

An examination of the localized corrosion model equations demonstrates that in general as the nitrate chloride ratio increases the probability of localized corrosion decreases. This is illustrated in SAR Figure 2.3.6-27. SAR Figures 2.3.6-24 and 2.3.6-26 present the localized corrosion model predictions that suggest the potential for localized corrosion of Alloy 22 decreases with a decrease in the ratio of nitrate to chloride. The intersection of the E_{rcrev} and E_{corr} curves does not establish whether localized corrosion will take place; rather the curves represent the probability of localized corrosion taking place as explained in Section 1.2 of this response. Thus, while the figures indicate a slight change in the voltage separation between the open-circuit potential and repassivation potential, the model still predicts a certain probability of localized corrosion taking place in both of the aforementioned cases. Therefore, experimental observations as noted by Dunn (2005) and King (2005) of localized corrosion taking place in a region where the curves have crossed are consistent with the model presented in the SAR.

1.1 RELEVANT CONSERVATISMS OF THE LOCALIZED CORROSION MODEL PRESENTED IN SAR SECTION 2.3.6

The waste package outer barrier (WPOB) crevice corrosion initiation model presented in *General Corrosion and Localized Corrosion of Waste Package Outer Barrier* (SNL 2007) is used to evaluate the crevice corrosion initiation behavior of the Alloy 22 WPOB. Localized corrosion of the WPOB is considered to initiate when the open-circuit corrosion potential (E_{corr}) is equal to or greater than a critical potential (the crevice repassivation potential [E_{rcrev}] in the current model), that is, ΔE ($E_{rcrev} - E_{corr}$) ≤ 0 (SNL 2007, Section 6.4.4.3). In constructing the model for the crevice repassivation potential, only specimens which underwent localized corrosion were utilized. This is conservative because, in many instances, only a subset of the samples underwent localized corrosion for a given environment. To ensure that the contribution

of those samples that underwent localized corrosion was not deemphasized, the samples that did not undergo localized corrosion were removed from the distribution.

If the exposure temperature is greater than or equal to 20°C and less than or equal to 120°C, then the WPOB crevice corrosion initiation model is implemented. If crevice corrosion is determined to initiate, then crevice corrosion is assumed to occur at a constant rate throughout the simulation period regardless of changes in the bulk chemical exposure environment. This is a conservative modeling assumption and is used because the crevice corrosion model does not account for the possibility of crevice corrosion repassivation or stifling.

Nitrate ions inhibit localized corrosion initiation (SNL 2007, Section 6.4.4.3). In addition, carbonate and sulfate ions may have an inhibitive effect on localized corrosion. Therefore, because only nitrate ions are accounted for in the model, the results for solutions with significant amounts of other potentially inhibitive ions in addition to nitrate ions are conservatively modeled. The model results reflecting the beneficial effects of the inhibitive ions (nitrate, in this case), combined with alkaline pH conditions of the typical carbonate-containing waters in the repository are consistent with the experimental observations on the immunity of Alloy 22 to localized corrosion in those waters (SNL 2007, Section 7.2.3).

1.2 SUMMARY OF DATA OF INTEREST IN SAR SECTION 2.3.6

As illustrated by SAR Figures 2.3.6-24 and 2.3.6-26, model predictions suggest the probability for localized corrosion initiation on Alloy 22 decreases with a decrease in the ratio of nitrate to chloride. In the aforementioned figures, this is manifested as an apparent increase in the voltage difference between the repassivation potential and the open-circuit potential as the concentration of chloride increases (SAR Figure 2.3.6-24) and the concentration of nitrate decreases (SAR Figure 2.3.6-26). With respect to each figure:

- *SAR Figure 2.3.6-24*: In this figure, the open circuit and repassivation potentials are shown for Alloy 22 at a temperature of 90°C in pH 7 solutions containing 3 m (moles per kg H_2O) nitrate and varying quantities of chloride (from 0 to 25 m). As the chloride concentration increases, the +2 standard deviation curve of the open-circuit potential crosses the −2 standard deviation curve of the repassivation potential at a concentration of approximately 7.5 m. As the chloride concentration increases, the separation between these two curves (i.e., $E_{rcrev} - E_{corr}$) also increases, becoming approximately 100 mV at a chloride concentration of 25 m.

- *SAR Figure 2.3.6-26*: In this figure, the open-circuit and repassivation potentials are shown for Alloy 22 at a temperature of 90°C in pH 7 solutions containing 6 m chloride and varying quantities of nitrate (0 to 6 m). As the nitrate concentration is increased, the +2 standard deviation curve of the open-circuit potential crosses the −2 standard deviation curve of the repassivation potential at a concentration of approximately 2.5 m. As the nitrate concentration continues to increase, the separation (i.e., $E_{corr} - E_{rcrev}$) also continues to increase, reaching approximately 50 mV at 6 m nitrate. It should be noted that these two curves are nearly parallel—at 0 m nitrate, the separation is approximately 20 mV in the opposite direction (i.e., $E_{corr} \approx E_{rcrev} + 20$ mV).

Although the two figures appear to illustrate a counterintuitive result, several aspects of the data must be considered. First, the crossing is at the second standard deviation, and these curves represent the 95th percentile of the data (assuming a normal distribution). As such, the intersection of these two curves does not establish whether localized corrosion can take place, rather they illustrate the probability of localized corrosion taking place. Secondly, the voltage difference only provides information on the driving force for a reaction to occur and does not describe the kinetics of the reaction. In other words, a specific positive or negative potential difference does not correspond to a specific rate. While the figures do illustrate a slight change in the voltage separation between the open-circuit potential and repassivation potential, the model still predicts a certain probability of localized corrosion taking place in both of the aforementioned cases. Thus, experimental observations of localized corrosion taking place in a region where the curves have crossed, as illustrated above, are consistent with the model presented in the SAR.

1.3 CONSIDERATION OF THE RESULTS PRESENTED IN KING ET AL. (2005) AND DUNN ET AL. (2005)

In the basis statement, two literature sources are referenced – King et al. (2005) and Dunn et al. (2005). It is stated that this information was not considered by DOE in developing the technical basis to support the evaluation of crevice corrosion. In fact, the references were used in the construction of the model and the use of these references is described in the two following sections.

1.3.1 Literature Results From King et al. (2005)

King et al. (2005) was used in Appendix VIII of *General Corrosion and Localized Corrosion of Waste Package Outer Barrier* (SNL 2007). In terms of relevance to the localized corrosion model, King et al. (2005) presents long-term open-circuit potential data (E_{corr}) for Alloy 22 in a series of environments, which represent a subset of the information used in the assembly of the localized corrosion model. As an example, Appendix VIII of *General Corrosion and Localized Corrosion of Waste Package Outer Barrier* (SNL 2007) lists many of the sample identification numbers. Thus, the data presented by King et al. (2005) has been considered by the DOE, and is already incorporated into the localized corrosion model.

1.3.2 Literature Results From Dunn et al. (2005)

Dunn et al. (2005) presents a model to assess the potential for localized corrosion of Alloy 22 under various repository-relevant conditions. This model was used as part of the validation exercise performed in *General Corrosion and Localized Corrosion of Waste Package Outer Barrier* (SNL 2007), in which values calculated using the model generated by Dunn et al. (2005) are compared directly to the results from the model utilized by TSPA (SNL 2007, Table 7-4). Crevice repassivation potential data presented in Table 7-4 of *General Corrosion and Localized Corrosion of Waste Package Outer Barrier* (SNL 2007) demonstrates that the model utilized by TSPA conservatively captures the results from Dunn et al. (2005).

2. COMMITMENTS TO NRC

None.

3. DESCRIPTION OF PROPOSED LA CHANGE

None.

4. REFERENCES

Dunn, D.S., O. Pensado, G.A. Cragnolino. 2005. "Performance Assessment of Alloy 22 as a Waste Package Outer Barrier." CORROSION 2005. Paper No. 05588. Houston, Texas: NACE International.

King, K.J., J.C. Estill, G.A., Hust, M.L., Stuart, and R.B. Rebak. 2005. "Evolution of the Corrosion Potential and Corrosion Rate for Alloy 22 in Chloride plus Nitrate Brines." CORROSION 2005. Paper No. 05607. Houston, Texas: NACE International.

SNL (Sandia National Laboratories) 2007. *General Corrosion and Localized Corrosion of Waste Package Outer Barrier*. ANL-EBS-MD-000003 REV 03. Las Vegas, Nevada: Sandia National Laboratories. ACC: DOC.20070730.0003; DOC.20070807.0007; LLR.20080414.0018.

RAI: Volume 3, Chapter 2.2.1.3.1, Second Set, Number 9:

Provide additional justification for the assumption that the repassivation potential is not underestimated by using the cyclic potentiodynamic polarization (CPP) method rather than an alternative method such as the Tsujikawa-Hisamatsu Electrochemical (THE) method.

Basis: DOE has used CPP testing to determine the localized corrosion repassivation potential, as described in SAR Section 2.3.6.4.2.2. Evans, et al. (2005) indicated that the CPP method can provide different results than the THE method, which is inconsistent with the justification in SNL (2007, Section 6.4.4.1) for using the CPP method. Additional information is needed to assess the use of the repassivation potential data in the performance assessment used to demonstrate compliance with 10 CFR 63.21(c)(15) and 63.114(b).

1. RESPONSE

For all measurements used in the development of the localized corrosion model, the cyclic potentiodynamic polarization (CPP) method yielded results which were equivalent to those obtained via the Tsujikawa-Hisamatsu Electrochemical (THE) method.

In the cyclic potentiodynamic polarization (CPP) method, the potential is swept in the positive direction until localized corrosion has initiated, then in the negative direction until it has repassivated. The point at which the reverse scan intersects the forward scan represents the repassivation potential. The second is the Tsujikawa-Hisamatsu Electrochemical (THE) method, in which a potentiodynamic scan in the positive direction is used to initiate localized corrosion; the active crevice corrosion site is then allowed to propagate at a fixed rate (i.e., galvanostatically), and then the potential is gradually moved stepwise in the negative direction until repassivation takes place. This technique has recently been formalized, and is described in detail in ASTM specification G192-08 (ASTM 2008)—as such, it will hereinafter be referred to as the "G192 technique". In simple terms, the G192 technique can be thought of as an extremely slow swept potential technique, where the potential is swept 10 mV every two hours, yielding an effective scan rate of 0.0014 mV/s—considerably slower than the scan rate of 0.1667 mV/s, used in the CPP experiments. This greatly reduced scan rate has a number of implications on the critical potential determined via the G192 technique. In both cases, physical evaluation of the resulting surface is required to visually verify that localized corrosion has indeed taken place.

As discussed by Evans et al. (2005), the CPP technique generally yields a more conservative (i.e., less positive) result for the repassivation potential in aggressive conditions. However, in benign conditions, the G192 technique yields a less positive critical potential due to the lower effective scan rate. Overall, however, the two techniques yield results which are close to one another. This is illustrated in Figure 12 of the journal article by Evans et al. (2005) where an empirical fit to the repassivation potential established via CPP is plotted along with the results taken from the G192 technique. As can be seen in the figure, the results are nominally identical for chloride solutions ranging from a relatively benign 1 mM up to a more concentrated 1 M

solution. Evans then went on to compare their results to data taken from the literature (Evans et al. 2005, Figure 13) where the results of the CPP and G192 experiments performed by Evans et al. (2005) yielded much less positive repassivation potentials than the literature values, which are conservative. Though the exact reason for this discrepancy was not determined, Evans et al. (2005) put forth the reasonable hypothesis that, "The discrepancy in the data could be related to the different nature and geometry (tightness) of the crevice former devices used in both sets of data."

To summarize, valid comparison of the results from the CPP and G192 techniques requires consideration of the materials and geometries being evaluated, as well as physical examination of the surface to determine if localized corrosion did in fact occur, and that any observed current was not the result of other processes, such as transpassive dissolution. The repassivation potential is not underestimated by using the CPP method compared to the G192 technique. For specimens of nominally the same geometry and base material, the results from the G192 and CPP techniques were nominally identical in determining the crevice repassivation potential over the range of conditions expected to exist in the repository. This was demonstrated by Evans et al. (2005) for Alloy 22 in chloride-bearing solutions ranging from 1 mM to 1 M in concentration. Thus, the CPP method does not underestimate the repassivation potential of localized corrosion used in the performance assessment.

2. COMMITMENTS TO NRC

None.

3. DESCRIPTION OF PROPOSED LA CHANGE

None.

4. REFERENCES

ASTM 2008. "Standard Test Method for Determining the Crevice Repassivation Potential of Corrosion-Resistant Alloys Using a Potentiodynamic-Galvanostatic-Potentiostatic Technique", Document No. G192-08. West Conshohocken, PA: ASTM International.

Evans, K.J., A. Yilmaz, S.D. Day, L.L. Wong, J.C. Estill, and R. Rebak. 2005. "Using Electrochemical Methods to Determine Alloy 22's Crevice Corrosion Repassivation Potential." *Journal of Metals*. Jan. pp. 56-61.

SNL (Sandia National Laboratories) 2007. *General Corrosion and Localized Corrosion of Waste Package Outer Barrier*. ANL-EBS-MD-000003 REV 03. Las Vegas, Nevada: Sandia National Laboratories. ACC: DOC.20070730.0003; DOC.20070807.0007; LLR.20080414.0018.

RAI Volume 3, Chapter 2.2.1.3.1, Second Set, Number 10:

Provide additional support for the treatment of the effects of microbially influenced corrosion (MIC) on Alloy 22 corrosion demonstrating:

- the enhancement factor used in the general corrosion model that appropriately accounts for the effects of MIC
- the technical basis for excluding microbially induced localized corrosion

Basis: DOE accounts for the effects of MIC on general corrosion by applying an enhancement factor of between 1 and 2 to Alloy 22 general corrosion rates for high relative humidities (SAR, Section 2.3.6.3.3.2). Results from scanning electron microscopy in SNL (2007, Section 6.4.5) show that test coupons that were exposed in nonsterile microcosm reactors for 57 months were clearly corroded (i.e., clear reduction of overall surface roughness), whereas the test coupons that were exposed to sterile microcosm reactors for 43 months showed no sign of corrosion (i.e., with clearly visible machining marks identical to that of the un-exposed coupons). These results may indicate that the effects of MIC on Alloy 22 general corrosion rates may be greater than a factor of two, as concluded in SNL (2007, Section 6.4.5) using electrochemical linear polarization resistance techniques in relatively short-term experiment (5 months). This requested information is needed to evaluate the use of Alloy 22 general corrosion rates in the performance assessment used to demonstrate compliance with 10 CFR 63.114(b).

DOE did not consider MIC effect on localized corrosion (SAR, 2.3.6.4). Alloy 22 test coupons that were incubated in nonsterile microcosm reactors developed micropits on the surface (SNL, 2007, Section 6.4.5). These micropits appear to have morphologies that are distinct from surface features associated with general corrosion. DOE did not provide a technical basis to explain why these micropits will not continue to propagate with time. This requested information is needed to evaluate the localized corrosion of Alloy 22 in the performance assessment used to demonstrate compliance with 10 CFR 63.114(f).

1. RESPONSE

Due to the nature of the in-drift environment, microbial activity in the repository will be severely limited and its impacts on the environment on the waste package surface, and hence any corrosion processes which may take place, are expected to be insignificant. An experimental program was conducted to establish if bacteria taken from the Yucca Mountain could result in enhanced dissolution of Alloy 22 under conditions which were highly conducive to bacterial growth (e.g., unlimited moisture, low temperature, and ample nutrients). While these environments are not repository relevant, some increased corrosion was observed. As such, DOE has conservatively incorporated a microbiologically induced corrosion (MIC) amplification factor which is applied to the general corrosion rate at the patch level (SAR Section 2.3.6.3.3.2).

It is appropriate to treat this increased corrosion as general corrosion rather than localized corrosion, because as discussed below the observed increased corrosion is distributed across the surface with no evidence of propagation.

1.1 THE ENVIRONMENTAL CONDITIONS AT YUCCA MOUNTAIN EFFECTIVELY INHIBIT MICROBIALLY INFLUENCED CORROSION

Microorganisms can be categorized into one of two broad groups based on different nutritional requirements as discussed in *Evaluation of Potential Impacts of Microbial Activity on Drift Chemistry* (BSC 2004, Section 7.1):

- Heterotrophs, which use organic carbon compounds as their energy source
- Autotrophs, which derive their metabolic energy from the oxidation of inorganic compounds and cell carbon from CO_2.

The in-drift environment at Yucca Mountain particularly the near absence of suitable nutrient sources will severely limit the development of both groups of microorganisms (SNL 2007, Section 6.4.5; SAR Section 2.3.6.3.3.2). With regard to heterotrophs, the repository supply of phosphate and organic carbon will be extremely low. For instance, Yucca Mountain groundwater contains only trace concentrations of these substances (SAR Section 2.3.6.3.3.2). Autotrophic microbial growth will be similarly limited due to the absence of available inorganic electron donors in the oxic repository environment. Additional factors which will inhibit the growth of microorganisms in the repository include the limited availability of water, as discussed in SAR Section 2.3.6.3.3.2, particularly during the thermal pulse (just after repository closure) when the relative humidity is low. Any potentially corrosive or nutrient containing seepage waters that may be in the drift will be prevented from contacting the waste package surface due to the presence of the drip shields, which will remain intact for much longer than 10,000 years. Although condensation on the underside of the drip shield is not anticipated (SNL 2008, FEP 2.1.08.14.0A), if it were to occur and contact the waste package surface, the condensate would have a composition similar to rain water (i.e., a very dilute solution of carbonic acid, pH ~ 5.6 with an extremely low dissolved ionic content and negligible chloride concentration) (SNL 2008, FEP 2.1.08.14.0A). Although the condensate could mix with the extremely small quantities of concentrated brines formed by deliquescence of salts in dust on the waste package, as described in excluded FEP 2.1.09.28.0B (SNL 2008), the quantities of these brines will be extremely low. Due to the aforementioned environmental constraints, microbial activity in the repository will be severely limited, therefore its impacts on drift chemistry and, subsequently, the environment on the waste package are expected to be insignificant, as discussed in SAR Section 2.3.6.3.3.2.

A recent, extensive review of the potential for deleterious MIC effects on nuclear waste containers in geological repositories including Yucca Mountain (King 2009) concluded that there is a large body of evidence to indicate that a number of factors result in deep geological repositories being hostile environments for microbial growth.

1.2 EXPERIMENTAL STUDIES CHARACTERIZING EFFECTS OF MICROBES ON ALLOY 22 CORROSION

1.2.1 Characterization of Temperature and Humidity Conditions for Biofilm Formation on Non-Immersed Alloy 22 Specimens

Biofilms can create microenvironments (variations in pH, nutrient concentrations, and oxygen levels) on a substrate (Else et al. 2003). As indicated in *General Corrosion and Localized Corrosion of Waste Package Outer Barrier* (SNL 2007, Section 6.4.5.1), most microbes can thrive only when the relative humidity is above 90%, although some microbes can be active at relative humidities as low as 75%. In a study to define the effects of temperature and humidity on biofilm formation on Alloy 22 (Else et al. 2003), specimens embedded in crushed Yucca Mountain repository tuff rock (without added nutrients) were placed in chambers along with bacterial microcosms at specific relative humidity and temperature values. Bacteria studied included native microorganisms from the subsurface at Yucca Mountain. Else et al. (2003) found that 100% relative humidity and 30°C (the lowest temperature studied) were the optimal conditions for bacterial attachment and biofilm formation. It was shown that as temperature increases (to 60°C or 70°C) or as relative humidity decreases below 100%, biofilm formation on Alloy 22 specimen surfaces was impeded. For instance, at 30°C, and at relative humidity values ranging from 32% to 84%, culturable counts after 12 months of exposure were below or near the minimum level of detection. The study concluded that the boundary conditions for microbe colonization on Alloy 22 surfaces required 100% relative humidity and 30°C for even minimal biofilm production after up to 18 months of exposure. Under these optimal conditions, the bacterial cell count (heterotropic plate count) was only about 500 per specimen. No surface attack was noted by scanning electron microscopy (SEM) examination of specimens exposed under these conditions. Thus, the use of test results obtained at low temperatures is conservative when applied to time domains when the waste package surface is at higher temperatures and/or lower relative humidities.

1.2.2 Effect of Yucca Mountain Bacteria on Long-Term Corrosion of Alloy 22 under Fully Immersed, Nutrient-Rich Environments

A series of experimental studies were performed utilizing bacteria taken from the Yucca Mountain site to establish if they could impact the corrosion behavior of Alloy 22 under conditions which promoted bacterial growth. While these results are from non-repository relevant conditions, they served to provide some insight into the capability of bacteria present at the Yucca Mountain site to influence corrosion processes under ideal growth conditions.

It has been shown that Yucca Mountain bacteria may enhance the general corrosion rate of Alloy 22 if the bacteria are provided sufficient nutrients and favorable exposure conditions. As discussed in SAR Section 2.3.6.3.2.3, a series of 12 strains of Yucca Mountain bacteria, including acid and slime producers, sulfate reducers, and iron oxidizers, were cultured from material taken from the Yucca Mountain site. The growth medium was supplemented with 100× concentrated simulated J-13 well water, 0.5% glucose, and 0.75% protease peptone. The Alloy 22 disc test specimens received in the mill-annealed condition were wet polished through 600-grit abrasive paper, cleaned with acetone and distilled water, and then sterilized by

autoclaving. Specimens for corrosion rate evaluation were fully immersed in the nutrient-rich solution and sterilized control solution at room temperature (about 22°C) for about 160 days. No localized corrosion was observed on any of the specimens. The degree of electrochemical activity on the Alloy 22 surface was assessed via polarization resistance measurements. The conservative assumption was made that all observed activity was the result of metal oxidation, even though some of the measured current may result from oxidation of reducing species produced by microbial activity (Yang et al. 2004). The Alloy 22 general corrosion rates calculated by making this assumption for samples in bacterially active environments were found to be about twice those of Alloy 22 specimens immersed in the sterile control solutions.

Electrochemical corrosion rate results were also obtained using the polarization resistance technique in a companion study on welded Alloy 22 specimens exposed to 100× J-13 water plus 0.1% glucose at ambient temperature (SAR Section 2.3.6.3.2.3). The testing was carried out in Yucca Mountain microorganism-inoculated and sterile environments for 70 to 125 days at room temperature. Corrosion rates obtained for welded specimens in nonsterile environments were only slightly higher than those in sterile environments and were consistent with the enhancement factor of, at most, two obtained from the nonwelded specimen data shown in SAR Table 2.3.6-3. Because the data in these studies using polarization resistance measurements were obtained in a nutrient-rich environment, the effects of microbial activity on corrosion rates in these tests are expected to be greater than they will be in the repository environment, which is expected to be limited by the factors discussed above and in SAR Section 2.3.6.3.3.2. Therefore, the effects of data uncertainty are adequately and conservatively represented in the MIC model.

In another study (Martin et al. 2004), Alloy 22 specimens were exposed at room temperature or 30°C with sterile or nonsterilized (supplemented with 0.1% glucose) Yucca Mountain tuff rock in simulated concentrated (10×) groundwater for almost 5 years. Alloy 22 specimens from microcosms held at 30°C were withdrawn, cleaned, and imaged using SEM. An unreacted Alloy 22 specimen was also cleaned in the same manner and imaged for comparison. Specimens incubated in the nonsterile microcosm reactors showed the development of micropores, primarily along the ridges formed by polishing, while specimens incubated in sterile microcosms and the unreacted specimen showed no evidence of micropore formation after one cleaning cycle (although repeated cleaning cycles resulted in formation of micropores). The micropores appeared uniform in shape except where they had grown together and ranged in size from 0.2 to 0.7 μm in diameter.

In this same study (Martin et al. 2004), Alloy 22 specimens exposed at room temperature (~22°C) to nutrient-enriched microbial environments for 17, 32, and 57 months also showed the presence of micropores (before and after cleaning). Similar behavior was not seen in sterile controls after 43 months of exposure. The observed micropores were of similar size (less than 1 μm in diameter) to those seen at 30°C; however, they were more numerous and not restricted to polishing ridges. Martin et al. (2004, Figures 7, 8, and 9) showed that the micropores formed during 17 months of exposure (the earliest time analyzed) have similar diameters as those formed during 34 and 57 months of exposure. This suggests that the micropores did not grow significantly during the 40-month period between 17 and 57 months of exposure, though new micropores may have nucleated. If these micropores were pits, then the lack of growth indicates

that once initiated, they were only able to propagate briefly before the local electrochemical conditions resulted in their repassivation.

1.2.3 Characterization of Bacteria Present in Long-Term Corrosion Test Facility Tanks

The Alloy 22 general corrosion rate distribution used in the TSPA is based on the measured weight loss of specimens exposed for about five years in the Long-Term Corrosion Test Facility (LTCTF). As discussed in *Microbial Effects on Nuclear Waste Packaging Materials* (Horn et al. 2005, Section 3), while microorganisms were not intentionally introduced into the LTCTF tanks, they were open to the laboratory environment. The microbial concentrations in several LTCTF tanks were evaluated. The tank test environments sampled for bacterial cell density counts included 60°C and 90°C; 1,000× J-13 groundwater, pH ~10.3 (simulated concentrated water (SCW)); 60°C; 1,000× J-13 groundwater, pH ~2.8 (simulated acidified water (SAW)); 60°C and 90°C, 10× J-13 groundwater, pH ~10.1 (simulated diluted water (SDW)). The greatest concentrations of microbes were found in the SDW tank at 60°C (4.6×10^6 cells/ml) and the lowest microbe concentrations were found in the SAW tank at 60°C (1.3×10^4 cells/ml) . For comparison, measurements of Yucca Mountain aerobic bacteria in 1× J-13 well waters at room temperature without glucose additions (about 5×10^6 cells/ml) were similar to the measured values in the 60° SDW tank (4.6×10^6 cells/ml). The composition of the microbial communities in three tanks was determined using direct DNA extraction of tank waters and swabs. Each 60°C tank was found to contain a different community of organisms, indicating the specimens were exposed to a range of different microbes. Among the bacteria detected in the tanks was *Thermus thermophilus*. The potential for thermophillic microorganisms, which can be active at 60°C and above, has been evaluated (Yang et al. 2004, Section 4.1.3) and could result in accelerated corrosion of nickel at 60°C. The presence of microbes including *Thermus thermophilus*, in the LTCTF tanks at 60°C and 90°C suggests that microbial effects at these temperatures may be included in the base Alloy 22 general corrosion rate.

1.3 TSPA TREATMENT OF MIC EFFECTS ON ALLOY 22 CORROSION

While no significant bacterial activity, and hence no microbiologically influenced corrosion, is anticipated to occur on the waste package surface, bacterial species taken from the Yucca Mountain site were observed to impact the corrosion behavior of Alloy 22 under conditions conducive to their growth. As a result, despite the fact that the latter observations were from non-repository relevant conditions, the DOE has conservatively added an amplification factor to the general corrosion rate to account for MIC.

As the damage observed in the studies described above was confined to the surface of the Alloy 22 specimens, an amplification factor applied directly to the abiotic general corrosion rate was determined to be the most appropriate method to account for such attack.

As discussed in SAR Section 2.3.6.3.3.2, the MIC enhancement factor, uniformly distributed between 1 and 2, is applied on the general corrosion rate when the relative humidity at the waste package outer corrosion barrier surface is above a threshold value of 75% to 90% (sampled uniformly) irrespective of the exposure temperature. The variation in the enhancement factor is attributed to variability across the waste package outer corrosion barrier surface. As discussed in

SAR Section 2.4.2.3.2.1.5, because sampling of the Alloy 22 general corrosion rates and the microbial enhancement factor occurs over the entire waste package surface of about 1,400 patches (subareas), the extremes of the sampled distribution of corrosion rates (equivalent to the 99.9th percentile value) will be sampled for at least one patch on each waste package. It is these maximum or near-maximum values of general corrosion rates, when combined with the thermal dependency of the general corrosion rate, the microbially influenced corrosion enhancement factor, and the thermal history that waste packages experience, that determine the time of first patch penetration of the waste package outer corrosion barrier.

1.4 SUMMARY AND CONCLUSIONS

The in-drift environment at Yucca Mountain will severely limit the development of microorganisms (SNL 2007, Section 6.4.5; SAR Section 2.3.6.3.3.2). Considering the highly stable passive film formed on Alloy 22 and the near absence of biological activity anticipated on the waste package surface, MIC is not expected to occur. As such, there is no impact anticipated from biological activity on either general or localized corrosion. A series of experiments performed under non-repository relevant conditions, using bacteria taken from the Yucca Mountain site, revealed that under conditions which promoted their growth, they were able to impact metal oxidation in the form of either enhanced electrochemical activity or the formation of micropores. As a result, the DOE has conservatively applied an amplification factor to the general corrosion model utilized by the TSPA. It is appropriate to treat this increased corrosion as general corrosion rather than localized corrosion, because the observed increased corrosion is distributed across the surface with no evidence of propagation.

2. COMMITMENTS TO NRC

None.

3. DESCRIPTION OF PROPOSED LA CHANGE

None.

4. REFERENCES

ASTM G 59-97. 1998. *Standard Test Method for Conducting Potentiodynamic Polarization Resistance Measurements*. West Conshohocken, Pennsylvania: American Society for Testing and Materials.

BSC (Bechtel SAIC Company) 2004. *Evaluation of Potential Impacts of Microbial Activity on Drift Chemistry*. ANL-EBS-MD-000038 REV 01. Las Vegas, Nevada: Bechtel SAIC Company. ACC: DOC.20041118.0005; DOC.20050505.0001; LLR.20080324.0016; DOC.20080814.0002; DOC.20050609.0001.

Else, T.A.; Pantle, C.R.; and Amy, P.S. 2003. "Boundaries for Biofilm Formation: Humidity and Temperature." *Applied and Environmental Microbiology, 69*, (8), 5006-5010. Washington, D.C.: American Society for Microbiology.

Horn, J.; Martin, S.; Carrillo, C.; and Lian, T. 2005. *Microbial Effects on Nuclear Waste Packaging Materials*. UCRL-TR-213915 Rev. 1. Livermore, California: Lawrence Livermore National Laboratory. ACC: MOL.20050728.0312

King, F. 2009. "Microbially Influenced Corrosion of Nuclear Waste Containers." *Corrosion, 65* (4), 233-251. Houston, Texas: National Association of Corrosion Engineers.

Martin, S.; Horn, J.; and Carillo, C. 2004. "Micron-Scale MIC of Alloy 22 After Long Term Incubation in Saturated Nuclear Waste Repository Microcosms." *Corrosion/2004, 59th Annual Conference & Exposition, March 28–April 1, 2004, New Orleans.* Paper No. 04596. Houston, Texas: NACE International.

SNL (Sandia National Laboratories) 2007. *General Corrosion and Localized Corrosion of Waste Package Outer Barrier*. ANL-EBS-MD-000003 REV 03. Las Vegas, Nevada: Sandia National Laboratories. ACC: DOC.20070730.0003; DOC.20070807.0007; LLR.20080414.0018.

SNL 2008. *Features, Events, and Processes for the Total System Performance Assessment: Analyses*. ANL-WIS-MD-000027 REV 00. Las Vegas, Nevada: Sandia National Laboratories. ACC: DOC.20080307.0003; DOC.20080407.0009; LLR.20080522.0166; DOC.20080722.0002.

Yang, L.; Birnbaum, S.; and Cragnolino, G.A. 2004. *Microbially Influenced Corrosion Studies of Engineered Barrier System Materials*. CNWRA 2005-01. San Antonio, Texas: Center for Nuclear Waste Regulatory Analyses. ACC: MOL.20070303.0228.

QA: N/A

UCRL-TR-213915 Rev. 1

LAWRENCE
LIVERMORE
NATIONAL
LABORATORY

Microbial Effects on Nuclear Waste Packaging Materials

Joanne Horn, Sue Martin, Celena Carrillo, and Tiangan Lian

September 15, 2005

Disclaimer

This work was performed under the auspices of the U.S. Department of Energy by University of California, Lawrence Livermore National Laboratory under Contract W-7405-Eng-48.

Contents

1. Introduction

Microorganisms may enhance corrosion of components of planned engineered barriers within the proposed nuclear waste repository at Yucca Mountain (YM). Corrosion could occur either directly, through processes collectively known as Microbiologically Influenced Corrosion (MIC), or indirectly, by adversely affecting the composition of water or brines that come into direct contact with engineered barrier surfaces. Microorganisms of potential concern (bacteria, archea, and fungi) include both those indigenous to Yucca Mountain and those that infiltrate during repository construction and after waste emplacement.

Specific aims of the experimental program to evaluate the potential of microorganisms to affect damage to engineered barrier materials include the following:

Indirect Effects

- Determine the limiting factors to microbial growth and activity presently in the YM environment.
- Assess these limiting factors to aid in determining the conditions and time during repository evolution when MIC might become operant.
- Evaluate present bacterial densities, the composition of the YM microbial community, and determining bacterial densities if limiting factors are overcome. During a major portion of the regulatory period, environmental conditions that are presently extant become reestablished. Therefore, these studies ascertain whether biomass is sufficient to cause MIC during this period and provide a baseline for determining the types of bacterial activities that may be expected.
- Assess biogenic environmental effects, including pH, alterations to nitrate concentration in groundwater, the generation of organic acids, and metal dissolution. These factors have been shown to be those most relevant to corrosion of engineered barriers.

Direct Effects

- Characterize and quantify microbiological effects on candidate containment materials. These studies were carried out in a number of different approaches, using whole YM microbiological communities, a subset of YM bacteria, and select reference organisms. Studies were carried out to determine morphological alterations to materials surfaces and using electrochemical methods to help quantify effects and modes of MIC, and to provide additional alternative means of evaluating MIC effects. They were carried out only under conservative conditions (low temperature, saturated conditions); thus, resulting conclusions may be considered an upper bound of potential biological effects on tested materials.

2. Present YM Microbial Community and Limiting Factors to Growth

In early studies, organisms were isolated from YM rock by plating on low-nutrient medium. This work was reviewed in the *Engineered Materials Characterization Report for the Yucca Mountain Site Characterization Project,* vol. 3, rev. 1, April 1997, section 2.6 (Reference 1). Microorganisms were isolated at 22° C, 30° C and 50° C under both aerobic and anaerobic conditions. Due to the limited conditions under which organisms were isolated, on growth medium containing an organic carbon source, only heterotrophic organisms (those that require reduced organic compounds as a source of cellular carbon and energy) were obtained. These were subsequently subjected to a battery of tests to determine if any possessed activities associated with corrosion (such as acid production, extrapolymeric or slime production, or sulfide generation through the process of desulfurylation. It was found that many of the isolates obtained had at least one of these activities, thereby showing the potential for MIC at YM. Iron-oxidizing bacteria, which obtain energy from the oxidation of ferrous iron or reduced sulfur compounds and cellular carbon from fixation of carbon dioxide, were also isolated from YM rock on a different medium selective for their growth. The presence of iron oxidizers may be significant for corrosion of carbon steel and titanium as they are capable of denitrification in the absence of an organic carbon source (see Section 4.2.3). Preliminary growth testing of the full complement of microbes contained in YM rock showed insignificant effects of temperature on growth rates or final yields (ca. 10^8 cells/mL added medium) of YM organisms at temperatures up to 50°C in low-nutrient medium. While temperatures above 50°C were not tested in this particular experiment, the results did show some heat resistance of at least a portion of the native YM community.

Later testing, using methods that avoid the need to grow organisms and simply rely on direct extraction of cellular membrane components from rock, showed the cellular density of organisms in YM rock to be approximately 4–7 × 10^4 cells/g of dry tuff. A series of experiments to assess growth-limiting factors demonstrated that sufficient nitrate and sulfate were contained in YM groundwater to support microbial growth. However, water availability was judged to be the primary limiting factor to growth. When unamended simulated groundwater was supplied to crushed YM tuff, the cell densities increased by 2–3 orders of magnitude. Secondary limiting factors were found to be both phosphate and organic carbon; when either of these was added to simulated groundwater, cell densities increased 1–2 orders of magnitude. In the absence of added organic carbon or phosphate, heterotrophic cell growth from YM tuff reached ca. 10^6 cells/mL added water. The phosphate required for cellular growth was probably solubilized by microbial acid production directly from YM rock; this process is recognized as commonly occurring and later analysis (presented later in this report) showed this to be the case. Only heterotrophic organisms were counted due to the methods used however, and it is not currently known what these organisms used as a source of carbon while growing in YM groundwater. These results are significant in that after about 1000 years following waste emplacement, groundwater is expected to drip into the repository environment. These experiments showed that significant microbial growth is possible when groundwater becomes available even absent of any added organic carbon (2).

The different types of microorganisms isolated from a given environment by growing on selective growth substrates is necessarily limited; it is estimated that only

0.1–1.0% of the individual species residing in a given sample can be isolated using this approach. Therefore, alternative methods that do not rely on growth were implemented to identify all the members of the extant YM microbial community. DNA was extracted directly from aseptically collected rock, a hyper-variable gene (16S rRNA) that enables species identification was amplified, the resulting clones (200) screened for unique gene sequences, and the results compiled. Sixty-five different species of eubacteria were identified using this approach. The frequency at which individual clonal variants were identified during the screening process allowed some estimation of the relative representation within the total community of each type of organism identified. Metabolic properties of identified organisms, with respect to their potential effects on repository materials, are summarized in Table 1. This work is detailed in Reference 3.

When ventilation was shut off to regions of the Exploratory Studies Facility (ESF), moisture accumulated in unventilated regions and prolific fungal growth ensued. Fungi, which are obligate heterotrophs (i.e., they require a reduced organic carbon source), were found to grow on virtually all organic materials introduced into the ESF. A wide range of species was identified, and air sampling followed by quantification of airborne spores showed over 10^4 fungal spores/m^3 of sampled air in affected areas (in comparison, less than 100 spores/m^3 is found in air outside the ESF). These studies are reviewed in Reference 4. The relevance of fungal growth to integrity of the EBS lies in the capacity of fungi to produce organic acids (e.g., oxalic acid), which may enhance corrosion of Alloy 22. However, these types of organisms require an organic carbon source to grow. Thus, if introduced organic materials are limited in repository construction and design, it seems most likely their growth will likewise be minimal.

Table 1. Potential Effects of Identified YM Microorganisms on Repository Performance

Type of Organisms	Relevant Properties	Potential Effect on Repository
Bacillus, *Clostridium*, *Arthrobacter*	Heat- and desiccation-resistant	May be able to survive initial heat pulse
Caulobacter, *Rhodobacter*	Able to maintain activity at extremely low nutrient levels	Metabolic products produced during low nutrient periods
Pseudomonas, *Arthrobacter*	Able to degrade complex organic compounds	Could degrade plasticizers, plastics, fuels
Microbacterium	Fermentative; produce organic acids and alcohols	Metabolic products can be corrosive to Ni-based alloys
Bacillus, *Pseudomonas*, *Clostridium*	Extracellular products: polysaccharides, enzymes, siderophores, hydrogen	Corrosive; may prevent reoxidation; chelators; potential embrittlement
Many identified organisms	Reduce nitrogen	Alters the chloride/nitrate ratio

3. Microbial Communities under Simulated Repository Conditions

Long-term corrosion testing conditions were evaluated to assess the potential structure of microbial communities under more representative repository conditions. Corrosion tests in the Long Term Corrosion Test Facility (LTCTF), aimed at evaluating candidate engineered barrier materials after long-term exposure under anticipated extreme repository conditions, were analyzed for microbiological colonization. Test vessels are on the order of 1000 L and contain simulated groundwaters at varying ionic strength, pH, and temperature (60°C or 90°C) and material coupons. Deionized water was used as a solvent for dissolved salts. Microorganisms were never intentionally introduced into these systems (no YM rock was included in these tests either); however, they are somewhat open to the surrounding laboratory, and therefore could be inoculated with organisms from the laboratory environment. Initial testing, performed by filtering tank waters with subsequent staining to microscopically visualize organisms, showed the presence of organisms in some tanks. Therefore, further analysis was undertaken to better evaluate the composition of the tank microbial communities, with the expectation that colonizing organisms may be indicative of what organisms would be anticipated to colonize the repository during periods where the environment approached those represented in the LTCTF tanks.

The composition of microbial communities in three LTCTF tanks was determined using direct DNA extraction of tank waters and swipes. Several liters of water were filtered from each sampled tank, and filters were combined with swabs that had been used to swipe the inner tank walls. Filters and swabs were pooled; and adsorbed organisms were desorbed and subjected to DNA extraction, 16S rDNA amplification, and cloning of amplified regions (as above). One hundred clones were screened from each tank to identify unique sequences/organisms and the clonal frequency of each unique sequence was calculated, based on the 100 clones screened (Fig. 1). Water and swipes were also assessed by phospholipid fatty acid (PLFA) analysis, which provides an estimate of total bacterial density (data not shown), and direct microscopic counts to provide another means of determining bacterial densities (Table 2).

As deduced from the bacterial density assessments (Table 2), bacteria were detected under all conditions tested. However, the greatest concentrations were associated with a 10-fold increased ionic strength of groundwater at 60°C, while the lowest densities were found in acidified, concentrated (1000×) groundwater. In terms of the types of organisms that colonized in the 60°C tanks tested, generally it was found that each tank contained a different community of organisms. This finding shows that in selective environments, those organisms best adapted to a particular set of conditions will prevail.

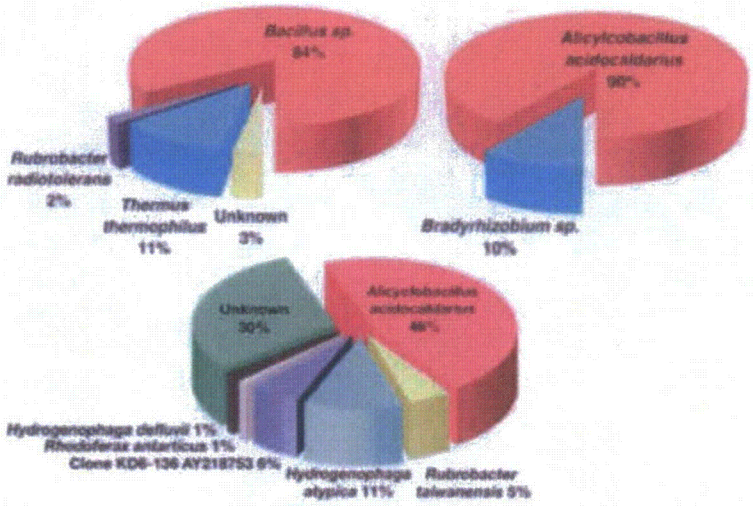

Fig. 1. Frequency of unique clone types (whose sequences indicate species) in LTCTF tanks. After amplification and cloning of 16S rRNA genes, 100 clones were screened; the frequency of occurrence of unique clones is depicted as the percentage of the total number of clones screened.

Table 2. Cell Density of LTCTF Samples Determined by Direct Microscopic Counts

LTCTF Sample	Direct Microscopic Counts* (cells/mL)
1000× groundwater, pH 2.8, 60°C	1.30E+04
1000× groundwater, pH 10.3, 60°C	1.19E+05
1000× groundwater, pH 10.3, 90°C	1.31E+06
10× groundwater, pH 10.1, 60°C	4.60E+06
10× groundwater, pH 10.1, 90°C	4.87E+05

*Desorbed cells from these samples were stained with Acridine Orange before microscopic counting in a chamber of known volume.

Alicyclobacillus acidocaldarius, which was a major component of the concentrated groundwater communities at both pH 2.8 and 10.3, has otherwise been isolated from acidic hot springs and contains hopanoid membrane lipids that harden the membrane to caustic or highly concentrated solutions. Although none of the identified organisms (with the exception of *Bacillus*) is generally known to inhabit environments such as those typified by the LLNL laboratory or Livermore, CA, in general, they were apparently able to transport to and colonize the LTCTF tanks. This demonstrates the broad distribution of organisms normally thought to inhabit extreme environments (such as hot springs) and supports the general tenet that transport is not a limiting factor for microbial colonization; it is generally thought that the environment is the selective force that determines which organisms inhabit a specific locale. Organisms that are able to survive in a given environment and are best suited to exploit the resources available. The organisms that colonized these tanks, therefore, may be an indicator of those that may colonize the repository environment during periods when conditions are similar to those in the LTCTF tests.

4. Microbiological Effects on Water Chemistry

4.1. Acid Generation and Associated Decrease in pH

The production of organic acids as products of microbial central metabolism is well documented (e.g., Reference 15, particularly Chapter 9; Reference 16, "Part II: Bioenergy and Metabolism"). The generation of acids has been both directly and indirectly linked to metal corrosion. Microbially generated acids have been shown to directly dissolve the protective calcareous film on stainless steel. Coupling of protons with electrons results in electron removal from the cathode, and forms hydrogen, which is a substrate for microbial sulfate reduction. Therefore, individual strains isolated from YM rock were screened and tested under various conditions for their effects on pH of the bulk growth medium. Results revealed that both growth and acid production were generally more rapid when the media were amended with glucose. This is not surprising given that acid production is largely a result of organic carbon utilization; addition of glucose provides at once more carbon and energy for growth, together with a greater potential rate of acid generation. However, about 10% of YM strains tested showed decreases in medium pH even without carbon addition. The lowest pH attained was 4.2. These results are further discussed in Reference 1.

Further experiments were carried out using the entire complement of organisms contained in YM rock, under varying growth conditions. It was found that sodium carbonate-based groundwaters (which are predicted to represent the bulk of repository seepage waters) effectively buffered biogenic acid production resulting in the maintenance of near neutral pH in the bulk solution. These findings are further detailed in Reference 5.

Fungal growth from YM rock was also tested for its effects on pH under a variety of conditions. When media containing adequate nutrients specific for fungal growth (i.e., high concentrations of reduced organic carbon) were employed, the pH of the medium was reduced to pH 3. However, when YM fungi were grown from YM rock in a simulated YM ground, water increased in ionic strength tenfold (from that found in situ,

10× J13). Initially, the pH decreased to pH 5 but was subsequently found to increase somewhat to pH 6, demonstrating the possible buffering effects of the sodium carbonate-based groundwater.

Sodium carbonate-based seepage waters have thus been shown to buffer the effects of potential acid production by microorganisms within the repository. This may counter the corrosive effects of microbial and fungal generated acids. However, it may also be important to consider that the measurements of pH effects have only been conducted on the bulk aqueous phase in which these organisms are growing. Within biofilms, the accumulation of cells and extracellular products produced by these organisms on surfaces, the concentrations of acids may be much greater than those that have been diluted in the surrounding medium. Furthermore, it is not known how well this observed buffering effect would function within the semi-solid biofilm matrix.

The types of organic acids generated by bacteria and fungi that have been found to accumulate on rock substrates include low concentrations (nM–μM) of lactate, formate, and oxalate. These same organisms grown under simulated in situ conditions have been shown to produce μM–mM concentrations of a broader range of organic acids including succinate, citrate, malate, pyruvate, and fumarate (6). Pure fungal cultures of *Aspergillus*, a fungi found to be prevalent in the ESF, has been shown to produce oxalate at a rate of 1.5 mM/hr (7); however, fungi do require a reduced carbon source to generate acids, and presumably, these would be minimal in the planned repository. Scoping studies were conducted with the full complement of organisms contained in YM rock with a continual feed of simulated concentrated groundwater (10× J13 with 0.1% glucose). Results of these studies show a steady-state concentration of acetate in the bulk aqueous phase of 3.2 mM and formate at 0.34 mM; lactate was detected (0.22 mM) in bulk cultures of YM rock containing microorganisms incubated with 10× J13 (with glucose). *Thiobacillus*, an iron- and sulfur-oxidizing organism that fixes carbon dioxide to supply cellular carbon and found in YM rock samples, generates formate (0.12 mM) in continuously fed cultures grown on a sulfur-based medium. A sulfate-reducing bacterium was found to generate acetate (40 mM) from lactate. Concentrations of these acids, as they were measured in the bulk aqueous phase of the cultures, do not appear great enough to affect corrosion of proposed EBS materials, and oxalate has not been found to affect breakdown of the Alloy 22 passive film in simulated crevice solutions. However, as was pointed out concerning overall pH effects, concentrations of organic acids may be expected to be much greater in biofilms colonizing these materials.

4.2. Nitrate Reduction

Nitrate counters the corrosive effects of chloride ions. The nitrate/chloride ratio of evolved groundwaters in the proposed nuclear waste repository at Yucca Mountain has therefore been acknowledged to be an important aspect to factor into the overall evaluation of potential corrosion of repository engineered barriers. Nitrate/chloride ratios above 0.2 to 0.5 have been shown to inhibit Alloy 22 corrosion, the proposed waste package corrosion barrier. Both nitrate and chloride are components of YM groundwater, present for example in J13 well water at concentrations of 0.155 mM and 0.195 mM, respectively. Microbiological reduction of nitrate may occur, causing a decrease in the nitrate/chloride ratio, thereby potentially contributing to corrosion of barrier materials.

4.2.1. Modes of Nitrate Reduction

Bacteria can reduce nitrogen by a number of different modes (Fig. 2). Nitrate can be directly incorporated into cells, then reduced intracellularly and incorporated into proteins, nucleic acids, and other cellular components (i.e., assimilated via anabolic metabolism). Assimilation of nitrate has been shown, however, to comprise a very minor component of overall nitrate consumption in soils and is relatively insignificant when compared to dissimilatory processes. This is because many nonphotosynthetic microorganisms are unable to reduce oxidized nitrogenous compounds for assimilation, so they must be supplied in a reduced state.

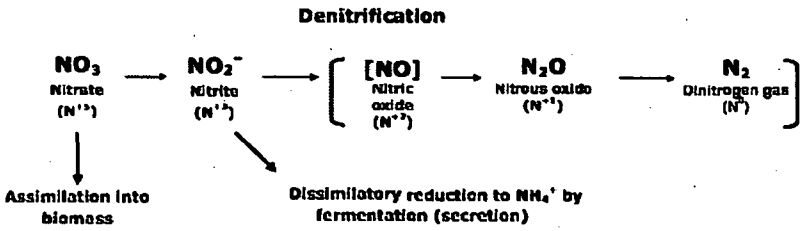

Fig. 2. Microbiological pathways of nitrate reduction. Names of specific compounds are designated together with the oxidation state of nitrogen in parentheses. The role of nitric oxide has been debated.

Alternatively, in microorganisms capable of carrying out fermentation (whereby a reduced organic substrate acts as both an electron donor and acceptor; one component of the original organic substrate is oxidized and the other reduced), a process known as dissimilatory nitrate reduction to ammonium (DNRA) results in the production of secreted ammonium from nitrate. This process has been determined to be favored when elevated organic carbon/nitrate ratios are prevalent. High nitrate concentrations are also required for DNRA to occur because generally the enzymes involved in the process have a low affinity for nitrate (100–500 μM). Greater redox potentials in addition to the requirement for elevated organic carbon also favor DNRA. The requirement for greater concentrations of fermentable organic carbon than of nitrate for DNRA to proceed makes it unlikely that this process will occur to any significant extent in the projected repository environment, as long as available carbon sources remain minimal.

4.2.2. Heterotrophic Denitrification

DNRA is distinguished from what may be termed "true" denitrification, which refers to the use of nitrate as a terminal electron acceptor with the evolution of nitrogenous gaseous products (as indicated in Fig. 2). Many aerobic organisms that use organic carbon as a source of energy and carbon (i.e., "heterotrophs") and normally employ oxygen as a terminal electron acceptor are capable of using nitrate in this latter

capacity if it is available in sufficient concentration. The process of heterotrophic denitrification can be represented by the following chemical reaction, using glucose as a model organic compound/electron donor:

$$4NO_3^- + 5/6\ C_6H_{12}O_6 + 4H^+ \rightarrow 2N_2 + 5CO_2 + 7H_2O$$

It has been estimated that denitrifying organisms comprise 1–5% of the total heterotrophic microbial community and 20% of the total anaerobic community (i.e., those organisms capable of using terminal electron acceptors other than oxygen) in soils. The bulk of these denitrifying organisms are adsorbed to particulate soil and mineral surfaces. In terms of the taxonomic distribution of microorganisms that carry out denitrification, *Alcaligenes*, *Bacillus*, *Corynebacterium*, and *Pseudomonas* isolates all have denitrification capacity; *Pseudomonas* and *Alcaligenes* have been implicated as major contributors to denitrification worldwide. All of these types of organisms have been identified as members of the microbial community now extant at Yucca Mountain. However, in addition to the ability to carry out denitrification, three other general requirements are necessary for denitrification to occur:

- Presence of nitrogen oxides
- Suitable electron donors
- Restricted oxygen availability

Clearly, nitrate is present in YM groundwaters presently; therefore, denitrification is not occurring to any major extent now. Restricted oxygen availability is not necessarily a relevant limiting factor because it is generally acknowledged that anaerobic microsites regularly occur in geologic media. Therefore, presence of suitable electron donors is the primary factor that may well limit the extent of denitrification now and whether denitrification will occur during repository evolution.

4.2.3. Autotrophic Denitrification

Some bacteria are capable of using nitrogen as a terminal electron acceptor (in place of oxygen) using inorganic, rather than organic electron donors. These organisms use either reduced sulfur compounds or ferrous iron as electron sources and are able to fix carbon dioxide to supply cellular carbon, so-called "autotrophic" metabolism. Thus, these types of organisms do not require an organic carbon source; they derive both their energy (electron) and carbon sources from inorganic compounds. It had been observed that ferrous iron–containing groundwaters never contained nitrate. This was originally thought to be a result of the abiotic chemical reduction of nitrate by Fe^{+2}, which had been observed in the presence of Cu^{+2} catalysts at circumneutral pH. However, attempts to observe denitrification in Fe^{+2}-containing aquifer samples that had been sterilized failed. Shortly thereafter, it was reported that *Gallionella ferruginea*, an autotrophic organism deriving reducing equivalents from ferrous iron, is able to reduce nitrate to nitrite. Nitrate can then be reduced to gaseous nitrogenous products by the oxidation of Fe^{+2} to Fe^{+3} via reactions including:

$$HNO_2 + Fe^{+2} + H^+ \rightarrow NO + Fe^{+3} + H_2O$$

$$2NO + 2Fe^{+2} + 2H^{+} \rightarrow N_2O + 2Fe^{+3} + H_2O$$

$$2HNO_2 + 6Fe^{+2} + 6H^{+} \rightarrow N_2 + 6Fe^{+3} + 4H_2O$$

Another autotrophic organism, *Thiobacillus denitrificans*, which oxidizes reduced sulfur (sulfide, thiosulfate, or elemental sulfur) to sulfate as an electron source, can use nitrate as a terminal electron acceptor. A series of field studies found that this organism caused the reduction of nitrate to nitrogen gas at the expense of endogenous ferrous disulfide (or pyrite):

$$5FeS_2 + 14NO_3^{-} + 4H^{+} \rightarrow 7N_2 + 10SO_4^{-2} + 5Fe^{+2} + 2H_2O$$

There is evidence that the ferrous iron produced as a product in this reaction also acted in an autotrophic biotically mediated process to reduce nitrate. Well waters containing ferrous iron were amended with nitrate and incubated; subsequent analysis showed decreases in nitrate and increases in ferric iron according to the following stoichiometry:

$$5Fe^{+2} + NO_3^{-} + 7H_2O \rightarrow 5FeOOH + 0.5N_2 + 9H^{+}$$

A study examined the geochemistry of a nitrate-containing aquifer that contained both pyrite and deposits of organic matter in the form of brown coal. The conclusion was that the bulk of denitrification, which was found in a region where the redox potential dropped sharply, was mainly fueled by pyrite as the principal electron donor; only 15% of nitrate reduction used the coal as an electron donor. However, this same report showed that although sulfate concentrations increased in the nitrate-reducing zone, ferrous iron remained, indicating that the Fe^{+2} generated by incomplete pyrite oxidation did not further contribute significantly to nitrate reduction.

Autotrophic denitrification has not been as extensively studied as heterotrophic denitrification; therefore, it is presently not clear how widespread or common this process is in various environments. Almost all studies to date regarding biogenic denitrification have focused on heterotrophic processes; the limiting factors and kinetics of the autotrophic physiology and metabolism are largely unknown. However, it has been shown in many field and laboratory studies that bacterial denitrification overall is often organic carbon-limited, indicating that autotrophic denitrification may not play a significant role in situ in reducing nitrates. However, if autotrophic denitrification were a factor in the evolution of the YM repository, it would decouple the requirement for organic carbon to fuel denitrification; denitrification could proceed without the need for organic carbon, fueled only by groundwater carbonate, and reduced iron or reduced sulfur.

4.2.4. Field Rates of Denitrification

Measured rates of denitrification in the unsaturated zone are more relevant to the anticipated conditions in the YM repository, since the repository horizon will be perched approximately 300 meters above the water table. However, very few studies have been conducted examining vadose zones at depth (>10 meters) in the subsurface. Both a study assessing denitrification activity to 289 meters in sand and clay and one determining

denitrification in limestone and overlying units to 180-meter depth did show significant decreases in denitrification with sampling depth (8, 9). The latter study showed a 100-fold lower denitrification rate (1.7 nM NO_3/g/day) at depths of 40 meters or greater than in surface soils. Deep clay sediments demonstrated little or no activity, which may be due to the lack of permeability in clays to infiltrating nitrate; in fact, this same study did show the *potential* for denitrification at all depths examined if nitrate were added to withdrawn sediment samples. Measurements in a sand/clay study below 150 meters deep in unamended samples show denitrification rates on the same order as those seen in limestone if no nitrate is added. Yet, if nitrate became available, rates increased up to 100-fold, demonstrating that denitrifying organisms were present in the deep sediments but required appropriate conditions to be active (8).

4.2.5. Observed Conditions for Nitrate Depletion of YM Groundwater

As noted above, organisms capable of carrying out at least heterotrophic denitrification are currently present within YM rock. Therefore, it could be that the limiting factor to denitrification presently in the YM subsurface is a lack of organic carbon or inorganic electron donors. It is unlikely that sufficiently reducing conditions are a limiting factor because anaerobic microsites are assumed to be available in geologic media. Recent experimental evidence, though, shows a somewhat more complex picture. Complete or near complete elimination of nitrate by YM organisms contained in YM rock supplied with a constant feed of simulated 10× J13 amended with 0.1% glucose was observed when either Alloy 22 or Stainless Steel 316 (SS 316) was present. Identical systems (Fig. 3) containing sterilized rock maintained the same approximate concentration of sulfate found in the background 10× J13 + 0.1% glucose (Table 3 and Fig. 4). Therefore, in the presence of these two alloys, either denitrification or nitrate assimilation was occurring. However, in systems run under the same conditions but

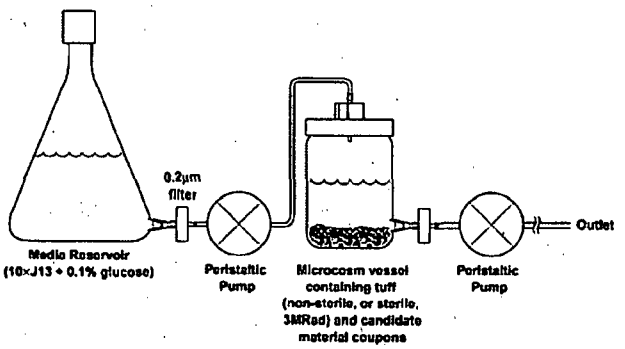

Fig. 3. Overall configuration of continual flow microcosms simulating a saturated repository environment. Simulated concentrated sodium carbonate-based groundwater amended with glucose was fed (2 mL/h) into a vessel containing either sterile or non-sterile YM rock and candidate material coupons. Microcosms were incubated at room temperature (22°C) or 30°C. Effluent was sampled on the outlet for chemical analysis. Periodically, coupons were withdrawn for surface analysis.

Table 3. Nitrate Depletion* in Saturated Repository Microcosms

EBS Material	Presence of YM Organisms	
	Unsterilized Rock	Sterilized Rock
Alloy 22	+	–
Stainless Steel 316	+	–
Titanium grade 7	–	–
No alloy	–	–

*Observed nitrate depletion is indicated by (+); lack of nitrate depletion is indicated by (–).

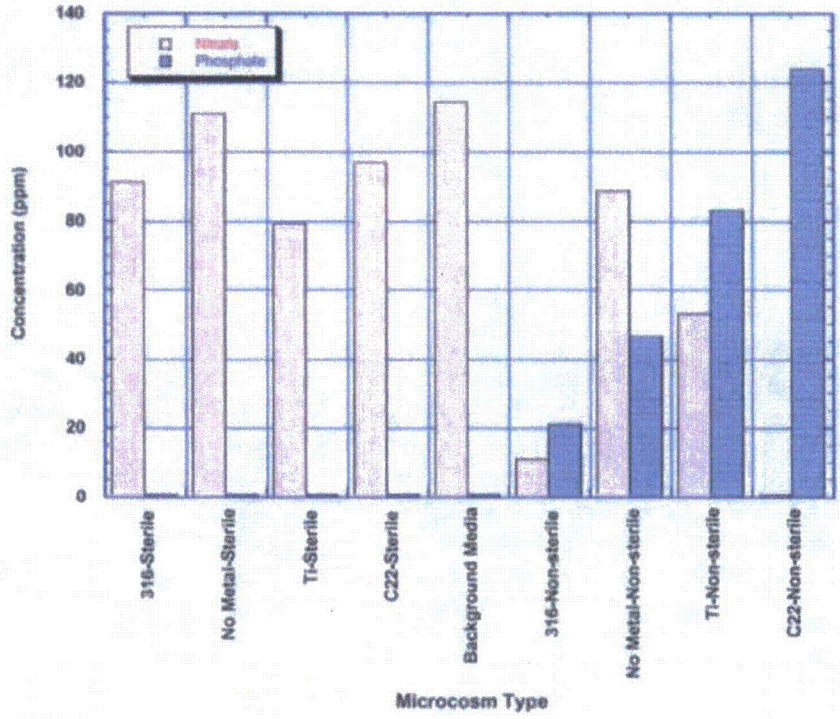

Fig. 4. Phosphate and nitrate concentrations in microcosm efflux solutions (i.e., spent 10× J13 + 0.1% glucose) from microcosms containing either different candidate EBS materials or no EBS materials. Concentrations of anions were determined using ion chromatography.

containing either no metal alloys or titanium grade 7 (Ti gr7), no significant reduction (no metals) or little reduction (Ti gr7) in nitrate concentration was observed in the presence or absence of YM microorganisms. (cf. Table 3 and Fig. 4).

The lack of nitrate depletion in microcosms containing either no metals or Ti gr7 strongly suggests that nitrate assimilation was not occurring in the vessels containing Alloy 22 or SS 316, because it would be generally expected for nitrate assimilation to occur equivalently under all tested conditions, no matter the type of alloy (or lack thereof) present. Likewise, if the glucose contained in the feed water were the source of reducing equivalents for nitrate reduction, then it would be expected for nitrate reduction to occur similarly across the types of alloys, since glucose was present in all microcosms. However, if autotrophic denitrification were occurring with an alloying component of Alloy 22 and SS 316 serving as an electron donor (while Ti gr7 could not supply reducing equivalents as readily) for nitrate reduction, then one might expect the observed result. An alternative explanation could be that microcosms containing different alloys contained different microbial populations because conditions encouraged the growth of differential populations of microbes from the rock, of which some were capable of nitrate assimilation or reduction, while others were not.

5. Materials Testing

5.1. Micrometer-Scale MIC of Alloy 22 in Saturated Repository Microcosms

5.1.1. Coupon Surface Analysis

Coupons of Alloy 22 were exposed to a simulated, saturated repository environment consisting of crushed rock from the repository site and a continual flow of simulated groundwater supplemented with 0.1% glucose (as was depicted in Fig. 3) for periods up to five years. Coupons were incubated with YM tuff that was either left unsterilized (with the YM microbial community left intact) or was pre-sterilized prior to being placed in the experimental vessels; vessels were incubated at either room temperature or 30°C. Surface analysis of the biotically incubated coupons shows development of both submicrometer sized pinholes or micropores; these features were not present on either sterile or untreated control coupons. The micropores formed on the Alloy 22 coupons exposed to be biotic environments are also referred to as micropits or micropitting in this document.

Alloy 22 coupons from microcosms incubated at 30°C were withdrawn, cleaned, and imaged using scanning electron microscopy (SEM). An unreacted Alloy 22 coupon was also cleaned and imaged in parallel for comparison. These SEM results are shown in Fig. 5. Coupons incubated in the non-sterile microcosm reactors showed the development of pinholes, primarily along the ridges formed by polishing, while coupons incubated in sterile microcosms and those that were not reacted in microcosms showed no evidence of pinhole formation after one cleaning cycle. The micropits appeared uniform in shape except where they had grown together and ranged in size from 200–700 nm in diameter.

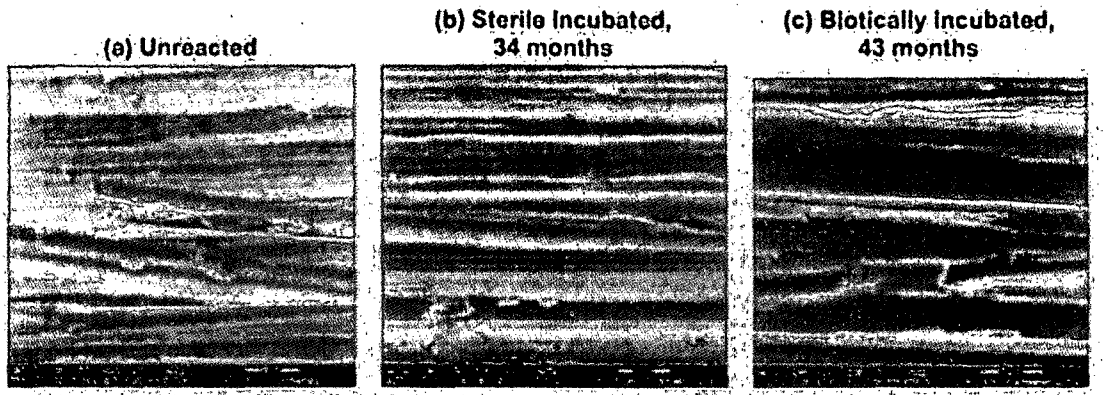

Fig. 5. Alloy 22 coupons incubated at 30°C: (a) unincubated/nonreacted coupon; (b) sterile-incubated coupon, and (c) non-sterile-incubated coupon. Coupons were cleaned and interrogated using scanning electron microscopy at a magnification of 8000× (a and b) or 10,000× (c). Pinhole formation, along the ridges formed by polishing, was evident on non-sterile coupons incubated 43 months (c), while sterile coupons incubated 34 months (b) and unreacted coupons (a) did not display pinhole formation.

In contrast to the Alloy 22 non-sterile coupons incubated at 30°C, coupons withdrawn after long-term incubation from biotic microcosms incubated at 22°C showed markedly different patterns of micropitting. Again, small micropores (generally less than 1 μm) were apparent on the surface, but their distribution and frequency was extensive, covering all regions of the coupon, and not restricted to polishing ridges. Furthermore, the micropores were less uniform in shape and size compared with those observed on the 30°C incubated coupons (Fig. 6). Coupons analyzed prior to cleaning contained a micropore density similar to those that were cleaned; cleaning effects, if any, were not observed. Unreacted coupons and those incubated under sterile conditions did not show micropore formation (Fig. 6). Coupons incubated biotically at room temperature for shorter durations (17 months and 32 months) also demonstrated micropore formation, indicating that the micropores were generated at the earlier sampling time points. Gravimetric analysis was inconclusive because many of the micropores were filled with deposited or precipitated minerals. Energy dispersive spectral analysis of pitted coupons showed that the micropits were often filled with siliceous material, which apparently originated from either dissolved and re-precipitated silica or particulate fines from the YM rock. Aluminosilicates were also present.

Atomic force microscopy (RMS analysis) indicated that the overall roughness of the non-sterile coupon surfaces incubated at ambient temperature decreased as a function of time, indicating a flattening of the coupon surface, even as microscale roughness increased due to micropore formation. Micrographs (SEM) also demonstrate surface smoothing; the polishing ridges have flattened, and only the gross features, such as surface gouges, remain (Fig. 6). The distribution of surface roughness (which includes the effect of micropores on biotically incubated samples) was evaluated using imaging analysis (Image Tool, v. 3.00, University of Texas Health Science Center, San Antonio; http://ddsx.uthscsa.edu/dig/itdesc.html) of SEM micrographs of Alloy 22 coupons incubated in microcosms for six years at ambient temperature. For sterilely incubated

coupons (3 coupons examined, a total of 15 fields analyzed), the median roughness density was 8.39 $\mu m^2/mm^2$ of coupon surface (maximum value 18.60 $\mu m^2/mm^2$; minimum value 0.021 $\mu m^2/mm^2$). For a biotically incubated coupon (10 fields analyzed), the median roughness density was 17.83 $\mu m^2/mm^2$ (maximum value 27.78 $\mu m^2/mm^2$; minimum value 9.45 $\mu m^2/mm^2$). Thus, the roughness density of biotically incubated samples is higher than that for sterilely incubated samples by a factor of about two (in large part due to the development of micropores). Because the depth associated with the difference in roughness could not be determined, the difference in total metal loss could not be estimated from the imaging analysis.

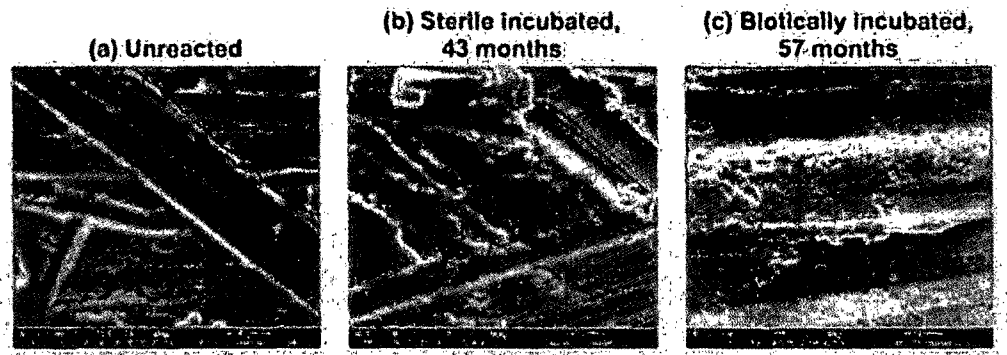

Fig. 6. Alloy 22 coupons incubated at room temperature (22° C): (a) unincubated, nonreacted coupon; (b) sterile incubated coupon (43 months); and (c) non-sterile incubated coupon (57 months). The micropores on the non-sterile coupons were ubiquitous and not uniform in shape (c).The unreacted (a) and sterile (b) surfaces are similar in appearance and are free of micropore features. All images are magnification 8000x.

It is not entirely clear why the distribution and frequency of micropores differ between biotically incubated coupons at room temperature as opposed to at 30°C. Clearly, the environments differ enough to create a sharply contrasting pattern of micropitting. This may be due to differences in the microbial communities, a result of the proliferation of different organisms from a single community when they are incubated under varying conditions (here, a temperature difference). To further probe this possibility, we performed analysis of the microbial communities, those pelagic organisms in the solution phase, and those adhered to coupons, in biotic room-temperature and 30°C microcosms. Purification of single colonies (which represent growth from a single cell) from microcosms incubated at room temperature and 30°C was undertaken, and these were identified using 16S rDNA analysis. The results showed that there were completely different microbial communities present in microcosms incubated at different temperatures, at least in terms of those that were culturable on the medium used for isolation (R2A, a low-nutrient formulation). In the room-temperature microcosm sampled, a *Pseudomonas* sp. and *Burkholderia cepacia* were identified, while the 30°C-incubated microcosm had an unrelated culturable community structure that included *Ralstonia pickettii*, *Sphigomonas paucimobilis*, and *Bacillus licheniformis*. The varying activities of these organisms may well account for the observed differential effects on Alloy 22 under these two test conditions.

5.1.2. Dissolution of Alloy 22 Determined by Effluent Chemical Analysis

Chemical analysis of bulk aqueous efflux solutions from microcosms were undertaken to determine the concentration of solubilized Alloy 22 elements. Solubilized metal from the coupons and contributions from the tuff and growth media were identified with ICP-MS on samples from sterile and non-sterile microcosms incubated at 30°C or room temperature. Note that ion chromatographic analysis of these same fluids resulted in the observations shown previously in Fig. 4.

A seven- to sixteen-fold elevation in Mn concentration was detected in the 30°C-incubated, non-sterile microcosm reactors containing tuff and metal coupons (exceeding 600 ppb), compared to the background media, the no-metal, non-sterile control reactors containing tuff (86 ppb), and sterile control reactors containing coupons and tuff (38 ppb) (Fig. 7a). Manganese is a component of both Alloy 22 and YM tuff; therefore, the Mn concentration in the no-added-metal, non-sterile reactors reflects Mn solubilized solely from tuff in the presence of YM bacteria (Mn concentration in YM tuff is 0.05–0.06 wt % and 0.26 wt % in Alloy 22). Sterile control reactors that contain Alloy 22 coupons and tuff contained small amounts of solubilized Mn in the absence of microbial activity. Since the Mn concentration was 86 ppb in the no-metal, non-sterile control reactors and 38 ppb in the sterile control reactor effluent, it is evident that the majority (>80%) of solubilized Mn in the non-sterile, 30°C reactors arose from the Alloy 22 coupons due to microbial activity. These findings were in contrast to those from the room-temperature-incubated microcosms, where chemical analyses of the bulk aqueous efflux solution did not indicate elevated concentrations of metals and dissolved salts above background and control concentrations, indicating that the metal lost from the surface had been either precipitated or adsorbed.

Molybdenum in 30°C-incubated non-sterile, coupon-containing microcosm reactor effluent was also elevated above background and control values, but the absolute concentration was low (10 ppb). The no-metal, non-sterile control was measured just above detection limits (0.4 ppb; Fig. 7b), showing that very little to none of the Mo originated from tuff. The coordinate sterile control reactors also contained Mo at levels just above detection, indicating that the solubilized Mo in non-sterile reactor effluent may have been due to microbial activity. These experiments are further discussed in Reference 10.

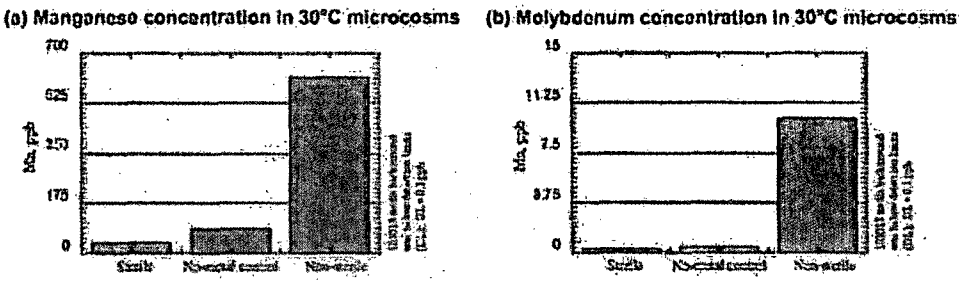

Fig. 7. Chemical analysis of bulk aqueous solutions from microcosm reactors incubated at 30° C shows that (a) there is an increase in soluble Mn compared to the no-added-metal, non-sterile and sterile controls and (b) molybdenum was detected in low concentrations in the non-sterile reactors but at higher values than for the sterile and no-added-metal (non-sterile) controls.

5.2. Biogenic Titanium Dissolution

An experiment was undertaken to evaluate more extreme conditions under which EBS materials might be susceptible to MIC. Iron-oxidizing organisms cultured from YM rock samples use carbon dioxide as a source of cellular carbon and derive energy from the oxidation of reduced sulfur or iron. *T. ferrooxidans*, a sulfur- and iron-oxidizing bacterium, was grown in continuous culture, with a constant supply of a growth medium containing thiosulfate as an energy source, generating sulfuric acid as an end product of metabolism. Culture conditions were aimed at generating an exponential-phase culture in which the organisms were metabolically vigorous over an extended period; material coupons were exposed to this continually growing culture throughout the incubation period of seven months. Our findings show that there was no discernable corrosion of Alloy 22; however, Ti gr7 did show signs of generalized corrosion on a micrometer scale using atomic force microscopy (AFM, Fig. 8). Consistent with signs of Ti gr7 corrosion observed using AFM, deposition of (presumably solubilized) Ti was found in the reactor and on Alloy 22 coupons resident in the same reactor as the Ti coupons (Table 4). Titanium coupons exposed to sterile thiosulfate medium did not display any signs of corrosion, thereby implicating *T. ferrooxidans* metabolic products of thiosulfate as potential corrosive agents on titanium. These results are further delineated in Reference 11.

These experiments show that given the appropriate growth conditions, particularly with respect to supplying a reduced sulfur compound as an energy source, sulfur-oxidizing organisms can enhance some corrosion of Ti gr7. Sources of reduced sulfur in the repository may be limited, however, possibly obviating this corrosion route.

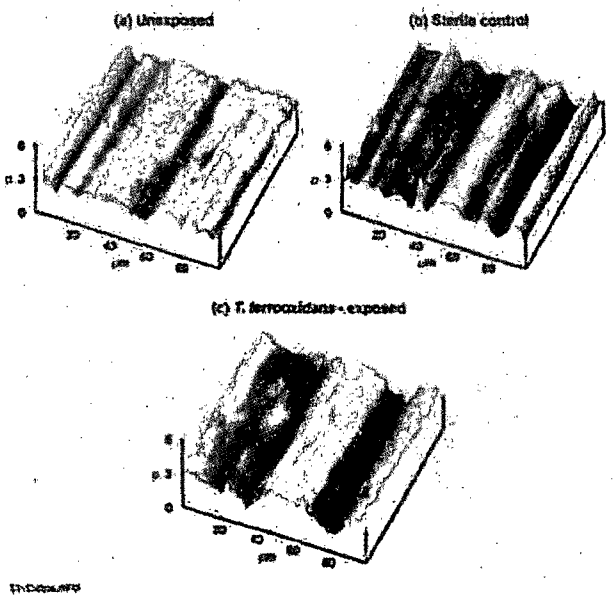

Fig. 8. AFM images of titanium grade 7 after fixation and acid washing: (a) unexposed starting material coupon; (b) after seven months incubation in sterile Thiosulfate medium alone; and (c) after seven months incubation in *T. ferrooxidans* culture grown in Thiosulfate medium.

Table 4. Elemental Analysis of *T. ferrooxidans* Bioreactor Effluent and Precipitates

Sample	Cr (mg/L)	Ni (mg/L)	Tl (mg/L)
Filtered effluent	1.36	0.521	0.023
Unfiltered effluent	0.98	0.352	0.023
Precipitate	0.19	0.068	0.269
Detection limit	0.01	0.01	0.02

5.3. Electrochemical Testing to Assess Corrosion Rates and Modes

Previous electrochemical testing showed relatively low rates of generalized corrosion (using polarization resistance measurements) of Alloy 22 in the presence of YM microorganisms, using unaerated batch systems supplied with a rich nutrient medium. The mean rates of corrosion of Alloy 22 in these systems, with the addition of YM microbes, was 0.2 µm/y. Biotic systems showed a twofold increase in corrosion rate compared with identical systems run under sterile conditions. Under these test conditions, anodic polarization behavior of Alloy 22 base metal shifted toward slightly higher current densities at lower applied potentials when YM bacteria were present versus in their

absence, indicating that YM bacteria caused somewhat greater anodic activity, in agreement with the observed increase in corrosion rates. These results are discussed further in Reference 12.

In a follow-on study, conditions were modified to: (a) provide a more representative aqueous medium, (b) generate a system that would not become nutrient- or oxygen-depleted over the test period, (c) enable better endpoint analysis of coupon surfaces, and (d) incorporate additional types of test materials than had been tested previously. These ends were accomplished by incorporating the following factors into the test plan:

- Simulated 100× J13 supplemented with phosphate and 0.1% glucose was used as a feed medium, to better simulate seepage waters; phosphate was added to mimic bacterial dissolution of phosphate from YM rock (as was depicted in Fig. 4).
- Vessels were fed in a constant flow mode (2 mL/h) with feed medium.
- Vessels were constantly sparged with air.
- Mirror finished coupons were used.
- Alloy 22 base metal, Alloy 22 weldments, and Ti gr7 base metal were tested.
- Tests were conducted under sterile and MIC (YM bacteria) conditions.
- All trials were performed in triplicate.

The test matrix is outlined in Table 5.

Table 5. Testing Matrix For Polarization Resistance Experiments on Alloy 22 and Ti Gr 7.

Specimens	Vessels	
	Sterile	Non-Sterile
Alloy 22 Non-Welded (MA)	7, 8, 9	16, 17, 18
Alloy 22 As-Welded (ASW)	1, 2, 3	10, 11, 12
Ti Gr 7 Non-Welded	4, 5, 6	13, 14, 15

Vessels 1-18 were in operation for several months. The time of operation was different for each vessel. The corrosion potential and the polarization resistance of the specimens exposed to vessels 1-18 were monitored regularly. The polarization resistance is inversely proportional to the corrosion rate. Results show that the corrosion potential (E_{corr}) for welded and non-welded Alloy 22 coupons more or less stabilized for exposure times higher than 125 days. For Ti Gr 7, the E_{corr} stabilized for times higher than 75 days. For the entire testing time, the polarization resistance measurement showed considerable scattering, both for the sterile and non-sterile environments. The corrosion rate (calculated from polarization resistance measurements) for the specimens exposed to both types of environments was averaged for times higher than 125 days (for Alloy 22) and for times higher than 75 days (for Ti Gr 7).

Figure 9 shows the average corrosion rate for welded and non-welded Alloy 22 specimens. The standard deviation is represented as error bars. For both types of Alloy 22

specimens, the corrosion rate in the non-sterile environment was slightly higher than the corrosion rate in the sterile environment by a factor of approximately two.

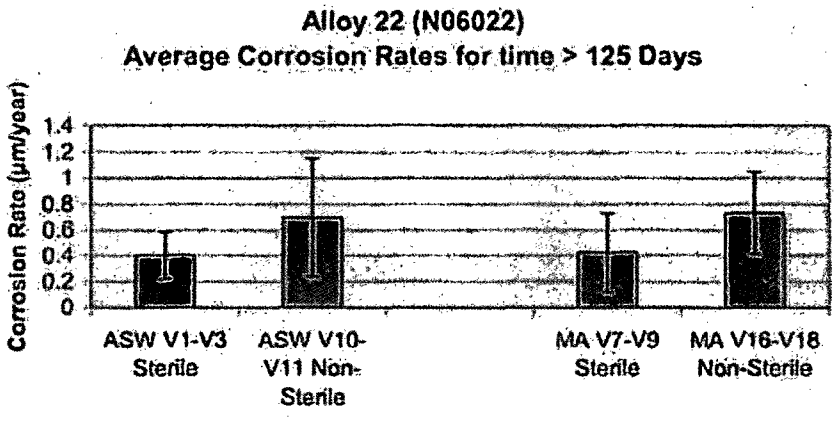

Fig. 9. Average corrosion rates determined by polarization resistance testing of welded and non-welded Alloy 22 for times higher than 125 days.

Figure 10 shows the average corrosion rates for Ti Gr 7 in sterile and non-sterile environments. For the sterile environment, the data from Vessel 5 was not included since it showed high corrosion rates. As was the case for Alloy 22, for Ti Gr 7 the corrosion rate in the non-sterile environment was higher than in the sterile environment approximately by a factor of two. The standard deviation for Ti Gr 7 in non-sterile conditions was larger than for Alloy 22 and considerably overlapped the data for the sterile Ti Gr 7.

Anodic polarization experiments were conducted on welded (Fig. 11) and base metal (Fig. 12) Alloy 22 specimens that had been reacted with and without inoculated YM microorganisms. All specimens were exposed for 211-215 days to a continual flow (2 mL/hr) of 100X J13 simulated water containing 0.1% glucose. These experiments suggest minimal impact of the microbes on the corrosion of Alloy 22 even though the local environment under a biofilm is expected to be different than in the absence of a biofilm. The sterile and microbial anodic polarization curves for both the welded and base metals are very similar. The critical potential, a qualitative indication of breakdown of the passive film, varies between 700 mV for the sterile experiments to 800 mV for the microbial incubated experiments. This difference may be attributed to the biofilm formed on the metal surface. Hysteresis in anodic polarization curves can be a qualitative measure of localized corrosion and is usually characterized by sustaining high current

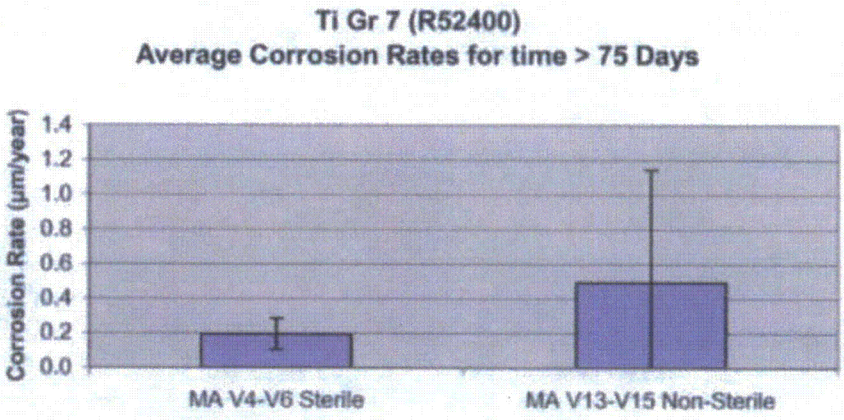

Fig. 10. Average corrosion rates determined by polarization resistance testing of Ti Gr 7 under sterile and non-sterile conditions.

density as the potential is ramped back down, which would represent an inability of the surface to repassivate. The hysteresis observed in both the sterile and microbial inoculated experiments is very narrow in shape, and thus not likely related to the occurrence of localized corrosion. Specimen surfaces were not examined to confirm this conclusion.

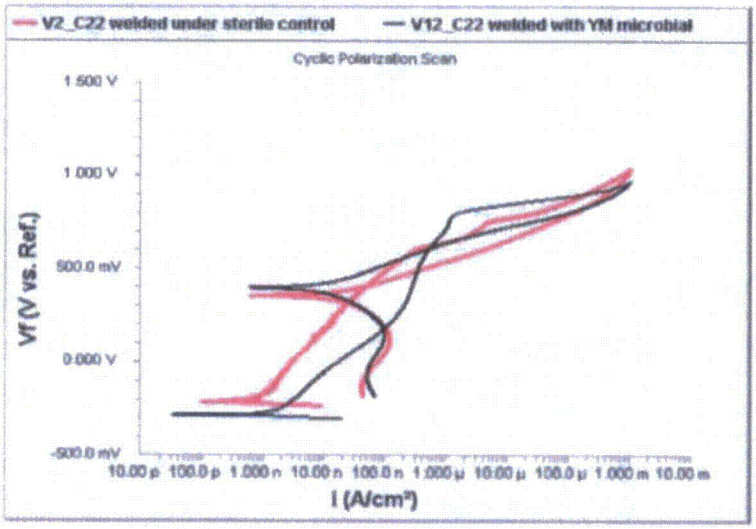

Fig. 11. Comparison of anodic polarization of an Alloy 22 welded metal coupon inoculated and incubated with YM bacteria with a coupon that was incubated under sterile conditions.

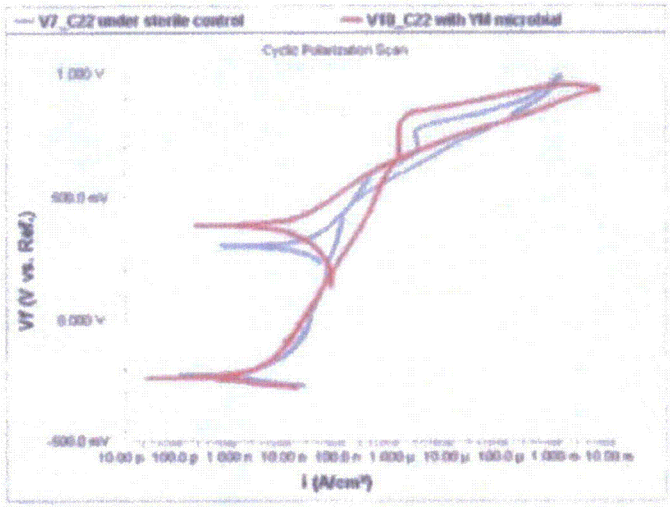

Fig. 12. Comparison of anodic polarization of an Alloy 22 base metal coupon inoculated and incubated with YM bacteria with a coupon that was incubated under sterile conditions.

5.4. Corrosion of Alloy 22 and Composition of the Biofilm

Although the effect of MIC on Alloy 22 is small, both the batch "reduced" experiment and the "oxidizing" flow-through experiment show that inoculated YM bacteria enhance the corrosion of Alloy 22 due to the presence of organic ligands or lower pH within the biofilm. We measured the composition of Alloy 22 films that formed in the sterile and non-sterile systems. Under reducing conditions, soluble Cr (1 ppm) and to a lesser extent Ni (0.1 ppm) were measured when coupons had been incubated with YM microorganisms (13). X-ray photoelectron spectroscopy (XPS) of the biofilm showed a thick carbonaceous layer with both Ni and Cr overlying the biotically incubated coupon (14). In the "oxidizing" system (Fig. 13), the biotically incubated coupon is again covered in a thick carbonaceous biofilm, which is clearly evident even after pre-sputtering for 25 minutes. Within the biofilm, Ni, Cr, and Mo are all evident, as they were in the prior analysis, indicating again the degradation of the alloy under the film, which is nominally at least 4 to 5 times thicker than the passive film formed on Alloy 22 in the sterile system. As the biofilm is traversed, progressing toward the metal surface, the accumulation of alloying elements within the film increased. However, base metal was never reached, as indicated by the lack of asymptotic concentrations of alloying elements. The biofilm also appears to change from an organic-rich film with minimal metal incorporation to a metal-(hydr)oxide-rich film with a smaller contribution from the organic film at depth, as is indicated by a constant oxygen, decreasing carbon, and increasing metal profiles with depth. The increasing hydr(oxide) component at depth reflects the incorporation of dissolved metals by the biofilm. This situation was in contrast to the sterile coupon, which had only a thin carbon surface layer (probably due to glucose in the medium), beneath which the oxidized passive layer is evident by

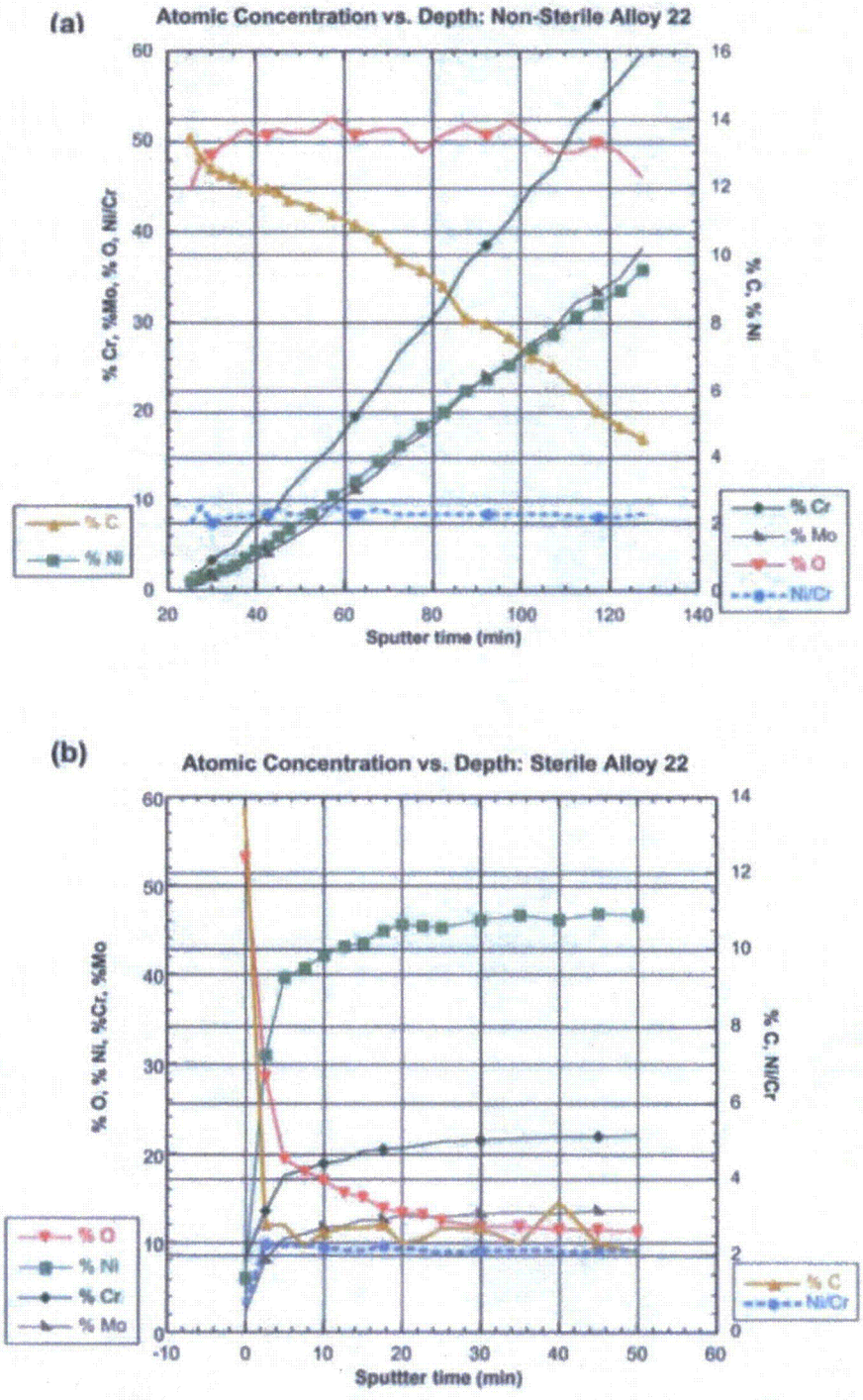

Fig. 13. Relative concentrations (atomic percent) of Alloy 22 alloying elements as a function of depth on: (a) a coupon incubated with YM bacteria and (b) a coupon incubated under sterile conditions.

intermediate levels of oxygen. Then at further depths, all alloying elements reach a steady value, indicating penetration of the base metal.

6. Concluding Remarks

The limiting factor for microbiological growth at Yucca Mountain is the availability of sufficient water either through deliquescence of salts or during groundwater seepage after the thermal pulse. Those microorganisms that do become established during this time, either those able to survive the thermal pulse or those that infiltrate may significantly alter the microbial community that is currently present, as was shown by community analysis of the contents of the LTCTF tanks.

Our experimental results using the present YM community suggest that microbes enhance Alloy 22 corrosion in the presence of a carbon source. Although this effect is small, MIC is seen in the formation of thick biofilm and micropits and in the enhancement of the corrosion rate using electrochemical tests. In addition, it should be noted that the described testing was carried out under relatively mild conditions, at neutral pH, at limited ionic concentrations, and with a carbon source. Further testing under more extreme conditions would need to be conducted to assess those periods during which the repository will experience harsher environmental conditions.

7. References

1. *Engineered Materials Characterization Report for the Yucca Mountain Site Characterization Project.* Vol. 3, Rev. 1, 1997. Section 2.6, Lawrence Livermore National Laboratory, UCRL-ID-119564. Also available as p. 2.6-1 through 2.6-25 of the full report: CRWMS M&O 1997 *Engineered Materials Characterization Report for the Yucca Mountain Site Characterization Project.* Vol. 3, Rev. 1, *Corrosion Data and Modeling.* Las Vegas, Nevada: CRWMS M&O. ACC: MOL.19971009.0589.
2. Horn, J.M., B. Masterson, M. Davis, A. Rivera, A. Miranda, S. Martin. 2004. Bacterial growth dynamics, limiting factors, and community diversity in a subsurface nuclear waste repository environment. *Geomicrobiology J.* **21**, 273–286.
3. Horn, J., C. Carrillo, and V. Dias. 2003. Comparison of the microbial community composition at Yucca Mountain and Laboratory Test Nuclear Repository environments. *Proceedings of Corrosion/2003*, Paper No. 556, National Association of Corrosion Engineers, March 17–20, San Diego, CA.
4. Horn, J., A. Jin, and R. Kelly. 2000. *An Evaluation of Fungal Growth in the Exploratory Studies Facility, Yucca Mountain NV*, Lawrence Livermore National Laboratory, UCRL-ID-141056.
5. *Engineered Materials Characterization Report.* Vol. 3, Rev. 1.1, 1995. Lawrence Livermore National Laboratory, UCRL-ID-119564.
6. Palmer, R.J., J. Siebert, and P. Hirsch. 1991. Biomass and organic acids in sandstone of weathering building: production by bacterial and fungal isolates. *Microb. Ecol.* **21**, 253–266.
7. Schrickx, J.M., M.J.H. Raedts, A.H. Stouthamer, and H.W. van Verseveld. 1995. Organic acid production by *Aspergillus niger* in recycling culture analyzed by capillary electrophoresis. *Anal. Biochem.* **231**, 175–181.
8. Francis, A.J., J.M. Slater, and C.J. Dodge. 1989. Denitrification in deep subsurface sediments. *Geomicrobiology J.* **7**, 103–116.
9. Morris, J.T., G.J. Whiting, and F.H. Chapelle. 1988. Potential denitrification rates in deep sediments from the southeastern coastal plain. *Environ. Sci. Technol.* **22**, 832–836.
10. Martin, S., J. Horn, and C. Carrillo. 2004. Micron-scale MIC of Alloy 22 after long term incubation in saturated nuclear waste repository microcosms. *Proceedings of Corrosion/2004*, Paper No. 04596, National Association of Corrosion Engineers, March 29–April 1, New Orleans, LA.
11. Horn, J., S. Martin, and B. Masterson. 2001. Evidence of biogenic corrosion of titanium after exposure to a continuous culture of *Thiobacillus ferrooxidans* grown in thiosulfate medium. *Proceedings of Corrosion/2001*, Paper No. 259, National Association of Corrosion Engineers, March 12–16, Houston, TX.
12. Lian, T., S. Martin, D. Jones, A. Rivera, and J. Horn. 1999. Corrosion of candidate container materials by Yucca Mountain bacteria. *Proceedings of Corrosion/99*, Paper No. 476, National Association of Corrosion Engineers, May 10–15, San Antonio, TX (Lawrence Livermore National Laboratory, UCRL-JC-132825, January 1999).
13. Horn, J., T. Lian, and S. Martin. 2002. Microbiologically-facilitated effects on the surface composition of Alloy 22, a candidate nuclear waste packaging material. *Proceedings of Corrosion/2002*, Paper No. 02448, National Association of Corrosion Engineers, April 7–11, Denver, CO.
14. BSC (Bechtel SAIC Company) 2004. Appendix 1, Surface Analysis of Corrosion Test Specimens for Dealloying (Response to Container Life and Source Term 1.02), Rev. 1. Las Vegas, Nevada: Bechtel SAIC Company. ACC: MOL.20040923.0130.
15. Cohen, G.N. 2004. *Microbial Biochemistry.* Boston: Kluwer Academic Publishers. 333 p.
16. Nelson, D.L., and Cox, M.M. 2004. *Lehninger Principles of Biochemistry*, Fourth Edition. New York: W.H. Freeman. 1100 p.